FRIEDRICH-ALEXANDER
UNIVERSITÄT
ERLANGEN-NÜRNBERG
NATURWISSENSCHAFTLICHE
FAKULTÄT

Department
Chemie und Pharmazie

Adsorption, Mobility and Reactions of Novel Porphyrins on Metal Surfaces

Adsorption, Mobilität und Reaktionen von neuartigen Porphyrinnen auf Metalloberflächen

Der Naturwissenschaftlichen Fakultät
der Friedrich-Alexander-Universität Erlangen-Nürnberg
zur Erlangung des Doktorgrades Dr. rer. nat.

vorgelegt von

Jan Brox

aus Neustadt an der Aisch

Als Dissertation genehmigt
von der Naturwissenschaftlichen Fakultät
der Friedrich-Alexander-Universität Erlangen-Nürnberg

Tag der mündlichen Prüfung:	22.06.2022
Vorsitzende/r des Promotionsorgans:	Prof. Dr. Wolfgang Achtziger
Gutachter/in:	Prof. Dr. Hans-Peter Steinrück Prof. Dr. Abner de Siervo

Table of Contents

1 Introduction 1

2 Experimental and fundamental Background 4

2.1 Principle of STM 4

2.2 Experimental Setup 6

2.3 Porphyrins 7

2.4 Substrate 10

3 Literature Review 12

3.1 Conformation 12

3.2 Diffusion and self-assembly behavior 13

3.3 Chemical surface reactions: Metalation, dehydrogenation, and network formation . 15

4 Results 18

4.1 Conformation and intermolecular interaction [P2, P4] 18

4.1.1 2HTNP and 2HTNBP on Cu(111) 19

4.1.2 2HTNP and 2HTNBP on Ag(111) 25

4.2 Coordination and metalation reaction with coadsorbed metal atoms [P1, P3] 31

4.2.1 Codeposition of Co atoms and 2H*trans*DCNPP 31

4.2.2 Codeposition of Zn and 2HTCNPP 38

5 Conclusion 46

6 Zusammenfassung 49

7 List of Abbreviation 52

8 References 53

9 Acknowledgements 60

10 Appendix 61

10.1 List of Publications 61

10.1.1 [P1] 62

10.1.2 [P2] 73

10.1.3 [P3] 85

10.1.4 [P4] 102

1 Introduction

In the upcoming years, technology will have an even bigger influence on our daily life compared to the present day. To tackle one of the most severe problems of our time, that is climate change, we need to progress in a variety of different fields. These include eliminating the dependency of fossil fuels by providing and storing clean energy, sustainable handling of our resources and decreasing the emission of greenhouse gases in the private and industry sector. The achievement of these goals requires a deeper understanding and optimization of the fabrication processes of relevant materials and products and the development of new technological concepts, *e.g.*, for energy conversion and storage. One promising route in this regard is the miniaturization of building blocks in fields like catalysis, energy storage and conversion, electronics, photonics, and information technology, to increase the efficiency in production cost and resource spending [1, 2]. Thus, the design and fabrication of functional materials at the nanoscale has become a major challenge and topic in industry and science [1].

Nanotechnology focuses on the fabrication, characterization, and manipulation of structures in the size range of 1 to 100 nm, in at least one dimension [3]. In the field of information technology miniaturization is vital and is achieved by doubling the number of transistors in dense integrated circuits approximately every two years following Moore's law [4]. To maintain the trend of fabricating smaller and smaller devices two powerful methods are used. The first is the top-down approach, which transforms larger components into smaller features in the nm regime by structuring techniques like photolithographic processes [5]. In the future, it will become increasingly difficult to develop lithographic processes, which can produce small enough features to keep up with the miniaturization trend predicted by Moore's law. The second route is the bottom-up approach, which is a promising strategy to overcome the mentioned size limitations [6]. In this approach, small building blocks in the atomic and molecular size range are used to fabricate nanostructures. A powerful strategy of the bottom-up approach is the self-assembly of functional molecules to form highly ordered nano-patterns, depending on the interaction motif of the selected building blocks [7]. Larger organic molecules have proven to be a suitable class for the formation of self-assembled nanostructures, due to their specific electronic and chemical properties, which can be tuned over a wide range [1, 8, 9]. Among the huge variety of molecules, porphyrins represent one of the most promising classes, since they offer interesting properties like a conformational flexible macrocycle, possible functionalities at the periphery and a reactive coordination center [10-12]. Their importance and versatility are shown by their omni-presence in nature, in vital processes in plants and mammals. Two of the most important porphyrins in nature are illustrated in Figure 1.1. These two examples reflect the importance of the central coordinated metal atom, which determines the functionality [13].

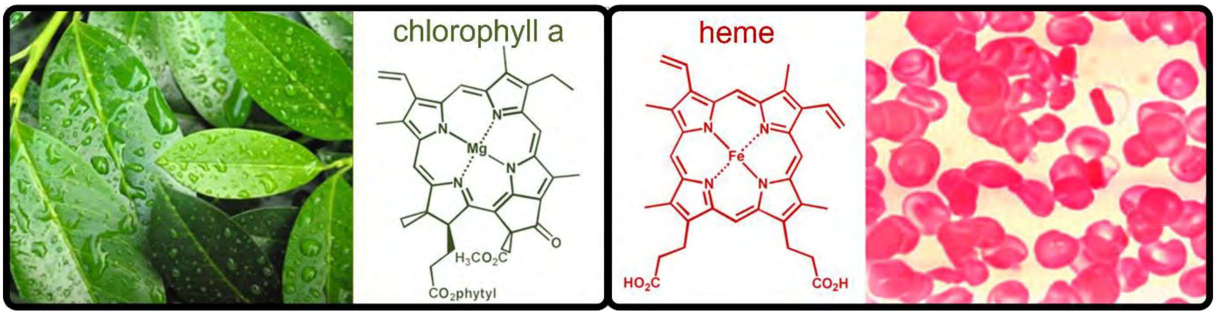

Figure 1.1: Illustration of the two most prominent metalloporphyrins chlorophyll a and heme in nature. Modified from [5].

Heme, being an Fe(II)-porphyrin, is responsible for the binding and transport of oxygen in the blood circle of mammals. On the other hand, chlorophyll a (Mg(II)-porphyrin) is involved in the light harvesting and electron transfer process in the photosynthesis of plants. This importance inspired researchers all over the world to build up applications based on porphyrins, which are already used in fields like solar energy conversion [14, 15], gas sensing [16] and catalysis [17, 18]. Their versatile functionality, structural flexibility, high thermal stability and low vapor pressure made them excellent candidates to study adsorption and self-assembly behavior on different single crystal surfaces of metals and oxides by various surface science techniques. To control the fabrication of functional nanostructures from porphyrins, a deeper understanding about their adsorption and self-assembly is needed. In this context, scanning tunneling microscopy (STM) emerged as an especially powerful tool for investigating nanoarchitectures.

The aim of this thesis is the investigation of different tetraphenylporphyrin derivatives by STM at and around room temperature (RT). It focusses on the molecular conformation, the diffusion behavior, the role of intermolecular interactions in the formation of supramolecular structures, and the interaction and reaction with coadsorbed metal atoms. The goal was to develop a deeper understanding of the adsorption properties of porphyrin molecules to set the stage for further developments of nanofabricated applications.

The thesis at hand is a cumulative thesis, which is based on four publications [P1-4] (attached in the Appendix). The studies in [P3], which address the properties of zinctetracyanophenylporphyrin on Ag(111), were performed in collaboration with the group of Prof. Dr. Abner de Siervo (University of Campinas, Brazil). The group of Prof. Dr. Norbert Jux (Friedrich-Alexander- University Erlangen-Nürnberg) provided the porphyrins, which were used in all four publications [P1-4].

In the following, the experimental setup and fundamentals are described in Chapter 2. In particular, an overview over the measuring technique, that is STM, and the used single crystal surfaces and porphyrin molecules is given. Chapter 3 summarizes the literature relevant for the thesis and related publications [P1-4]. In Chapter 4 the results of [P1-4] are presented in detail. Finally in Chapter 5, the findings are summarized in the conclusion.

2 Experimental and fundamental Background

2.1 Principle of STM

Scanning tunneling microscopy (STM) is a powerful method to image conducting and semiconducting surfaces in real space on the atomic level. Furthermore, the local density of states (LDOS) can be investigated by scanning tunneling spectroscopy (STS). Young et al. made the first suggestion of using the tunneling current for imaging surfaces in 1972 [19]. It took ten more years until Binnig and Rohrer presented the first working microscope to image surfaces with atomic resolution [20, 21]. Since then, STM has become an essential tool in condensed matter physics, material science, chemistry, and biology. The importance of the STM was acknowledged with the awarding of the Nobel-Prize in 1986 to Binning and Rohrer. The high potential of the STM is also used to manipulate individual atoms and molecules to form nanostructures on surfaces [22]. In the following the fundamentals of STM are reviewed. A more detailed theoretical description can be found in publications [22, 23].

STM measurements rely on the quantum-mechanical effect of electron tunneling. Compared to classical physics, an electron can tunnel through a potential barrier even though its kinetic energy is not high enough to overcome this barrier. The wave-particle dualism of quantum mechanics allows for describing the electron by its wave function Ψ, which decays exponentially in the potential barrier. As a consequence, the probability density $|\Psi^2|$ to find an electron at a position behind the barrier is non-zero behind a small and thin enough potential barrier and allows for electron transmission. This phenomenon occurs between two materials separated by a small gap (potential barrier for electrons), which is the distance d between the two materials. To observe a tunnel current I, typical a distance d in the range of 1 nm or below is needed. Equation 2.1 describes the dependency of the tunneling current I [24]:

$$I \propto U e^{\frac{-2d}{\hbar}\sqrt{2 m_e \Phi}} \tag{2.1}$$

In this equation Φ is the potential barrier height between the two materials, which can be described approximately by the average value of the work functions of the material A and B. The mass of the electron is given by m_e and U represents the applied bias voltage.

The potential barrier in a STM experiment is the gap d between tip and sample. Bringing the tip and sample in close enough distances, allows for an electron tunneling and thereby probing the sample according to the measured tunnel current. Equation 2.1 describes the exponential decay of the tunneling current I with increasing distance d, which enables an extreme height-sensitive probing of the electronic structure and topology of the sample. Based on this dependency, STM is used to scan flat conducting sample surfaces with a sharp metallic tip by probing the topography and electronic structure. Typical tip materials are tungsten or platinum-iridium alloys (9:1). The tips are mounted to a piezoelectric scanning unit, which uses the reverse piezoelectric effect to allow for a precise movement (Å-µm range) of the tip in x, y and z direction [25]. An image of the sample surface is generated by raster scanning the desired area in "constant height" or "constant current" mode. In the constant height mode, the z position of the tip is kept constant while scanning the surface. The change in tunnel current I(x, y) is depicted as the STM image, which reflects the corrugation of the surface. This mode enables a high scan speed, but is only limited to very flat surfaces, since the tip could crash into high surface corrugations. The constant current mode can be used for rougher surfaces, because the tip height is controlled by a feedback loop to keep the tunnel current constant at the cost of lower scan speed. The STM images consist of a map z(x, y) of tip height vs lateral position. STM images are always a combination of the topography and the electronic structure of the surface.

2.2 Experimental Setup

All experiments and sample preparations were performed in a two-chamber ultrahigh vacuum (UHV) system at a background pressure in the low 10^{-10} mbar regime. The whole set-up is resting on three Newport I-2000 laminar flow stabilizers (1.5-2.0 bar) to isolate against external low frequency vibrations. This chapter describes the UHV system and its components briefly.

The variable temperature scanning tunneling microscope is a RHK UHV VT STM 300 equipped with RHK SPM 100 electronics and a variable gain low noise current pre-amplifier (FEMTO DLPCA-200). Cut Pt/Ir tips were used as STM probes in the Besocke STM design scan head [26]. Radiative heating and a flow cryostat enable sample temperatures in the range of ~200-500 K. The STM images were recorded in constant current mode and the bias voltage refers to the sample. All STM raw data was processed with WSxM© software and typically moderate filtering (Gaussian smoothing, background subtraction) was applied for noise reduction in the images [27].

The homebuilt preparation chamber houses various sample preparation components like a SPECS IQE11/12 sputter gun and electron bombardment heating from a filament of an Osram halogen light bulb (250 W) to clean and anneal the substrates, respectively. A Knudsen cell evaporator was used for deposition of organic materials, until it was replaced with a home-build 3-fold Knudsen cell evaporator, which allows for the evaporation of three different porphyrins. A 3-fold Omicron Focus EFM 3 electron beam evaporator is attached to the chamber for metal deposition, which was equipped with Cu and Pd rods. Zn was evaporated from a Mo crucible. Additionally, a single Omicron Focus EFM 3 electron beam evaporator is used for Co (rod) evaporation, in combination with a quartz crystal microbalance (INFICON SQM-160) controlling the evaporation rate. Furthermore, several gas inlets offer the possibility of dosing gas into the chamber. For sample characterization, a SPECS ErLEED optics for low energy electron diffraction (LEED) and a Pfeiffer HiQuad QMG700 (m/z = max. 2000) mass spectrometer to detect large organic molecules (such as porphyrins) are installed.

2.3 Porphyrins

Porphyrins are based on the heterocyclic porphin macrocycle which consists of four pyrrole groups linked by four methane bridges (Figure 2.1, center).[13] The macrocycle is a highly conjugated π-system which is aromatic following the Hückel rule [28]. In the free-base configuration the macrocycle hosts two hydrogen atoms which leads to two aminic and two iminic pyrrole rings. By splitting off the hydrogen atoms, the macrocycle can coordinate a variety of metal atoms, leading to metal-porphyrins (Figure 2.1, left side). Furthermore, functional groups can be attached at different positions in the periphery of the porphyrin macrocycle leading to a wide variety of porphyrin derivates (Figure 2.1, right side).

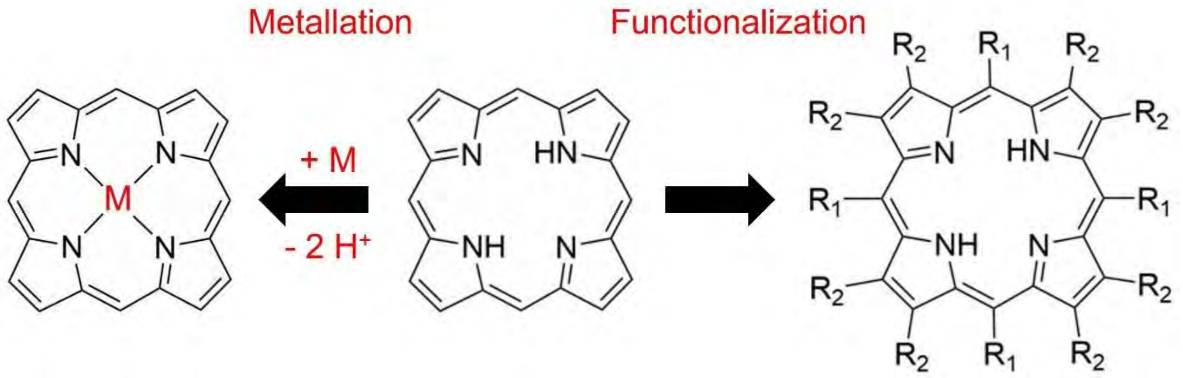

Figure 2.1: Schematic drawing of a metalated, free-base and functionalized porphyrin macrocycle.

This complexity makes the nomenclature of porphyrins difficult and inconsistent in literature. In this thesis, the most common nomenclature will be used to describe the used porphyrins [29]. The macrocycle can be functionalized in two different positions. A substitution of the hydrogen atoms of the pyrrole groups is referred as a *β*-substitution, while the functionalization of the linking methine bridges is called *meso*-substitution [29]. The porphyrins investigated in this thesis are depicted in Figure 2.2 with their macrocycle being highlighted in red. All molecules depicted in Figure 2.2 are functionalized with a variation of the functionalized phenyl groups in the *meso*-position. The molecules belong to the class of “tetraphenylporphyrins”. The left column shows molecules, which are functionalized with an additional benzene ring attached to the *meso*-phenyl function. The porphyrin is labeled after the corresponding naphthalene molecules, that is, as “tetranaphthylporphyrins”. A fourfold functionalization of the macrocycle with isoindole groups leads to the class of “tetrabenzoporphyrins”, which got their name from the addition of a benzene ring to the *β*-positions of the macrocycle. If this benzoporphyrin is additionally functionalized with four naphthyl groups, it is denoted as “tetranaphthyl-tetrabenzoporphyrins” (Figure 2.2b). This is the only porphyrin in this thesis, which has a fully functionalized macrocycle.

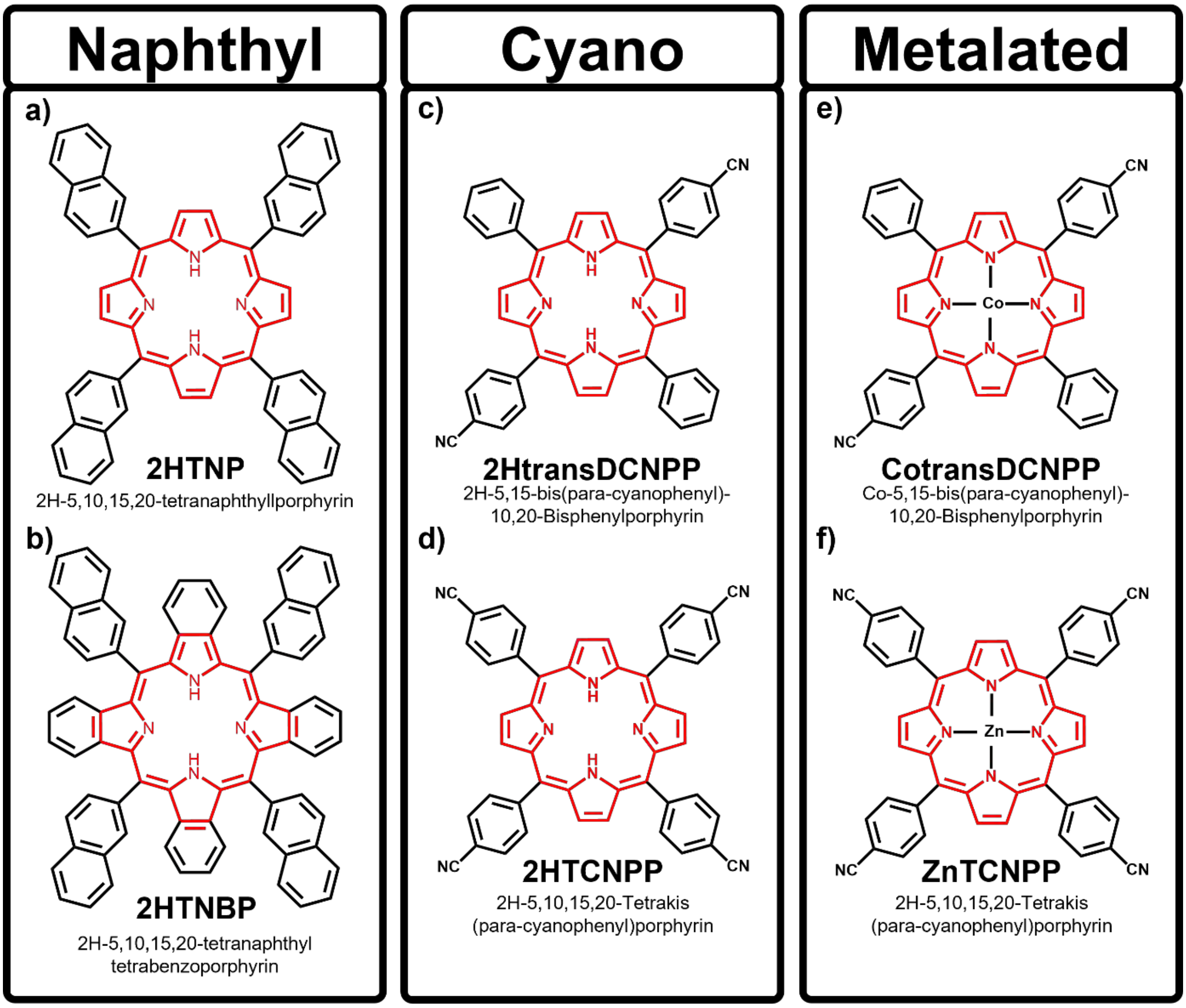

Figure 2.2: Schematic drawing of all porphyrins investigated in this thesis. The macrocycle is highlighted in red and the functionalization in black.

The middle column of Figure 2.2 shows tetraphenylporphyrins, which are partly or completely functionalized with cyano-groups in the *para*-position of the phenyl groups. This class of porphyrins is labeled as “cyanoporphyrins”. The right panel shows the corresponding cobalt and zinc metalated “cyanoporphyrins”, which were studied in this thesis.

By looking at the structural formula and the huge aromatic system one might expect a rather flat conformation of the molecule. Due to steric reasons, the orientation of the subgroups within the molecule deviates from this flat-looking appearance, especially also upon adsorption on a surface. A closer look shows the geometric flexibility of porphyrins with several rotation and tilting angles within the molecule, which are highlighted in Figure 2.3. All angles correlate to the macrocycle plane, with the tilting angle δ describing the outwards tilting of the pyrrole rings. The intramolecular conformation in Figure 2.3 shows that two opposite pyrrole rings (yellow) are tilted outwards the macrocycle plane with downwards pointing iminic nitrogen atoms (in blue). The aminic nitrogen atoms (blue) point upwards with the downward bent pyrrole rings. The angle θ represents the rotation around the σ-bond between the *meso*-substituent and the macrocycle and is caused by the steric repulsion of the aromatic side legs and the pyrrole rings of the macrocycle [8, 30-40]. Since all the phenyl-functionalized porphyrins have a symmetry axis along this bond direction, no different surface conformers are expected. The naphthyl groups, however, introduce an asymmetry around this bonding. The identification of the molecular adsorption conformation plays a major part in this thesis and the influence of the different side groups on the adsorption will be discussed in detail in Chapter 4.

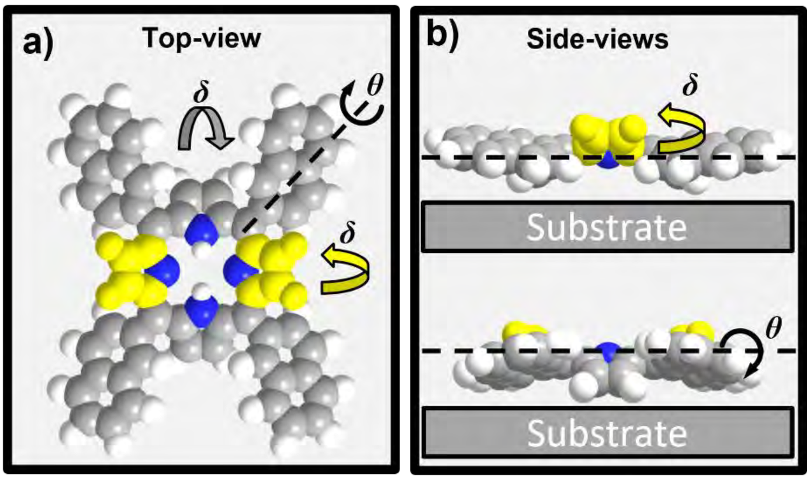

Figure 2.3: Top-view and side-view of a space filling model of 2HTNP to illustrate the conformation flexibility of the macrocycle. The upright standing iminic pyrrole groups are highlighted in yellow and the corresponding tilting angle of pyrrole groups out of the macrocycle plane is δ. The angle θ describes the rotation of the *meso*-substituents. The rotation of asymmetric groups like naphthyl could lead to several possible surface conformers.

All porphyrin compounds shown in Figure 2.2 were synthesized by the group of Prof. Dr. Norbert Jux from the Chair of Organic Chemistry II at the Friedrich-Alexander-University Erlangen-Nürnberg. The porphyrins were deposited on the single crystal surfaces (held at RT) by thermal sublimation from a home build Knudsen cell [41].

2.4 Substrate

The adsorption behavior of various porphyrins on copper and silver single crystal surfaces is investigated by STM. To understand the adsorption behavior of organic molecules on the substrate, detailed knowledge about the atomic arrangement and the electronic structure of the surfaces is necessary. Copper and silver crystallize in the face centered cubic lattice (fcc), which is shown in Figure 2.4. The bulk lattice parameter is 0.361 nm for Cu and 0.408 nm for Ag. The distance between two neighboring atoms in the closed-packed <111> plane is 0.255 nm for Cu and 0.289 nm for Ag.

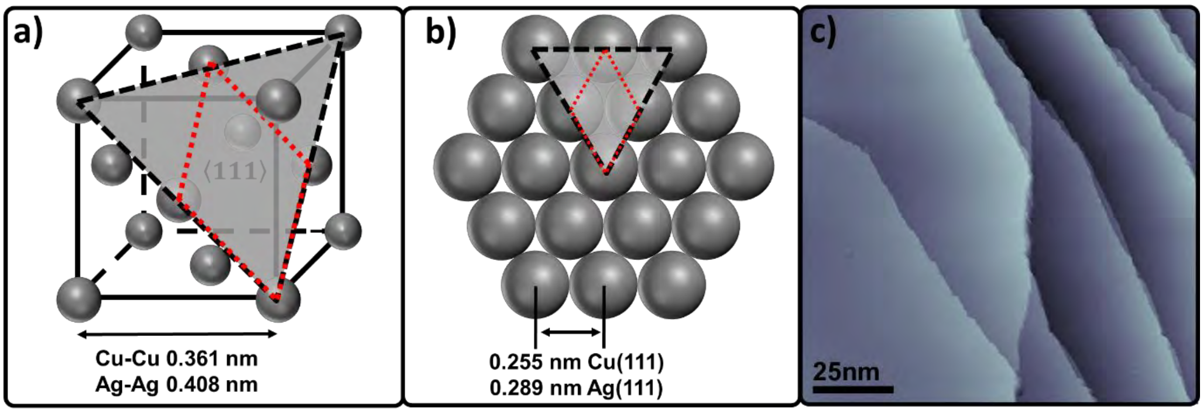

Figure 2.4: a) Illustration of face centered cubic (fcc) unit cell with the indicated <111> plane in grey. b) Top-view of the stacking order of the <111> plane. c) STM image of a clean Cu(111) surface with broad terraces (U = -1V, I = 29 pA).

Both crystals exhibit the same surface geometry, but the Cu substrate is considered as the chemically more reactive substrate. The difference in reactivity makes both surfaces good candidates to study the adsorption behavior of different porphyrins. The molecular-substrate interactions are expected to be stronger on the reactive Cu surfaces, since the iminic nitrogen atoms of the porphyrin macrocycle interact strongly with the surface atoms. On the other hand, molecule-molecule interactions will dominate on the comparatively less reactive silver surface. By comparing experiments on both surfaces the influence of different functional groups for the adsorption behavior of porphyrins can be studied. The Cu(111) single crystal was purchased from MaTeck, and the Ag(111) crystal was bought from Surface Preparation Laboratory. The crystals have a specified purity of >99.99 % and an alignment of <0.1° with respect to the nominal orientation. The crystals are cleaned by repeated cycles of Ar^+-ion sputtering (600 eV, sample current between 5-10 µA for 3h) at an Ar background pressure of 5 x 10^{-5} mbar. The annealing step is programmed to follow a temperature rate of 1 K/s to 850 K. This temperature is held for 10 minutes followed by cooling down to RT with a rate of 0.3 K/s. The rather slow preparation procedure leads to a size-increase of terraces and the number of step edges is reduced. During the annealing of Cu(111) the manipulator was cooled down and kept around 170 K, to avoid contamination of single crystal surface with molecules desorbing from the manipulator (for more details refer to [42]).

3 Literature Review

3.1 Conformation

In a simplified picture, the conformation of surface adsorbates depends on the balance of steric repulsion of molecular subgroups (intermolecular interaction) and the interaction forces with the surface (adsorbate/substrate interactions). For porphyrins, this means that the tilting of *meso*-substituents (i.e., phenyl group) is linked to the tilting of the pyrrole units of the macrocycle [43]. A flatter macrocycle would lead to more upright standing phenyl groups, while planar lying phenyl legs would cause a strong deformation of the macrocycle. For porphyrins derivates, the saddle-shape conformation was assumed on metal surfaces [33, 38, 40, 44-48]. One very well understood reference system for this behavior are 2H-tetraphenylporphyrins (2HTPPs), which feature four phenyl groups in the *meso*-position of the macrocycle on Ag(111), Au(111), and Cu(111) [10, 11, 35, 36, 49]. The situation is more complex on Cu(111). Jarvis *et al.* studied 2H-tetra(4)bromophenylporphyrin on Cu(111) with STM and density functional theory (DFT) calculations. They proposed a saddle-shape conformation based on van-der-Waals-forces being the dominant molecular-substrate interactions and ruled out more specific chemical bonds [37]. Contrary to that, additional studies of the adsorption conformation of 2HTPP on Cu(111) by atomic force microscopy (AFM), STM + DFT, and normal incidence X-ray standing waves (NIXSW) describe a different conformation, in which the iminic nitrogen atoms of the pyrrole rings form a strong coordination with the underlying substrate yielding nearly upright standing pyrrole rings [50-52]. This conformation is drastically different than the saddle-shape and is called “inverted” structure according to Lepper *et al.* [51]. Besides the interaction of the macrocycle with different surfaces, the modification of the periphery of the macrocycle can have a huge influence on the surface conformation. A bowl like structure was observed for 2H-terakis-(3,5-di-tert-butyl)phenyl-porphyrin (2HTTBPP) on Cu(111), by adding two bulky tert-butyl groups to the *meso*-phenyl groups [32]. Summarizing, the adsorption conformation of porphyrins is strongly linked to their molecular structure and the corresponding molecular-substrate interactions. However, the conformation of the adsorbates also has influence of the molecular mobility and the intermolecular interactions, which will be discussed in the following sections.

3.2 Diffusion and self-assembly behavior

Besides the discussed effects of the functionalization of the porphyrin macrocycle on the adsorption conformation, it has a major influence on the diffusion behavior and self-assembly of the molecules as well. Only a minor modification of 2HTPP to 2H-tetraphenyl-benzoporphyrin (2HTPBP) with the addition of four benzene rings to *β*-position macrocycle changes the mobility of the molecules drastically. For 2HTPP, individual adsorbed molecules are observed at low coverages on Cu(111), while 2HTPBP are very mobile as individual species on the surface and only observable when they assemble into islands [53]. Another example is the slight modification in the *meso*-substituents from phenyl (2HTPP) to pyridyl for 2H-tetrapyridylporphyrin (2HTPyP), which is a replacement of the *para*-carbon atom of the phenyl group with a nitrogen atom. This results in a change of the long-range square ordered structure of 2HTPP to a herringbone structure for 2HTPyP [54, 55]. Furthermore, the strong influence of the underlying substrate plays a critical role and is highlighted in Figure 3.1.

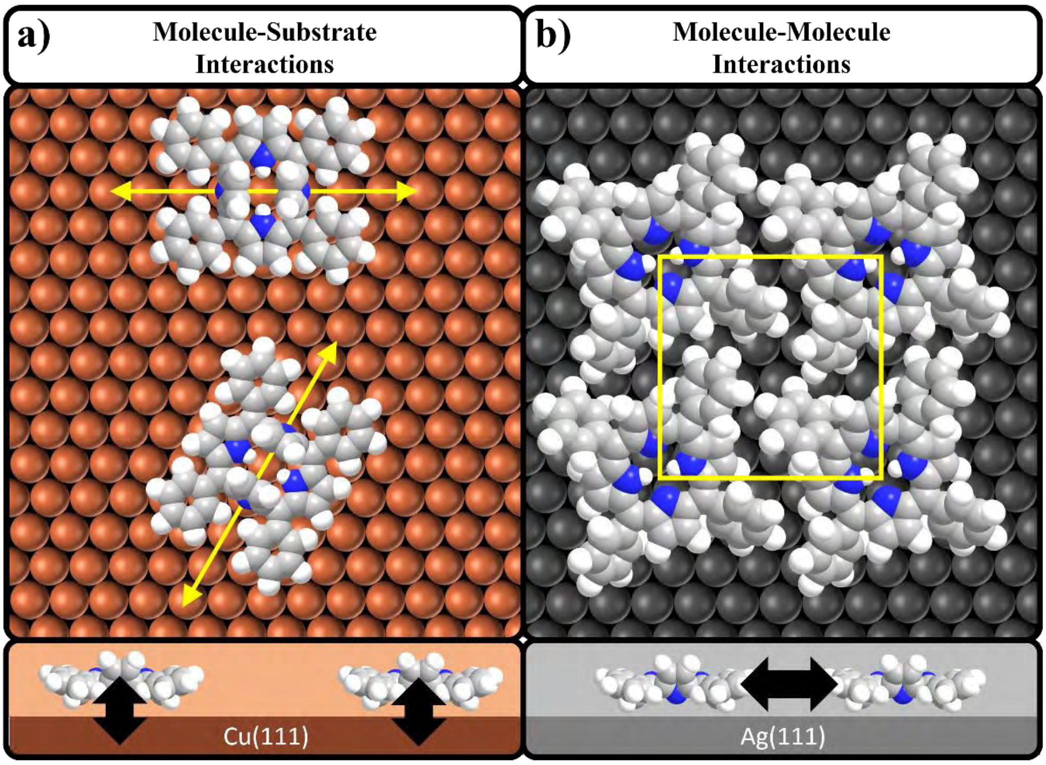

Figure 3.1: Illustration of the influence of molecule-substrate and molecule-molecule interactions on the adsorption behavior of 2HTPP. a) On Cu(111) ,the strong molecule-substrate interaction leads to the adsorption of 2HTPP as individual molecules orientated along the high symmetry axis (yellow arrows). b) On Ag(111), the molecule-molecule interaction dominates and a square supramolecular order (yellow square) is formed by stabilizing T-type interactions of neighboring porphyrins.

For 2HTPP, two different conformations are observed on Cu(111) and on Ag(111), which govern their adsorption behavior. As mentioned above, 2HTPP has stronger interaction with the surface atoms, leading to its “inverted” structure. Consequently, it is adsorbed as an individual molecule with a well-defined orientation along the main crystallographic axis (yellow arrows in Figure 3.1a) and can diffuse only along these directions. On the other hand, on Ag(111) 2HTPP adsorbs in its saddle-shape conformation, which has a weaker interaction with the substrate and allows for a rapid diffusion in all directions on the surface such that the molecules cannot be. imaged at RT. The diffusion enables the molecules to assemble into long-range ordered structures stabilized by T-type interactions (see Figure 3.1b). These three examples show the huge effect of the interplay between molecule-substrate and molecule-molecule interactions on different substrates.

3.3 Chemical surface reactions: Metalation, dehydrogenation, and network formation

The versatile ability of the porphyrin macrocycle to coordinate a broad range of different metal atoms in different oxidation states drew increasing interest of this reaction in the surface science community [10, 11, 56, 57]. The different metal centers influence the electronic state of the macrocycle and could act as active sites, making them interesting for applications in catalysis, sensor technologies or gas storage by adsorbing small molecules [58, 59]. The *in-situ* metalation was studied with pre- or post-deposited metal atoms or in form of "self-metalation" with surface adatoms. 2HTPP acted again as a well understood reference system and its in-situ metalation was studied extensively by STM, STS, AFM, X-ray photoelectron spectroscopy (XPS), and near edge X-ray absorption fine structure (NEXAFS). The wide variety of different metal atoms, which undergo a metalation reaction including Co [49, 60], Cu [38, 61] at RT and Fe [62, 63], Zn [64, 65], Ni [66, 67], and Ce [68] at slightly higher temperatures was studied for 2HTPP. Besides the metalation with coadsorbed metal atoms, porphyrins can react with already present substrate atoms. This reaction was first observed for a freebase protoporphyrin IX on Cu(110) and Cu(100) at RT by Gonzalez-Moreno *et al.*, while Diller *et al.* introduced the terminology "self-metalation" [38, 69]. Further studies showed the ability of porphyrins to undergo self-metalation reactions on surfaces like Cu, Ni and Fe [38, 40, 70-73], while so far no self-metalation reaction are reported on Ag(111) and Au(111). These results show the importance of the reactivity of the substrate to undergo in-situ reactions like self-metalation. Ditze *et al.* investigated the activation energy of the metalation reaction by Arrhenius analysis at low coverages with the STM [73]. Interestingly, the metalation process was linked to a drastic change in adsorption behavior, since metalated porphyrins lose their strong interaction with the surface and start to rapidly diffuse on the substrate [40].

Based on these results, Lepper *et al.* could show in a similar study on cyano-functionalized phenylporphyrins that the metalation reaction is depending on the functionalization of the periphery [74]. With an increasing amount of cyano-functionalization the self-metalation rate dropped, which show the importance of the side group. For further insight into the mechanism of metal coordination at the macrocycle, DFT calculations on 2H-porphyrin have been performed in the gas phase [64]. A three-step reaction pathway was suggested: Firstly, the metal atom is coordinated to the nitrogen atoms of the macrocycle. This step is followed by a one-by-one transfer of the two aminic hydrogen atoms onto the metal center, before they react to H_2 and are released from the porphyrin [64]. Studies of the metalation reaction in solution and at the solid-vacuum interface propose an intermediate reaction state, the so called "sitting atop"

(SAT) complex, in which the metal atom coordinates with the macrocycle while the aminic hydrogen atoms are still bound to the pyrrole nitrogen [75-80]. Shubina *et al.* investigated the metalation of 2HTPP with bare Zn atoms on a Ag(111) surface with XPS and found a similar complex [64]. The rate limiting step for metalation is the transfer of the first hydrogen to the metal atom. This step varies for different metal centers. For coadsorbed Fe and 2HTPP on Ag(111), the adcomplex could be identified already at 100 K [79], which Yamada *et al.* were able to image with low-temperature STM at 78.5 K. The original 2HTPP, a 2HTPP precursor adcomplex "α" state (Fe atom on top), and a 2HTPP precursor adcomplex "γ" state (Fe atom inside) were identified by DFT calculations, STM and STS [81]. A detailed understanding of the metalation reaction is, however, still missing and the involved influences like substrate, metal center and side groups need further investigations.

A further on-surface reaction is the dehydrogenation at elevated temperatures around 450 to 500 K. Röckert *et al.* observed a self-metalation reaction of 2HTPP on Cu(111) at 400 K with STM, XPS and temperature programmed desorption (TPD) [82]. At 450 and 500 K a partial loss of hydrogen leads to the intramolecular bond formation between the pyrrole rings of the macrocycle and the adjacent *meso*-phenyl legs, which results in a planarization of the macrocycle. Furthermore, the dehydrogenation reaction is not limited to intramolecular bond formation but can be used to crosslink other carbon-based molecules with porphyrins. Annealing porphyrins and graphene sheets on Ag(111) to 620 K, He *et al.* reported a bond formation between the corresponding molecules [83]. Furthermore, a covalent linking of porphyrins can lead to the formation of supramolecular structures by utilizing the on-surface Ullmann reaction of bromine-functionalized porphyrins [84]. Strictly speaking, the coupling reaction does not follow the definition of self-assembly by Whitesides, but nevertheless is a powerful tool to fabricate supramolecular frameworks. A particular interesting route to fabricate self-assembled nanostructures is the use of metal-coordinated organic frameworks like shown by Lepper *et al.* for cyano-functionalized porphyrins on Cu(111). The cyano-function is interesting due to its capability to interact via H-bonding, dipolar coupling, and metal organic bond formation [74, 85-87].

To conclude, it can be stated that the metalation of porphyrins occurs already at or slightly above RT, while dehydrogenation or network formation require higher thermal activation energy. All the reaction pathways are promising candidates for the manipulation of porphyrins *in-situ* and could be a promising route for the fabrication of highly functionalized nanostructures.

4 Results

This chapter is an extended summary of the results of the publications [P1-4] and puts them into perspective to the reviewed literature. By analyzing the behavior of the different porphyrins regarding their adsorption, mobility, and reaction, one can achieve fundamental insights into the processes, which are required to build up functional nanostructures based on porphyrins. The publications [P1-4] give a detailed overview of the results of the individual systems and are attached in the Appendix.

Our results focus on the adsorption behavior of porphyrins in a well-defined environment by using ultra-high vacuum conditions and single crystal metal surfaces. This limits the possible adsorption sites to regular and defined surface regions and minimizes the influence of surface contaminations. For a detailed understanding of the involved processes, a detailed consideration of the molecule-substrate and molecule-molecule interaction is needed. Thereby, the molecular conformation plays a huge role for the interaction with substrate and with neighboring molecules and is thus studied in detail. In this thesis, the connection of molecular conformation with the adsorption behavior and thus mobility, reactivity and supramolecular order was studied on Cu(111) and Ag(111) surfaces. The first chapter (4.1) summarizes the results of exchanging the symmetric phenyl group by an asymmetric napththyl group and by adding a benzo-group to the pyrrole groups (or in other words by introducing isoindole groups). The second chapter (4.2) focusses on the interaction of metal atoms like Co and Zn with the functional side groups (cyano) and the coordination and reaction with the macrocycle in form of metalation reactions.

4.1 Conformation and intermolecular interaction [P2, P4]

The interaction of 2HTPP on various single crystal surfaces has been studied in great detail and become a well-understood reference system [38, 51, 62, 64, 73, 88]. As discussed in the sections before, the molecule-substrate interaction has a strong influence on the adsorption behavior. on Cu(111), the strong chemical interaction between the iminic nitrogen atoms and the Cu substrate atoms leads to a peculiar intramolecular conformation, the so called “inverted structure”, while on Ag(111) a saddle shape conformation is preferred [50, 51]. This chapter focuses on the changes that are introduced replacing the symmetric phenyl group with a asymmetric naphthyl group. Furthermore, the influence of adding a benzo group to the pyrrole rings (forming isoindole groups) is studied.

4.1.1 2HTNP and 2HTNBP on Cu(111)

As a first step, we describe and discuss the adsorption behavior of 2HTNP and 2HTNBP on Cu(111) and thereafter address the behavior on Ag(111), based on the results of [P2] and [P4]. Figure 4.1 shows a very low coverage STM image of 2HTNP molecules adsorbed as isolated molecules on Cu(111). The appearance of individual molecules is dominated by two (sometimes merged to one) elongated parallel protrusions in the center of the molecule, which are surrounded by four dimmer protrusions in the periphery.

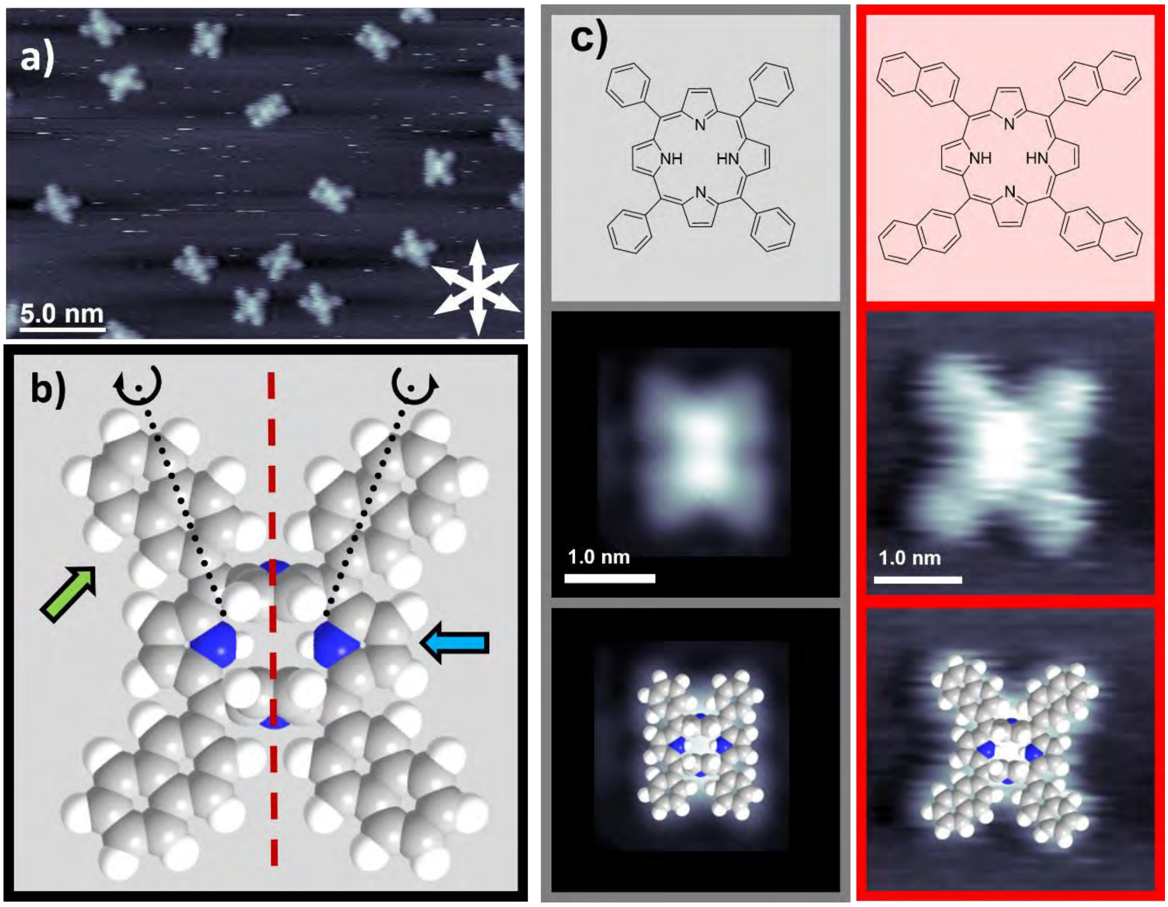

Figure 4.1: a) Constant current STM image of a low coverage of 2HTNP, prepared and measured at RT. b) Top-view of a space-filling model of the inverted structure of 2HTNP: Each naphthyl substituent (indicated by a red arrow) can be oriented away (α) or towards (τ) the main axis of the molecule through the iminic pyrrole groups (dashed line); also shown is the tilt angle of the iminic (=N-) pyrrole group; the aminic pyrrole group is indicated by the blue arrow. c) Chemical structure, high resolution STM image and structural overlay of inverted space-filling models of 2HTPP (left) and 2HTNP (right) for comparison. (a) U_{bias}= -1150 mV, I_{set} = 300 pA; (c) U_{bias}= -1400 mV, I_{set} = 370 pA. Modified image from [P2] with permission.

Similar to the well-investigated 2HTPP (Figure 4.1c, left panel), the specific molecular appearance arises from strong molecule-substrate interactions via the iminic nitrogen atoms of the porphyrin macrocycle and the Cu-substrate. 2HTNP adsorbs in an inverted structure, meaning that the iminic pyrrole groups are rotated by more than 90° out of the macrocycle plane, which is oriented almost parallel to the surface. A molecular space-filling ball model of the "inverted" 2HTNP is depicted in Fig. 4.1b, with the aminic pyrrole (blue arrow) and naphthyl (green arrow) groups being parallel to the surface.

For 2HTPP (Figure 4.1c, left panel), the phenyl groups are parallel to the surface and rotation around the linking C-C bond by 180° leaves the appearance and symmetry of the molecule unchanged. In contrast, for 2HTNP, rotation of the flat-lying naphthyl groups (green arrow) around the linking C-C-bond (black dotted line) by 180° changes the appearance and symmetry of the molecule, which leads to a variety of possible conformations. The α/τ-notation allows for a classification and description of the different conformers. In the α-orientation, the naphthyl group points away from the main molecular axis through the iminic pyrrole groups (red dashed vertical line in Fig. 4.1b), while in the τ-orientation it points towards this axis. By indicating the orientations of the four groups clockwise, starting in the left upper corner of the molecule, we obtain 16 possible conformations. The STM overview images in Fig. 4.2a show the ten distinguishable color-coded conformers of 2HTNP on Cu(111). All molecules are orientated along one of the three high symmetry-axes of the substrate. Of the theoretical 16 different conformations according to the α/τ -notation only ten are observed, because some molecules are rotamer pairs. In such a case, a rotation by 180° does not lead to a new appearance, which means that two different α/τ-notations describe the same conformation. For example, the $\alpha\alpha\tau\tau$ conformer is equal to the $\tau\tau\alpha\alpha$ conformer (see Fig. 4.2). The observed conformations are identified by their appearance and characterized according to their α/τ-notation, symmetry elements and point group. An overview of all conformers can be found in Figure 4.2. The first two conformers are the X- and I-shape. Both have in common that the elongated central protrusion is surrounded by four dimmer protrusions in a symmetrical fashion. For the X-shape, the molecule forms almost a square, while the I-shape is rectangular. According to the α/τ-notation, this results in $\alpha\alpha\alpha\alpha$ (X) and $\tau\tau\tau\tau$ (I) conformation and both belong to the C_{2v} point group. The conformations K and T are a mixture of the first two (X and I) and belong to the C_s point group. The K-shape has one mirror plane perpendicular to the main axis of the molecule. The notations of the corresponding rotamer conformations are $\tau\alpha\alpha\tau$ and *αττα*. For the T-shape, the mirror plane is along the molecular axis and the notations of the corresponding rotamers are *ααττ* and *ττάα*.

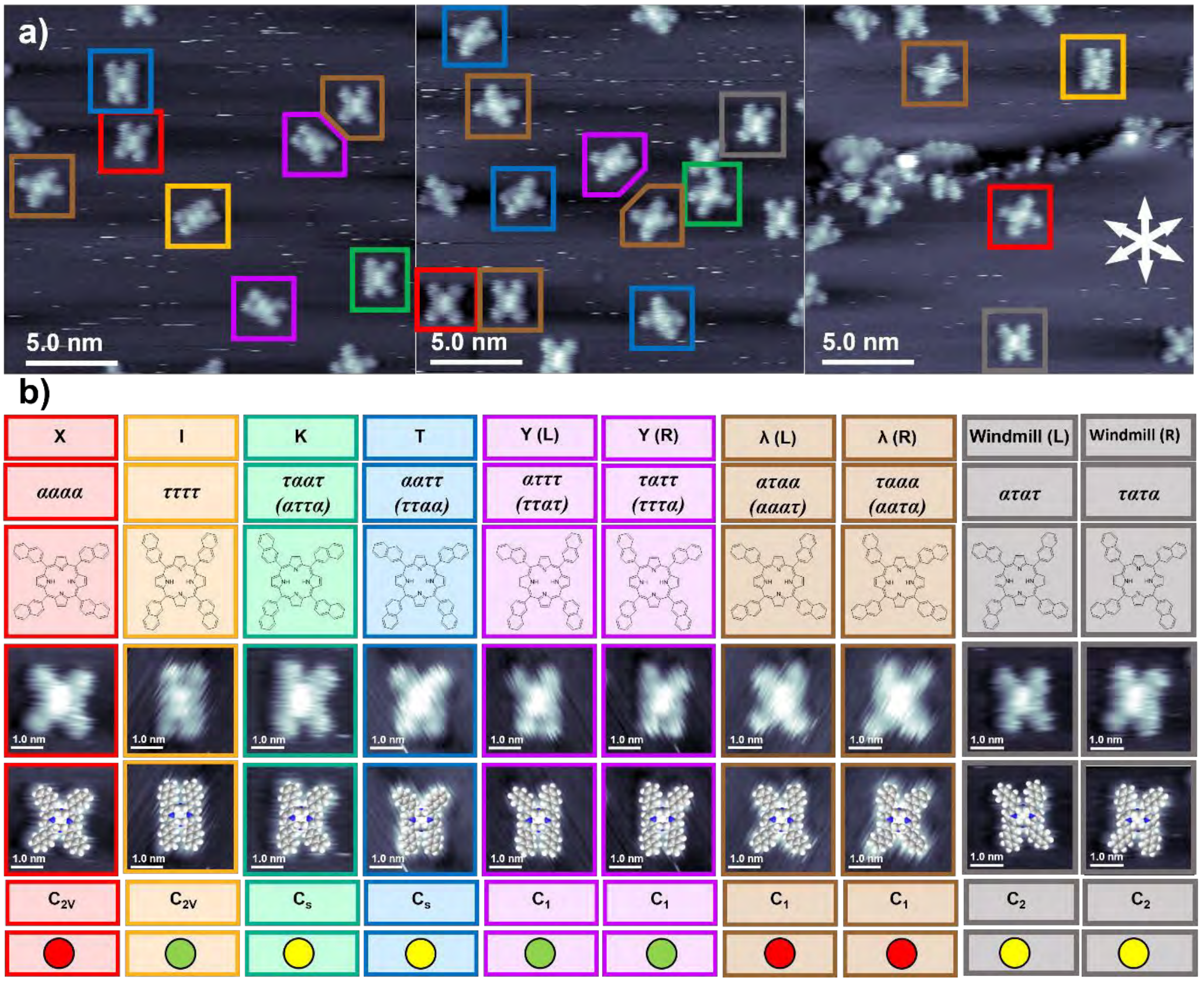

Figure 4.2: a) Three constant current STM images showing the 10 distinguishable surface conformations of 2HTNP highlighted by differently colored boxes. b) Name, α/τ-notation, chemical structure, high resolution STM image of a single molecule, STM image overlaid by a scaled space-filling model, point group, and mobility ranking (red: immobile, yellow: medium, green: fast) for all possible conformations. In case of equivalent rotamers, two α/τ-notation are denoted. (a) U_{bias}= -1150 mV, I_{set} = 300 pA. Original images from [P2] with permission.

All before mentioned conformations are achiral adsorption motives. The remaining conformations are surface-chiral, which means that each of them is present as an enantiomeric pair on the surface. The first enantiomeric pair is the windmill shapes, in which the naphthyl-group orientation alternates. Thereby, the *ατατ* conformer has a counterclockwise orientation (L) and the *τατα* conformer a clockwise orientation of the naphthyl groups (R). Both belong to the C_2 point group with the rotation point in the center of the macrocycle. The Y-shape is closely related to the I-shape, with one of the naphthyl groups pointing away from the main molecular axis. The naphthyl-groups are either orientated $\alpha\tau\tau\tau$ (L) or $\tau\alpha\tau\tau$ (R) for this enantiomeric pair. The opposite of the Y-shape is the λ-shape, which corresponds to $\alpha\tau\alpha\alpha$ (L) and $\tau\alpha\alpha\alpha$ (R) conformers. The Y-shape and the λ-shape both have no symmetry element, and thus belong to the C_1 point group. The observed conformations are stable at RT, and we never observed a switching of the orientations of the naphthyl groups and thus a change in molecular conformation.

Similar to 2HTNP, 2HTNBP adsorb as individual molecules on Cu(111) (see Fig. 4.3). They appear as a singular circular protrusion, which unfortunately gives no further information about the molecular conformation or the orientation of the naphthyl groups. This behavior is untypical for benzoporphyrins, since they typically form islands on the Ag(111) and also Cu(111) surfaces at RT [53, 89, 90]. The observed behavior indicates a better coordination of the iminic nitrogen atoms of the isoindole groups to Cu substrate atoms, like for 2HTPP and 2HTNP in the inverted structure. A fully inverted structure can however not be formed due to steric hinderance by the other isoindole groups. An additional driving force for the strong molecule-substrate interaction could be the larger footprint of the naphthyl groups. 2HTNBP has an even larger footprint compared to 2HTNP (isoindole instead of pyrrole groups) and benzoporphyrins (naphthyl instead of phenyl groups). Both effects could contribute to an increased adsorption energy.

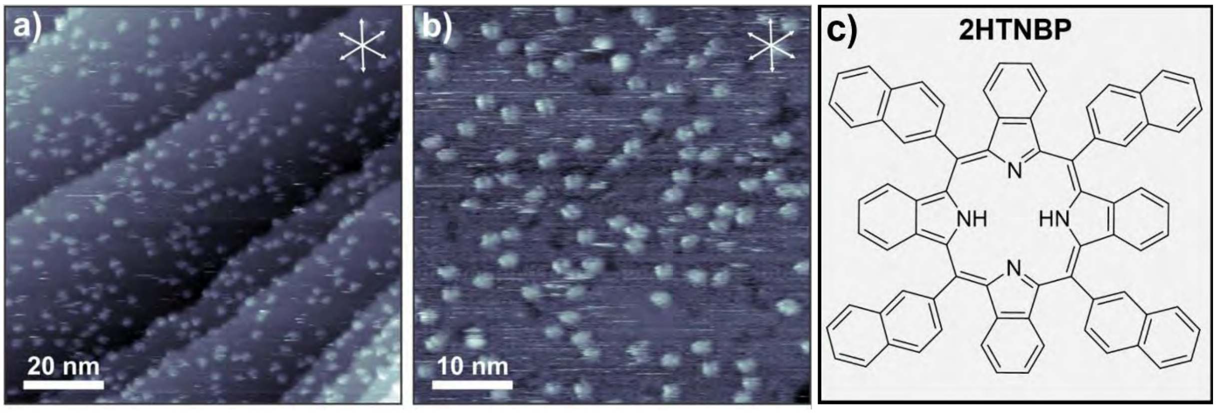

Figure 4.3: a) and b) STM images of 2HTNBP on Cu(111) measured at RT. c) Chemical structure of 2HTNBP. (a) U_{bias}= -1000 mV, I_{set} = 290 pA; (b) U_{bias}= -800 mV, I_{set} = 300 pA. Modified image from [P4] with permission.

To obtain further insights, the dynamic behavior of 2HTNP and 2HTNBP was also studied. Especially for 2HTNP the influence of the orientation of the naphthyl groups on the mobility of the different conformers is quite pronounced: In Fig. 4.4 motion-pathway-plots are shown for 2HTNP (top) and 2HTNBP(bottom). For 2HTNP, the ten conformers can be classified into three groups (red: immobile, yellow: medium mobility and green: fast). The X- and both λ-shapes both are immobile; they stick to their position and are hardly moving at all. The K-, T- and both windmill shapes diffuse short distances along a crystallographic axis. Y- and I-conformers are very mobile and diffuse the longest distances along a crystallographic axis. This behavior demonstrates that the molecular conformation of adsorbed 2HTNP significantly influence the mobility, that is, its diffusion behavior. The detailed analysis of the different conformations shows clear systematics behind our observations. Conformations with 4 (I) or 3 (Y) naphthyl groups in τ-orientation (smallest footprint), have a higher mobility and diffuse larger distances (green). Molecules with two naphthyl groups in τ-orientation (K, T, windmill) behave intermediate mobile (yellow). Finally, conformations with only 1 (λ) or 0 (X) naphthyl groups in τ-orientation (largest footprint), are immobile (red). One possible explanation for the molecules with all naphthyl groups in α-orientation is its larger footprint, meaning the interaction potential has a larger corrugation, and thus the whole molecule is stronger bound (immobilized).

For 2HTNBP (Figure 4.4c and d), we again observe three different behaviors: Most of the molecules are immobile (red) and diffuse only occasionally in close vicinity to their original position in the starting frame. This diffusion occurs in no preferred direction. Species with medium mobility are marked in orange and they diffuse faster, along one of the high symmetry axes (closed packed rows) of the Cu(111) substrate. Occasionally they hop to a neighboring closed-packed row. Furthermore, these molecules switch their direction of diffusion (alignment with the high symmetry axis) by 120°. Finally, very mobile species (green) are observed, which move too fast on the surface at RT to clearly capture their appearance as individual molecules in an STM frame of the movie; they rather appear as streaky protrusions, which diffuse with no preferred direction on the surface.

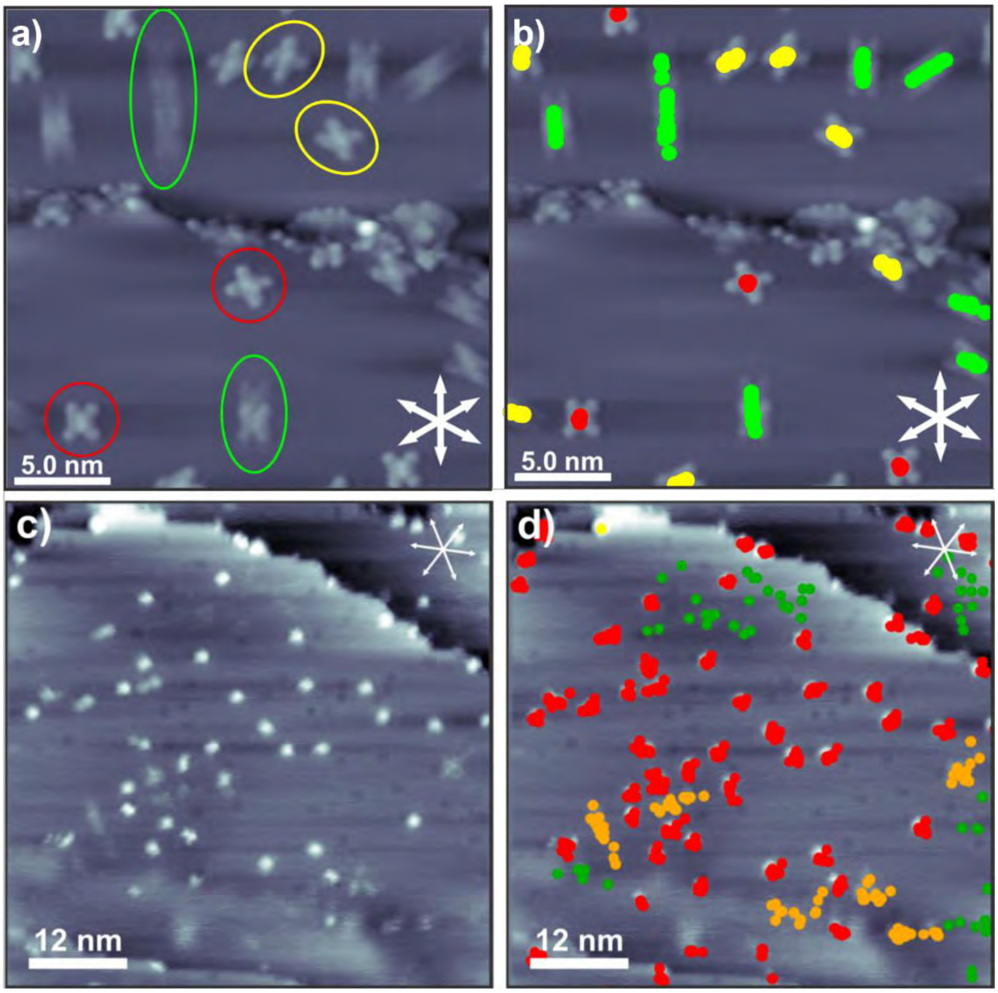

Figure 4.4: a) Average frames of STM movies of 2HTNP on Cu(111) at RT. b) Same image with the positions of the molecules color-coded in each single STM image, according to the observed mobility (red: immobile, yellow: medium, green: fast), and then superimposed over the corresponding STM average frames. c) Average frames of STM movies of 2HTNBP on Cu(111) at RT d) Same image with the positions of the molecules color-coded in each single STM image, according to the observed mobility (red: immobile, orange: medium, green: fast), and then superimposed over the corresponding STM average frames.. (a and b) U_{bias}= -1150 mV, I_{set} = 300 pA; (c and d) U_{bias}= -1000 mV, I_{set} = 300 pA. Modified images from [P2] and [P4] with permission.

After annealing 2HTNP at 400 K only three of the 10 conformations are observed. The X-shape is by far the dominant conformer, and λ(L)- or λ(R)-shape enantiomers were rarely observed (Figure 4.5). From the lack of mobility and the fact that the other molecules are converted to this conformation by overcoming an activation barrier, we conclude that the X-shape is the thermodynamically most favorable conformation (poses an energetic minimum). The other species are initially trapped in a metastable state at RT.

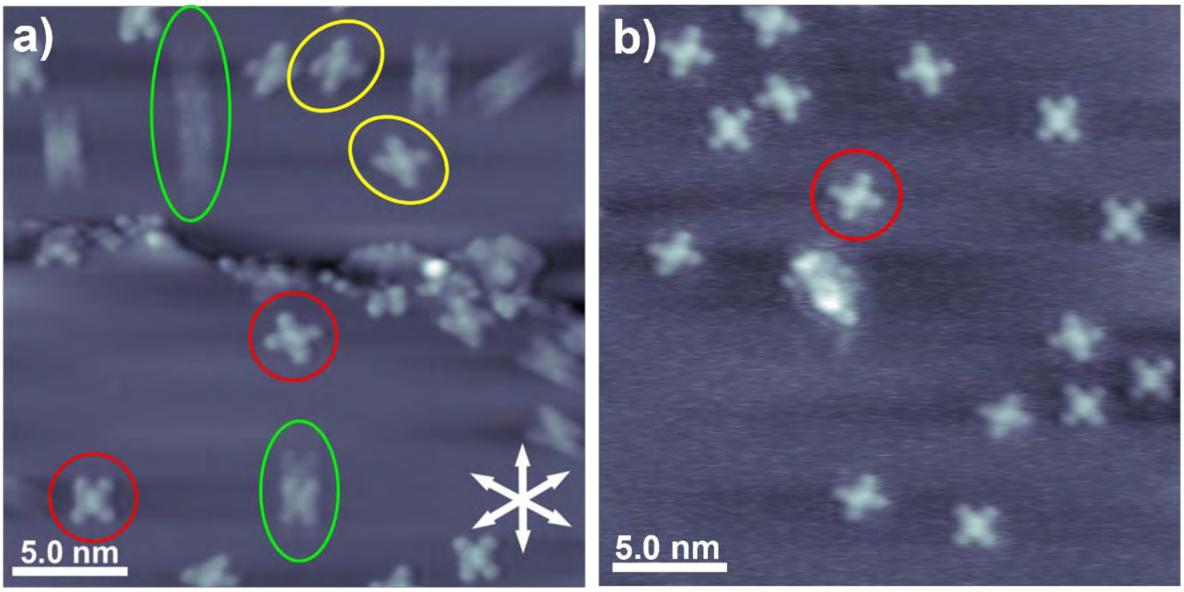

Figure 4.5: a) Average frames of STM movies of 2HTNP on Cu(111) at RT. b) Average frames of STM movies of 2HTNP on Cu(111) measured at RT after annealing to 400 K for 1h; all molecules are found to be immobile, as exemplarily indicated for one molecules (red circle). (a) U_{bias}= -1150 mV, I_{set} = 300 pA; (b) U_{bias}= -1100 mV, I_{set} = 300 pA. Modified image from [P2] with permission.

4.1.2 2HTNP and 2HTNBP on Ag(111)

For a deeper understanding of the adsorption behavior of naphthyl-functionalized porphyrins and their intermolecular interaction, we studied 2HTNP and 2HTNBP also on Ag(111) at RT. The chemical structure and space filling ball models of 2HTNP and 2HTBNP are displayed in their saddle-shape conformation in Figure 4.6 with the two upright standing pyrrole groups of 2HTNP and isoindole groups of 2HBNTP highlighted in yellow.

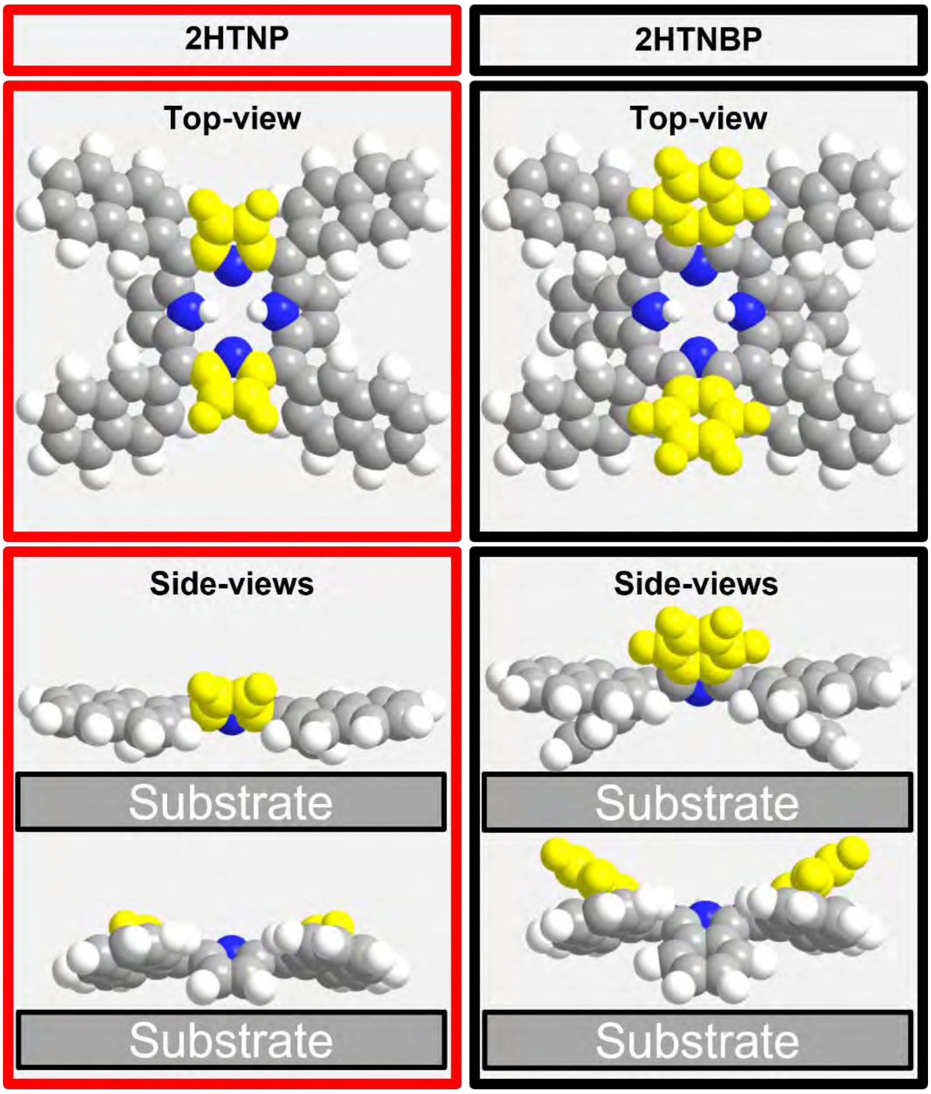

Figure 4.6: Top/side-views of a space-filling model of the saddle shape of 2H-Tetranaphthylbenzoporphyrin (left side) and 2H-Tetranaphthylporphyrin (right side). The yellow highlighted isoindole/pyrrole groups are pointing away from the surface. Modified image from [P4].

Figure 4.7 shows the adsorption behavior of 2HTNP at a coverage below a closed molecular layer. Perfectly long-range ordered regions and disordered regions of molecules coexist on the surface. The macrocycle is visible as a central depression, which is surrounded by four smaller protrusions which are assigned to the naphthyl groups. The molecules appear elongated in one direction, which would resemble a $\tau\tau\tau\tau$-orientation of the naphthyl groups. The long-range ordered structures are built up by parallel rows of neighboring porphyrins. The nearly rectangular unit cell is described by the vectors b_1 = 2.01 ± 0.04 nm, b_2 = 1.28 ± 0.04 nm and α = 84° ± 5°. The intermolecular distance along b_1 is larger than the length of one molecule and matches 7 Ag-Ag distances (2.02 nm). It is perfectly aligned along one of the high symmetry axes of the substrate. Since the b_2 vector is also a combination of substrate lattice vectors (see below), the molecules have a favorable adsorption site on the surface. This indicates a repulsive intermolecular interaction at a row distance below 7 Ag-Ag distances. Thus, a stronger repulsive interaction due to a denser packing of neighboring rows (e.g. 6 Ag-Ag distances along the surface vector a) cannot be overcompensated by the energy gained by more molecules at specific adsorption sites. The angle $\alpha = 85°$ reflects the closest packable surface site in b_2 direction, which would lead to the observed island pattern (along the direction of b_1). The proposed $\begin{pmatrix} 7 & 0 \\ -2 & 5 \end{pmatrix}$ structure is commensurable with the surface and the experimental unit cell parameters match with the calculated parameters for the commensurate superstructure (b_1 = 2.02 nm ($7a$), b_2 = 1.26 nm ($\sqrt{19}a$) and $\alpha = 83.4°$). Interestingly, island formation normally occurs mostly caused by intermolecular interactions without adsorption site specificity on the less reactive Ag(111) for other porphyrin molecules [36, 53, 55].

In Fig. 4.7e, the outer phenyl ring of the naphthyl groups sits on the same adsorption site as the center of the macrocycle. The apparent overlap of the naphthyl groups is not present in the actual structure. The naphthyl group is tilted against the surface, which cannot be seen from the top view perspective. Furthermore, our STM images cannot clarify whether the adsorption sites are top, bridge or hollow sites.

Annealing 2HTNP to 600 K, leads to a change of the island structure with the unit cell being no longer orientated along one of the high symmetry axes. The main molecular axis (line through iminic isoindole groups) is rotated by 16° ± 2°. Otherwise, the molecular appearance remains the same (see Fig. 4.7d). The length of unit cell vector c_1 stays comparable to seven close-packed Ag-Ag distances, even though it is not aligned anymore with one of the high symmetry axes of the surface. This results in a decrease of the angle between the unit cell vectors to 71°. The unit cell parameters are c_1= 2.02 ± 0.04 nm, c_2 = 1.22 ± 0.04 nm. Fig. 4.7f proves that the overlaid molecules in this structure do not have the same adsorption sites and that the structure is not commensurable with the substrate anymore. Considering the orientation of the molecular unit cell on the surface, only every third molecule could sit on the same adsorption site as the first. The potential driving force for this structural change can be the increased molecular density (0.39 molecules/nm^2 at RT to 0.43 molecules/nm^2 after annealing).

In this case, the energy gained by additional adsorbed molecules exceeds the energy of the molecule sitting on specific adsorption sites.

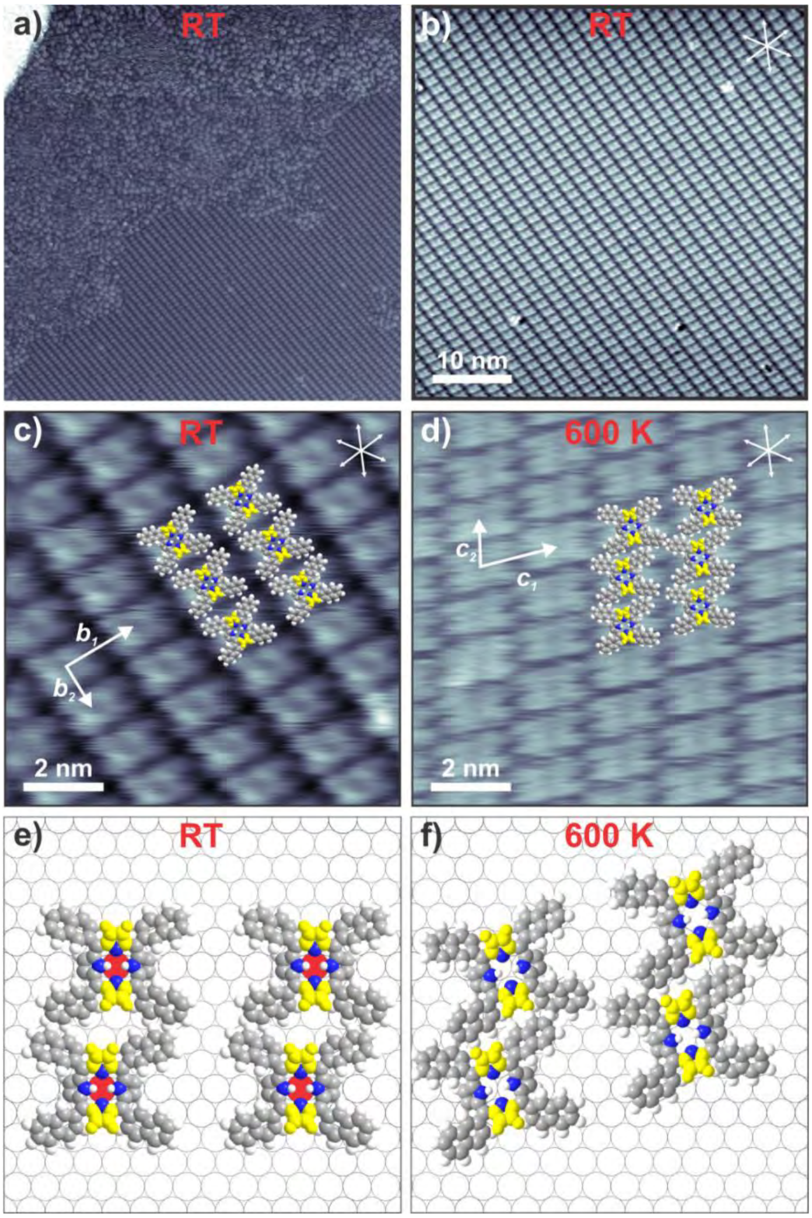

Figure 4.7: a, b) STM images of islands formed by 2HTNP on Ag(111) at RT. c) High resolution STM images overlaid with space-filling molecular models of 2HTNP and its unit cell vectors (white) at RT. d) High resolution STM images overlaid with space-filling molecular models of 2HTNP and its unit cell vectors (white) after heating to 600 K. e) Molecular models overlaid on an atomic Ag(111) surface to emphasise the adsorption sites at RT. The on top adsorption site was used for illustration. f) Molecular models overlaid on an atomic Ag(111) surface to emphasise the adsorption sites after heating to 600 K. The on top adsorption site was used for illustration. (a-c) U_{bias}= -100 mV, I_{set} = 300 pA; (d) U_{bias}= -1050 mV, I_{set} = 290 pA.. Original image from [P4] with permission.

We next move on to the adsorption of the larger 2HTNBP molecule on Ag(111). Figure 4.8a and b show close-packed, long-range ordered supramolecular structures, which are surrounded by a 2D gas phase of fast diffusing molecules (stripy features). In contrast to 2HTNP, the macrocycle and the naphthyl groups of 2HTNBP are not visible and the molecules are identified as two parallel elongated protrusions (yellow circles Figure 4.8d). These protrusions resemble the two upright standing isoindole groups of the macrocycle in the saddle-shape conformation. Figure 4.8d shows the superposition of molecules onto the STM images, and the square arrangement of the unit cell with $d_1 = 1.58 \pm 0.04$ nm, $d_2 = 1.54 \pm 0.04$ nm and $\alpha = 90° \pm 5°$. The d_1 and d_2 vectors of the unit cell coincide with one of the [110] and [211] axes of the Ag(111) surface. The molecules are aligned along the d_2 vector of the unit cell with the main molecular axis being the line separating the two upright standing isoindole units (yellow ellipses). Every second molecule along d_1 and every molecule along d_2 occupy the same adsorption site. Compared to the adsorption behavior on Cu(111), intermolecular interactions dominate due to the weaker and less site-specific molecular-substrate interactions (weaker porphyrin-Ag coordination). Figure 4.8d shows the well-known T-type interaction of aromatic systems for the neighboring naphthyl group points directly to each other [36, 91, 92].

Figure 4.8e and f summarize the results of the annealing of 2HTNBP molecules on Ag(111) to 500 K. The big blue oval highlights a domain wall, which consists of one row of molecules with a different azimuthal orientation compared to the orientation in the adjacent right and left domains. The molecules within the domain wall and larger domains share the same appearance as two parallel elongated protrusions like seen at RT in Figure 4.8d (red ovals: large domain, blue ovals: domain wall). The molecules within the domain wall still interact in a T-type fashion between neighboring naphthyl groups. Furthermore, the interaction at the domain boundary is T-type as well. Within the larger domains, the interaction pattern between neighboring naphthyl groups is π-π stacking (the apparent overlap of the molecular models in Figure 4.8f is only due to the of the top view perspective). The unit cell of the annealed structure is again nearly quadratic with parameters $e_1 = 1.50 \pm 0.04$ nm, $e_2 = 1.49 \pm 0.04$ nm and $\alpha = 88° \pm 5°$. The alignment with respect to the substrate does not change compared to the structure at RT (see above). Every third molecule along e_1 and every molecule along e_2 occupy the same adsorption site. The driving force is again the energy gain by an increase in molecular density from 0.41 molecules/nm^2 at RT to 0.45 molecules/nm^2 at 500 K.

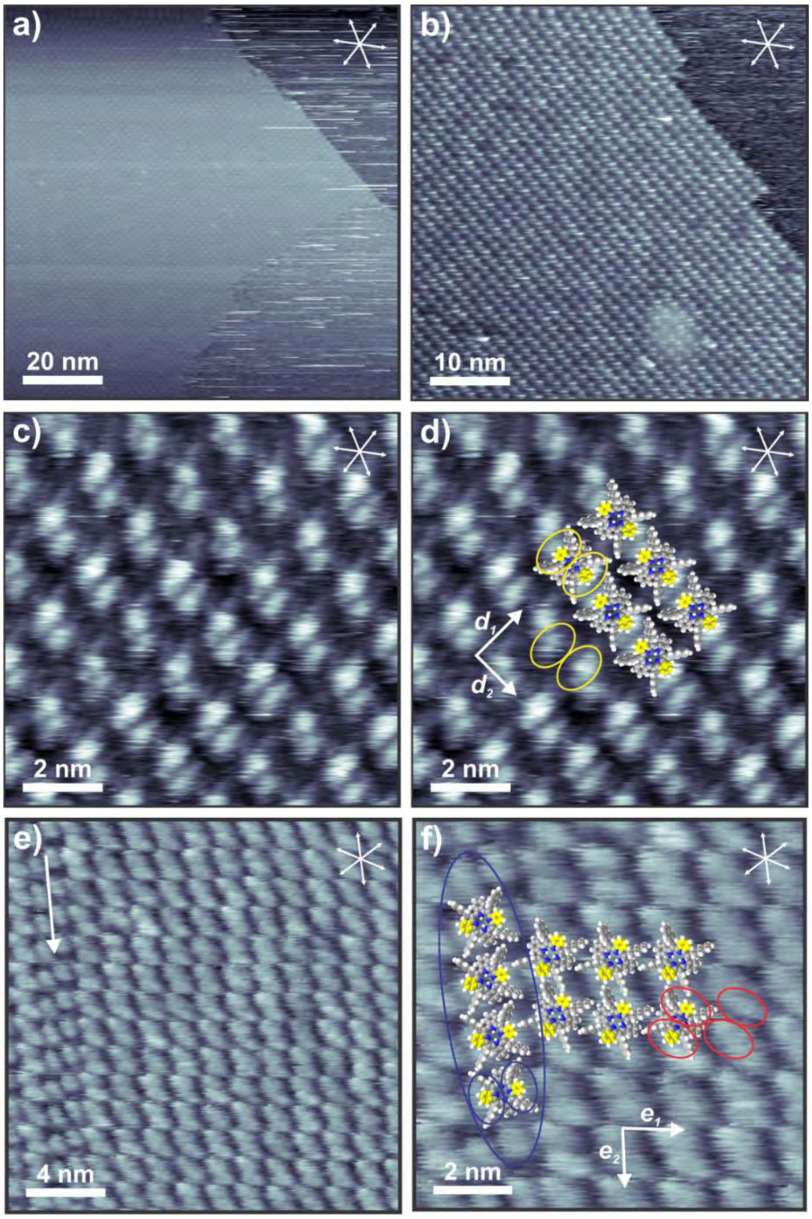

Figure 4.8: a, b and c) STM images of islands formed by 2HTNBP on Ag(111) at RT. d) High resolution STM image overlaid with space-filling molecular models of 2HTNBP and its unit cell vectors (white) e) High resolution STM image after annealing to 500 K. The island has a line defect (white arrow), in which the molecules are rotated against the molecules of the main island. b) Overlay of space filling molecules to show the different orientations in the line defect (blue oval indicate the upward bent isoindole groups) and the island (red ovals). For further details see text. (a) U_{bias}= -1000 mV, I_{set} = 200 pA; (b) U_{bias}= 1000 mV, I_{set} = 200 pA; (c and d) U_{bias}= -1910 mV, I_{set} = 290 pA; (e and f) U_{bias}= -2500 mV, I_{set} = 310 pA. Original image from [P4] with permission.

4.2 Coordination and metalation reaction with coadsorbed metal atoms [P1, P3]

After looking at the dependency of the conformation based on the functionalization of the macrocycle in the periphery, this chapter focusses on the coordination and metalation behavior of porphyrins with Co and Zn atoms based on the results of [P1] and [P3]. Metalation reactions are a powerful and flexible route towards an in-situ modification of the adsorption behavior of porphyrins. The choice of the metal center has a strong influence on the functionality of the porphyrin like seen in the nature examples chlorophyl and heme. The versatility of the porphyrin metalation is quite interesting, since nanostructures can be built by evaporating metalated porphyrins, metalation on the surface by pre- and post-deposited metal atoms, or even by reacting with the surface itself in form of self-metalation. As mentioned in the literature review in Chapter 3.3, a detailed understanding of the metalation reaction is still missing and the involved factors like substrate, metal center and side groups need further investigations. We concentrated on porphyrins with cyno-functionalized phenyl groups.

4.2.1 Codeposition of Co atoms and 2H*trans*DCNPP

To elucidate the interaction and reaction of Co with 2H*trans*DCNPPs, the island structure of the molecules and their individual appearance must be clarified first. At RT, 2H*trans*DCNPP on Ag(111) forms a close-packed and well-ordered supramolecular structure shown in Fig. 4.9. The lattice vectors of the unit cell are e_1 = 1.61 ± 0.04 nm and e_2 = 2.65 ± 0.03 nm, with an enclosed angle γ = 90 ± 3°, yielding a molecular density of 0.47 molecules per nm^2. Fig. 4.9c and d show a high resolution STM image of one molecule incorporated in the two-dimensional island with a scaled space filling model of 2H*trans*DCNPP. The molecular appearance of 2H*trans*DCNPP, as four protrusions in the periphery around a core with a depression in the center, is very similar to that of 2HTPP and 2HTCNPP [36, 62, 87]. On a closer look, the four protrusions show different lateral size, with two opposite larger (cyano-phenyl) and the two smaller protrusions (phenyl). The scaled molecular model overlayed the STM image in Figure 4.9d is in good agreement.

The interpretation of the appearance of individual 2H*trans*DCNPP molecules helps to analyze and describe the supramolecular structure. Fig. 4.9e and f show a high resolution STM image and superimposed scaled models of 2H*trans*DCNPP. All molecules within a row (I) are oriented along the same direction while neighboring rows (II) consists of 90° azimuthally rotated molecules. Consequently, the molecular orientation switches between alternating rows. Van der Waals interactions and intermolecular hydrogen bonding between nitrogen atoms of the cyano groups and hydrogen atoms of pyrrole groups of adjacent molecules in the neighboring rows stabilizes this supramolecular order [55, 61]. Closer inspection reveals that the cyano groups "avoid" direct interaction with each other, due to electrostatic repulsion.

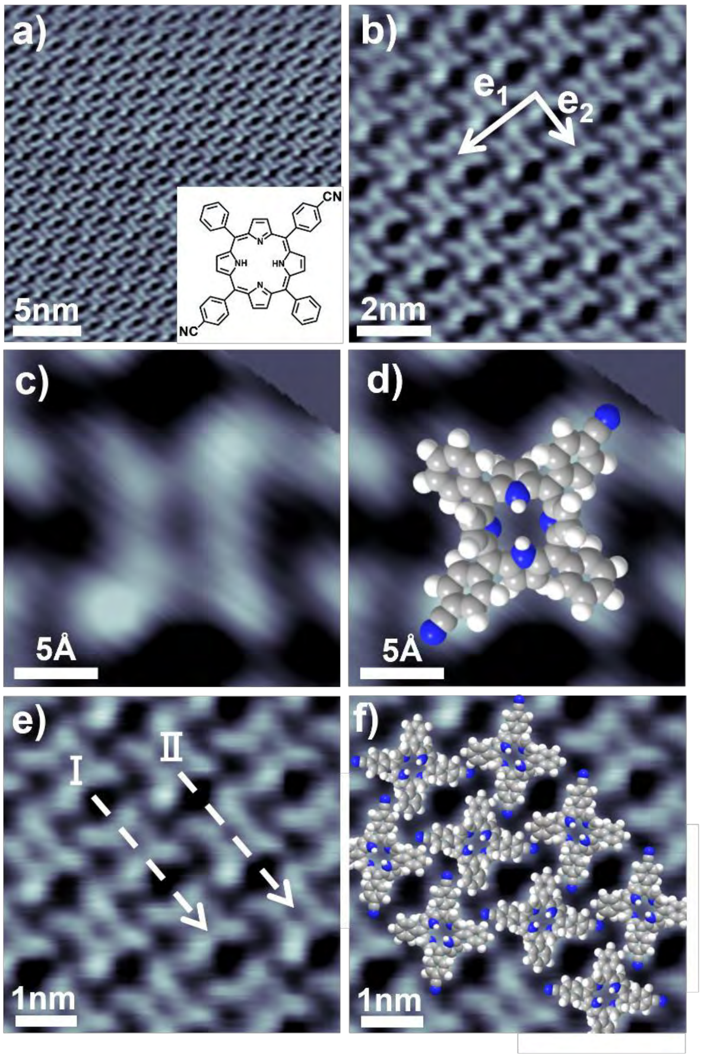

Figure 4.9: a) and b) Constant current STM images of the self-assembled 2H*trans*DCNPP on Ag(111). A unit cell is overlaid in b). c) Close-up STM image of one 2H*trans*DCNPP molecule. d) Same image overlaid with the corresponding space filling model. e) Magnified detail of the center part of a), and in f) the same image overlaid with the corresponding scaled molecular models. (a-f) U_{bias} = -100 mV, I_{set} = 270 pA. Modified image from [P1] with permission from the Royal Society of Chemistry.

To study the metalation reaction of 2H*trans*DCNPP, Co was deposited onto a porphyrin covered Ag(111) surface. The amount of cobalt is roughly the amount required to stoichiometrically metalate 33 % of the porphyrins on the surface. Figure 4.10a shows a fraction of the molecules appearing as protrusions in the STM images, while the others remain unchanged after the Co deposition. The protrusion resembles the enhanced tunneling contribution through the Co(II) $3d_z$ orbitals of metalated porphyrins. The fraction of Co*trans*DCNPP (31%) is in good agreement with the amount of deposited Co. The STM images of Fig. 4.10b and c were acquired after the successive deposition of equal amounts of Co (first evaporation) onto the molecular structure, yielding 66% and 99% of deposited Co, respectively to metalate porphyrins. The number of protrusions resembling Co*trans*DCNPP molecules, increases roughly proportionally to the amount of deposited Co. The fraction of metalated molecules in Figure 4.10 are (a) 31%, (b) 73% and (c) 97%. These values are in good agreement with the values expected for a stoichiometric reaction, which would be (a) 41%, (b) 82% and (c) 120%, considering the effective starting coverage of 85 % for 2H*trans*DCNPP. Assuming a margin of error for the amount of deposited Co (25 %), it becomes immediately evident that the efficiency of the metalation reaction is close to 100%. Notably, the supramolecular structure maintains intact during the metalation process, despite the known affinity of cyano groups to Co atoms favoring the formation of metal–organic networks at RT with related linkers [93-95]. Since, the evaporation of Co atoms on the surface is a statistical process, it can be ruled out that all Co atoms directly adsorb at the center of a 2H*trans*DCNPP molecule. Therefore, a percentage of Co atoms must diffuse to the non-metalated molecules before they can coordinate to the macrocycle [56]. Similar results were also reported for other metal-porphyrin systems [49, 60, 62, 93, 94, 96-99].

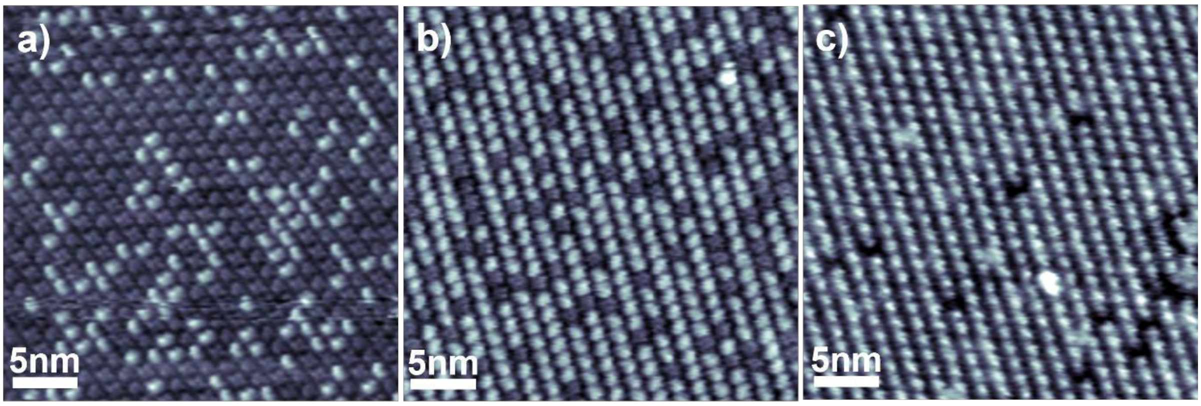

Figure 4.10: Constant current STM images of a monolayer of 2H*trans*DCNPP molecules after the incremental deposition of Co (stoichiometrically amount needed to metalate 33% of the porphyrins in each step). (a-c) U_{bias} = -1000 mV, I_{set} = 290 pA. Original image from [P1] with permission from the Royal Society of Chemistry.

The next logical step was the investigation of the metalation reaction by changing the sequence of the deposited materials. Fig. 4.11a and b show the STM images of a Ag(111) surface before and after the deposition of Co at RT. The Co atoms agglomerate and form three-dimensional islands which decorate the step edges of the Ag(111) surface. The deposition of roughly a closed monolayer of 2H*trans*DCNPP onto the Co precovered Ag(111) at RT yielded a homogeneous adlayer of 2H*trans*DCNPP. A coexistence of Co cluster at the steps and the same supramolecular structure of 2H*trans*DCNPP, like seen on the clean Ag(111), was observed (see Fig. 4.11c). The simultaneous presence of Co clusters and free-base porphyrins in the undisturbed island structure indicates that the metalation reaction at RT is very slow at the given conditions. Annealing to 500 K led to the partial formation of Co*trans*DCNPP (Figure 4.11d). Again, the bright protrusions are assigned to Co*trans*DCNPP (43%) and the dim species to 2H*trans*DCNPP (57%). The required activation barrier for the metalation reaction indicates that the Co atoms are relatively strongly bound within the Co clusters. The heating is required to dissolve the Co clusters and allow for the diffusion of individual Co atoms to metalate a 2H*trans*DCNPP molecule. This means that, metalation with pre-deposited Co atoms is kinetically hindered, and overcoming of the activation barrier *via* heating is necessary [56, 62, 65]. At higher annealing temperatures, the supramolecular order breaks up, and the uniform shape of the molecules is no longer observable (not shown). This is most likely due to the decomposition of the molecules.

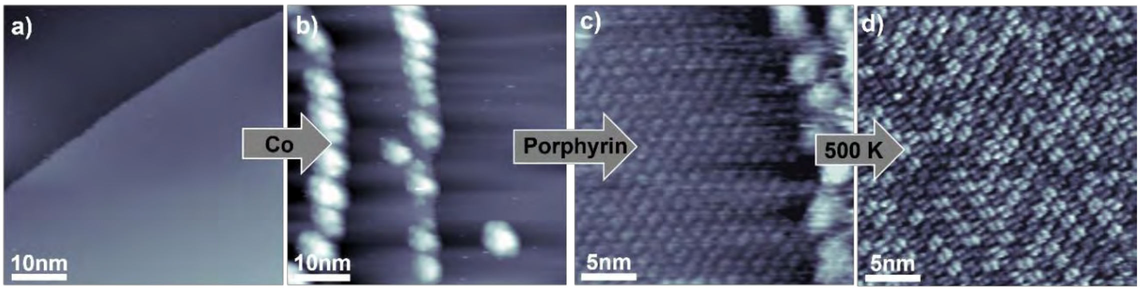

Figure 4.11: a) STM image of clean Ag(111) surface. b) STM image showing the nucleation of Co on step edges of Ag(111). c) 2H*trans*DCNPP monolayer evaporated on the surface depicted in b). d) STM image of c) after annealing to 500 K. The bright spots in the image are assigned to Co*trans*DCNPP. (a) U_{bias} = -1000 mV, I_{set} = 290 pA; (b) U_{bias} = -1300 mV, I_{set} = 300 pA; (c and d) U_{bias} = 1000 mV, I_{set} = 300 pA. Modified image from [P1] with permission from the Royal Society of Chemistry.

Additional deposition of more than double the amount of Co needed to fully metalated a layer of 2H*trans*DCNPP breaks up the supramolecular structure into a variety of disordered intermolecular arrangements (Fig. 4.12a). This effect is even more pronounced after annealing to 400 K, when most molecules have agglomerated in disordered clusters or cannot be imaged any more (Fig. 4.12b). Literature proves that deposited Co atoms and cyano-functionalized polyphenyl molecules form ordered metal–organic networks by coordination of a Co atom by three cyano groups with an angle of 120° between each other [95, 100]. The coordination motif of the molecules depends on the ratio between Co and cyano functions. Various pore shapes based on 4-, 5- and 6-fold coordination of Co atoms were observed, for different amounts of deposited Co atoms [95]. Urgel *et al.* reported that cyano-functionalized porphyrins form 3-fold prevailed metal–organic coordination motifs with codeposited Co atoms on a Ag(111), which are very similar to our system (2H*trans*DCNPP) [93]. Upon Co deposition, first the metalation reaction of the free-base 2*Htrans*DCNPP at RT takes place. With further increase of Co above the amount needed for complete metalation, coordination structures of Co-coordinated CotransDCNPP start to form. However, the supramolecular arrangement needs to break up to form these coordination structures. The coordination is promoted by annealing to 400 K, which indicates that an additional energy barrier for the rearrangement of molecules must be overcome. Fig. 4.12c and d display the STM images of two representative motifs and an overview of all observed motifs (see Fig. 4.12e). The appearance of all motifs is the same with two to six protrusions surrounding one central protrusion (marked in red in Fig. 4.12e), with the 4-fold coordination being the dominating form. A statistical analysis of ~800 molecules was performed and shows the distribution of coordination numbers. The 4-fold coordination bond seems to be the energetically favored option, but the energy difference between the motifs is not sufficient to significantly favor one binding motif over the others. For all coordination motifs the average distance of an "outer" protrusion to the central protrusion is 1.0 ± 0.1 nm, which is too small to account for all protrusions to a Co*trans*DCNPP molecules. This is evident, considering the lattice parameter e_1 = 1.61 ± 0.04 nm estimated for the molecular order discussed in detail above. As discussed above, the outer protrusions could be assigned to Co*trans*DCNPP molecules, because at negative bias voltages a strong contribution of an orbital-mediated tunneling process *via* the hybrid Co(d_{z^2})–Ag orbital of the adsorption complex, induced by molecule–substrate interactions would explain the bright round appearance in the STM images [56, 101]. Since the central protrusion is ruled out to be a porphyrin due to the short protrusion–protrusion distances, we propose that the central protrusions are Co atoms coordinated by the cyano groups of surrounding Co*trans*DCNPP molecules. The identical appearance can be attributed to the similar chemical environment of a Co atom coordinated by two to six cyano groups and a Co atom coordinated by the porphyrin macrocycle. The STM images give no further insight whether a single Co atom or Co-clusters are present in the central protrusion.

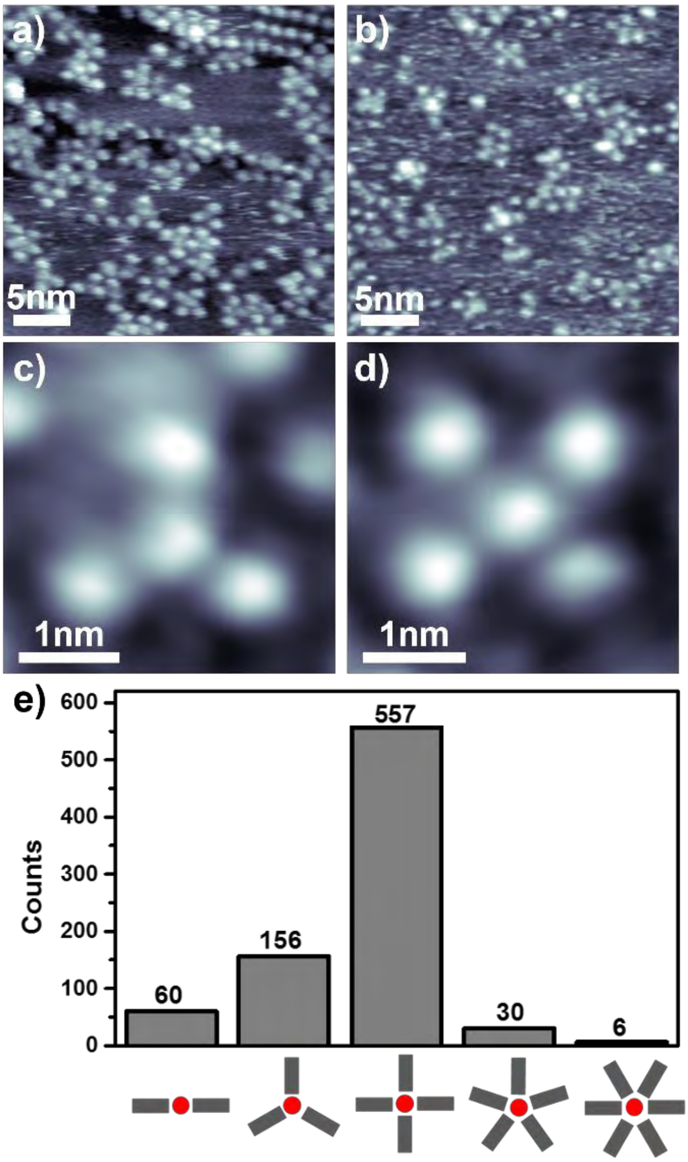

Figure 4.12: a) STM image of amorphous metal-organic structure of Co*trans*DCNPP and Co formed at RT. b) STM image of the amorphous coordination structure observed after annealing the sample to 400K. c) and d) STM images of two representative coordination motifs observed in experimental results. e) Distribution of the number of Co*trans*DCNPP molecules coordinating to a Co atom. (a-d) U_{bias} = -1000 mV, I_{set} = 290 pA. Original image from [P1] with permission from the Royal Society of Chemistry.

To verify our interpretation STM images at the same position with both negative and positive bias voltages were acquired. At positive bias voltage the corresponding STM images of Co-porphyrins should rather reflect the topography of the molecules than the pronounced electronic effect at negative bias. Fig. 4.13 shows the experiments of the bias switching with the left column being the negative bias STM image, the middle column positive bias and the right column has the corresponding image overlayed with scaled molecular models.

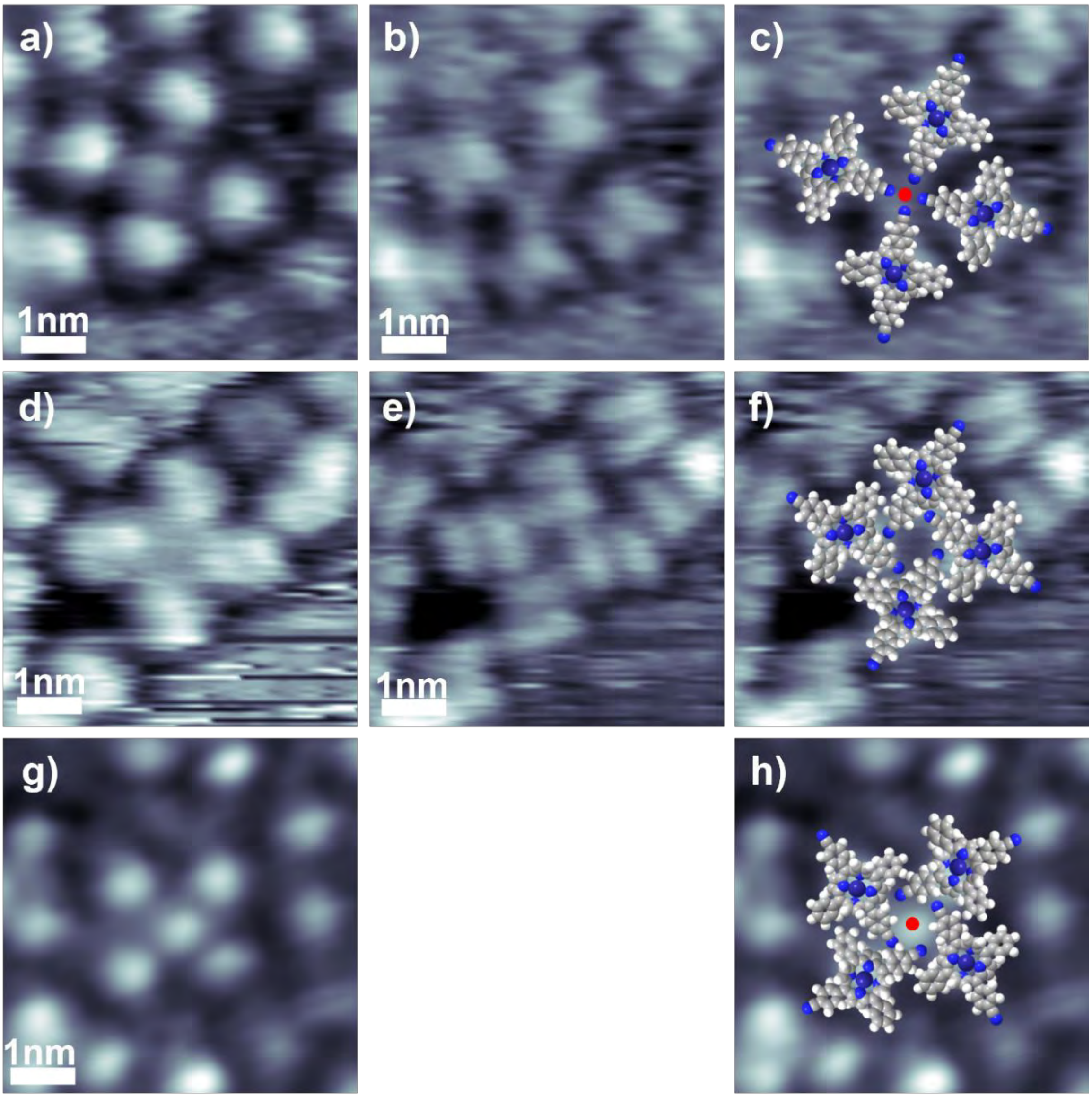

Figure 4.13: Bias dependent STM measurements. The first column (a, d and g) presents images with negative bias. The second column (b and e) depicts the images measured at the same position with positive bias. In the middle column (c, f and h) the images presented with overlayed scaled models. (a and d) U_{bias} = -1000 mV, I_{set} = 290 pA; (b and c) U_{bias} = 1000 mV, I_{set} = 290 pA; (e) U_{bias} = 1700 mV, I_{set} = 290 pA; (g and h) U_{bias} = -100 mV, I_{set} = 300 pA;. Modified image from [P1] with permission from the Royal Society of Chemistry.

The 4-fold motif is the most frequently observed structure. The STM images clearly allow for the identification of the four outer protrusions as Co*trans*DCNPP molecules, while at the central position only a small protrusion is observable in the positive bias STM image, which is assigned to Co. The superimposed scaled molecular models and the Co center indicated as red dot are shown in Fig. 4.13c, f and h. The 4-fold protrusion motif shown in Fig. 4a-c has an enlarged distance of with 1.2 ± 0.1 nm compared to the average value of 1 ± 0.1 nm. The typical distance is depicted by the STM images shown in Fig. 4.13d-f. In this case the central spot is missing at negative bias as depicted in Fig. 4.13a, which is due to a temporary tip modification. However, in the latter case it was not possible to image at positive bias. The “windmill” arrangement is the dominating motif since it also perfectly resembles the average distance of the central Co atom to the surrounding Co*trans*DCNPP molecules. The oxidation state of Co in Co*trans*DCNPP (2+) and in coordination nodes might differ [60, 61, 94]. A 0-oxidation state of central Co center might explain its invisibility in Fig. 4.13d. Under the used preparation parameters, no extended 2D networks formation was observed, which could be due to symmetry and lattice mismatch between the coordination structure and the hexagonal substrate [93].

4.2.2 Codeposition of Zn and 2HTCNPP

In order to study the interaction and metalation of 2HTCNPP with post-deposited Zn on Ag(111), we first separately studied the adsorption of 2HTCNPP and the potential reaction product ZnTCNPP at RT. The individual molecules are clearly resolved with sub-molecular resolution, as is evident from Figure 4.14 (left panel). The molecules adsorb in the so-called “saddle shape” conformation, with a slight depression in the center of the molecule being the macrocycle, and the four cyanophenyl groups identified as protrusions at the periphery of the molecule. The appearance ZnTCNPP is slightly different (right panel). It is dominated by four bright protrusions due to the cyanophenyl groups at the periphery of the molecule, with the macrocycle being less bright and no obvious depression in its center. The central Zn atom is not visible, since the 4s and 3d orbitals are completely occupied. Both molecules assemble into long-range-ordered 2D supramolecular structure with a square unit cell with similar lattice vectors in the range of g_1 = 1.49 ± 0.04 nm and g_2 = 1.45 ± 0.04 nm, with an enclosed angle of α = 87° ± 5°. After post-deposition of Zn atoms onto the 2HTCNPP islands, the formation of three different new island types, A, B and C in coexistence was observed (see Figure 4.17). Notably, in all three islands the molecular appearance of some molecules changes towards a bright double protrusion (sometimes single broad protrusion), which differs both from 2HTCNPP and ZnTCNPP. The number of bright species correlates with the amount of deposited Zn, but the before mentioned observation rules out a metalation reaction at this stage.

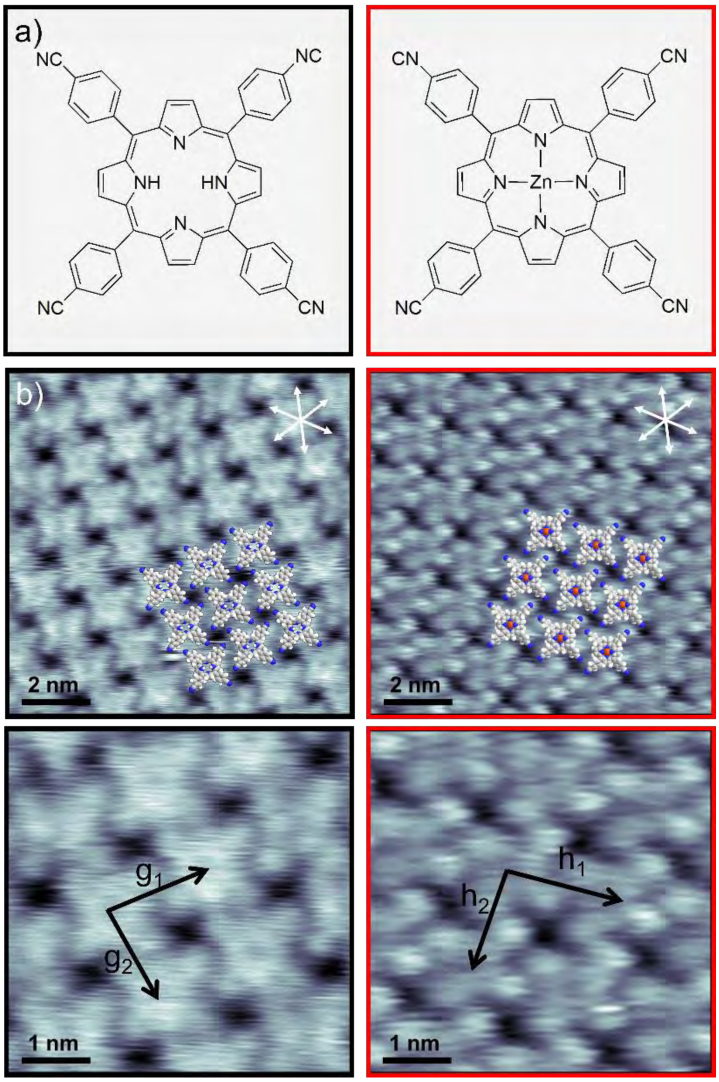

Figure 4.14: a) Chemical structure of 2HTCNPP (black) and ZnTCNPP (red). b) Constant-current STM images of an island of 2HTCNPP (black) and ZnTCNPP (red) on Ag(111) at RT and higher resolution of the respective unit cells. Overlaid molecules indicate the structure of the ordered 2HTCNPP and ZnTCNPP layers; the central Zn atom in ZnTCNPP is depicted in red. (b) 2HTCNPP: U_{bias} = -850 mV, I_{set} = 190 pA; ZnTCNPP: U_{bias} = -190 mV, I_{set} = 300 pA. Modified image from [P3] with permission.

In DFT calculations, Shubina et al. proposed the formation of a so called “SAT” (sitting atop) complex for 2HTPP plus Zn, in which the Zn atom coordinates the macrocycle without the release of hydrogen [64]. This 2H-SAT complex is the first intermediate in the metalation reaction of 2HTPP to ZnTPP. For the final metalation to ZnTPP an activation barrier of 32.6 kcal mol^{-1} must be overcome [64]. Based on this report, we assign the bright protrusions seen in the three new structures in Figure 4.17 to metastable SAT complexes formed by Zn and the macrocycle, prior to the metalation reaction to ZnTCNPP and the release of hydrogen. The different island patterns will be discussed in a later stage.

A heat treatment of the 2HTCNPP + Zn layer was performed to check whether the metastable SAT complexes can be metalated like 2HTPP plus Zn [64, 65]. All bright protrusions, which were observed for all three coexisting island types after Zn deposition at RT, transform into the same quadratic structure (with some disordered regions). In Figure 4.15, high resolution STM images of ZnTCNPP (a) and of 2HTCNPP + Zn after annealing to 500 K (b) are compared. The molecular appearances in both images are identical and the unit cell of the 500 K-annealed 2HTCNPP + Zn layer ($h_1 = 1.54 \pm 0.04$ nm, $h_2 = 1.46 \pm 0.04$ nm, $\alpha = 85° \pm 5°$) matches that of ZnTCNPP ($h_1 = 1.51 \pm 0.04$ nm, $h_2 = 1.49 \pm 0.04$ nm, $\alpha = 85° \pm 5°$), within the margin of error. This similarity shows that the metalation is hindered by an activation barrier and confirms the presence of a metastable intermediate SAT complex.

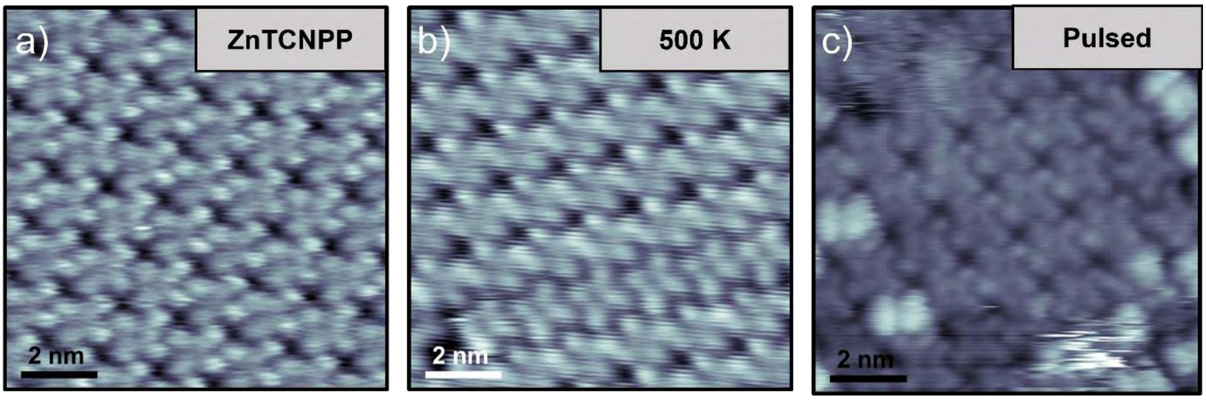

Figure 4.15: a) High resolution STM image of ZnTCNPP. b) High resolution STM image of 2HTCNPP + Zn + 500 K. c) High resolution STM image of 2HTCNPP + Zn + pulse(+2.73 V). (a) $U_{bias} = -190$ mV, $I_{set} = 300$ pA; (b) $U_{bias} = -1000$ mV, $I_{set} = 220$ pA; (c) $U_{bias} = -1660$ mV, $I_{set} = 300$ pA. Original image from [P3] with permission.

Additionally, temperature is not the only possibility to overcome the energy barrier to induce a conformational change or metalation reaction. The SAT complex species can also be affected by tip pulsing. Applying a positive voltage pulse between 1.5 to 4 V (referred to the sample), the molecular appearance of a small area within the island changes, while the molecules further away from the pulse center remain unchanged. This can be attributed to a voltage-induced change of the molecules and not to a contrast-change (due to a tip change).

Over the course of a “STM movies” (10 Frames, 0.1 fps) the stepwise change induced by a 2.73 V pulse can be monitored (see Figure 4.16). The pulse was applied in the middle of Frame

3 and the change of the structure was observed afterwards. Remarkably, the structural change did not occur instantaneously, but over time by switching 4 to 7 molecules in between frames. For the intermediate SAT complex, two possible voltage-induced reactions pathways are possible. Firstly, the back reaction to 2HTCNPP under the release of the Zn atom, and the second is the formation of ZnTCNPP under the release of hydrogen. The newly formed species arrange into a regular pattern of ~20 molecules (e.g., 4 times 5) with a quadratic lattice (h_1 = 1.54 ± 0.04 nm, h_2 = 1.46 ± 0.04 nm, α = 86°± 5°), like that of ZnTCNPP or 2HTPP. The visibility of the four cyanophenyl groups and the vanishing bright protrusion of the SAT complex allows for the assignment of the molecules as ZnTCNPP. We thus conclude that the SAT complex reacts towards ZnTCNPP. Another strong evidence for the formation of ZnTCNPP is that other reaction pathways like bias-induced transfer of the coordinated metal atom to the tip, which are observed for lead-phthalocyanine molecules, could be ruled out [102]. A subsequent demetallation of neighboring molecules in the timescale of seconds is highly unlikely. The switching behavior occurs in all three island types.

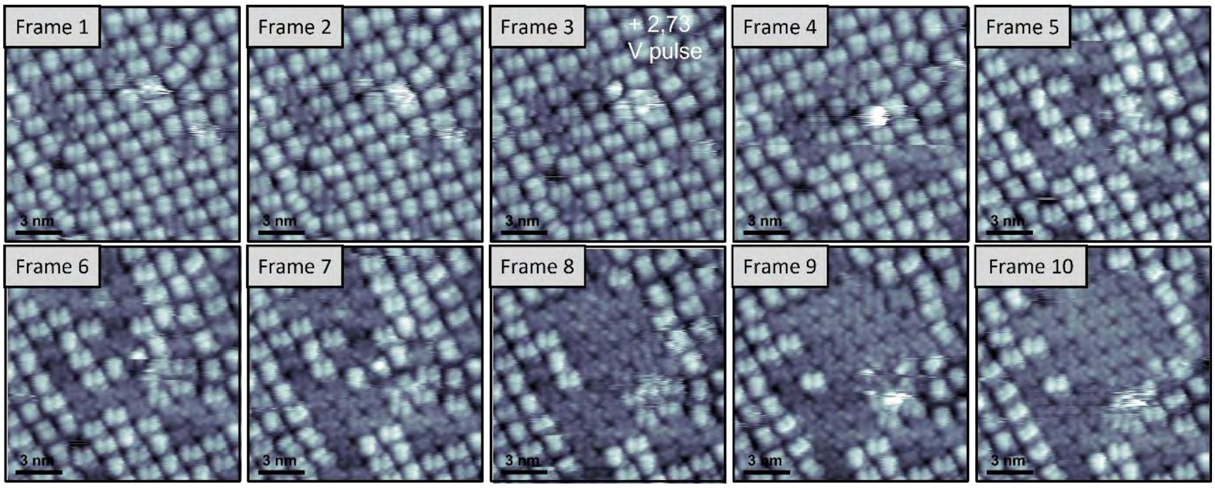

Figure 4.16: Consecutive STM frames of an 2HTCNPP island (structure A) covered with Zn. During Frame 3, a 2.73 V tip pulse was executed, which leads to a change in molecular conformation and supramolecular ordering (compare Frames 9 and 10). U_{bias} = -1660 mV, I_{set} = 300 pA. Original image from [P3] with permission.

A possible explanation for the switching occurring not only at the time of the pulse but continuing on the time scale of seconds afterwards is the released hydrogen in the course of the reaction of the SAT complex to ZnTCNPP. It adsorbs on the surface and modifies the local electronic properties such that the activation barrier for the metalation reaction of neighboring SAT complexes is lowered.

The selectivity of the switching with only positive voltage pulse can be explained by the population on a specific molecular state in the LUMO, which induces deprotonation and therefore metalation. Wang et al. have studied the reversible metalation/demetalation of the Sn atom in Sn-phthalocyanine [103]. The injection of electrons in the LUMO+1 gives rise to a negatively charged and thus transiently reduced molecule. Upon leaving the molecule, the electron may transfer energy to vibrational excitations and thus initiate the molecular switching. However, for ZnTCNPP molecules with a stronger coupling to the metal surface rapid transfer of the attached electron may suppress switching and thus no reversible switching could be observed.

Figure 4.17 gives an overview of the different island types seen for 2HTCNPP +Zn. The first and dominant island type A is a square ordered 2D structure ($i_1 = 1.52 \pm 0.04$ nm, $i_2 = 1.48 \pm 0.04$ nm, $\alpha = 85° \pm 5°$). Both the SAT complexes and the remaining 2HTCNPP molecules are rotated against the lattice vectors, but are aligned along the high symmetry axes of the Ag(111) substrate. The similar packing of island-type A compared to 2HTCNPP at RT results from the adsorption of Zn onto 2HTCNPP in the square islands without a rearrangement of the porphyrin molecules.

The second island type B is a slightly disordered densely packed hexagonal structure. The overall interaction theme within the structure is that three CN-groups of neighboring molecules point towards each other. The double protrusions are predominantly orientated parallel to Ag(111) high symmetry directions.

The third island type C is a regular porous 2D structure built by pores, which are surrounded by eight molecules. An alternative description of this structure is as an arrangement of two alternating types of rows: the first being a fully occupied row and in the second only every second site occupied. The structure has several defects by occasional filling of the pores by a molecule and a break of the alternating row symmetry. With better resolution, circular bright features are observed within the pores, which could be attributed to fast diffusing Zn metal atoms. The molecules are oriented again along the high symmetry direction of the substrate but now also along the rows. The overall lattice is again close to quadratic ($j_1 = 1.66 \pm 0.08$ nm, $j_2 = 1.50 \pm 0.07$ nm, $\alpha = 88° \pm 5°$).

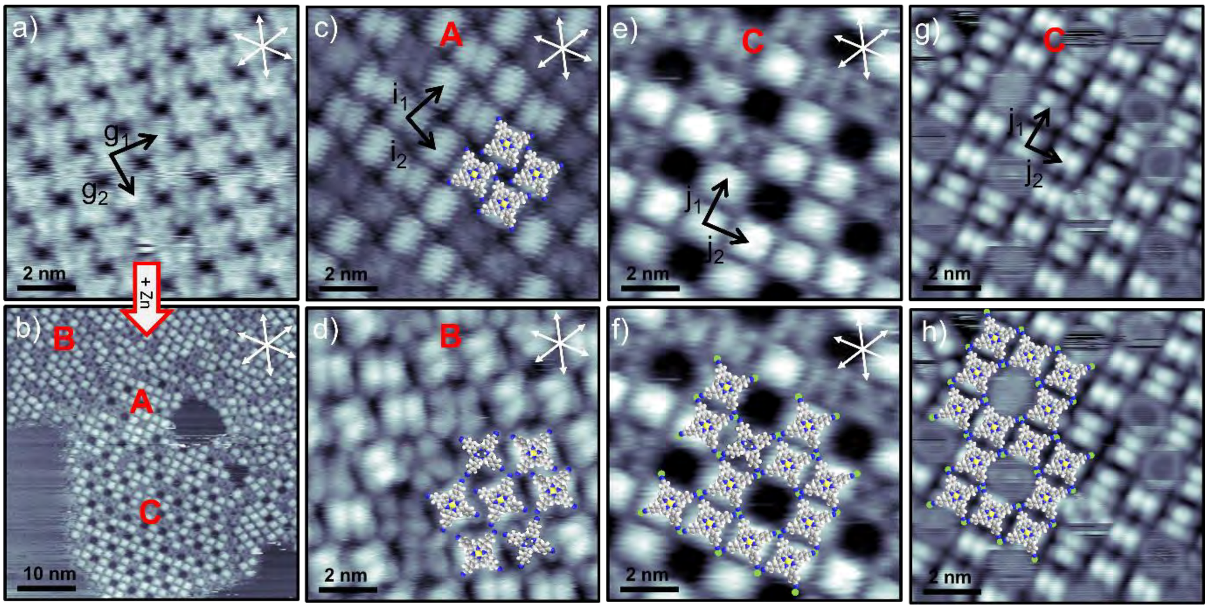

Figure 4.17: a) High resolution STM image of 2HTCNPP. b) The addition of Zn forms the three structures seen in the lower left overview. c) High resolution STM image of structure A. d) High resolution STM image of structure B, where each molecule has an average of six neighbors. e and f) High resolution STM images of structure C with regular missing molecules within the structure. g and h) High resolution STM images of structure C (different contrast; measured in Campinas/Brazil) with circular features within the holes of the structure. Overlaid molecular models indicate the structure of the different layers. The central Zn adatom in the SAT complex is depicted in yellow, and the coordinating Ag adatoms in green. (a) U_{bias} = -850 mV, I_{set} = 190 pA; (b) U_{bias} = -1660 mV, I_{set} = 300 pA; (c) U_{bias} = -810 mV, I_{set} = 340 pA; (d) U_{bias} = -1660 mV, I_{set} = 300 pA; (e and f) U_{bias} = -1660 mV, I_{set} = 300 pA; (g and h) U_{bias} = -1488 mV, I_{set} = 130 pA. Modified image from [P3] with permission.

Since three cyano groups of neighboring molecules are pointing towards each other, we propose a cyano-metal-cyano coordination as the binding motif. For Zn, a +3-oxidation state is highly unlikely, due to its electronic structure, which would refer to the only alternative of Ag adatoms, which are present on the surface. Very similar porous Au-coordination structures formed by cyano-functionalized triarylamines were observed on a Au(111) surface [85]. These molecules have a threefold symmetry which results in a hexagonal structure, while in our case the fourfold symmetry of the porphyrin core yields a square structure.

Nevertheless, the absence of this type of coordination prior to Zn evaporation onto 2HTCNPP and the structure of ZnTCNPP itself, indicates that Zn is involved in the formation of island type C. An explanation is a geometric/electronic shift in the structure of the SAT complex compared to 2HTCNPP and ZnTCNPP, such that the formation of the coordination network becomes energetically favorable. It appears that island types A and B represent two intermediate steps towards type C upon deposition of Zn onto 2HTCNPP. Firstly, Zn interacts with 2HTCNPP to form the SAT complex without changing the long-range order. In a next step the molecule tends to arrange into the porous type C. As driving force, we propose the formation of the Ag-coordinated network, with three molecules coordinated to one Ag adatom. Type B has a disordered intermediate structure during this reorganization, in which three neighboring molecules are already coordinated, but the differently oriented quadratic lattice is not yet formed. The coexistence of structures A, B and C indicates that the energetic differences are small. Otherwise, exclusively type C islands would be expected.

The post-deposition of Zn onto ZnTCNPP gives rise to an outstandingly long-range order, even across substrate step edges. The islands consist of parallel rows of molecules with identical orientation and form a square lattice (see Figure 4.18a). The superstructure shows periodic “line defects”, consisting of single rows of molecules with different azimuthal orientation (see Figure 4.18a and b. The space between the defect rows can vary from 3 to 8 regular rows in between, without periodicity. On other spots, the long-range islands are broken by line defects every fixed number of molecules (e.g., 3 regular rows in between – see Figure 4.18c). The overall island orientation remains the same after the row of different orientation, but a shift by half a molecule (“antiphase shift”) is observed. This phenomenon is also present for 2HTCNPP and 2HTCNPP + Zn (for images refer to [P3]), but is particularly pronounced for ZnTCNPP. The start of the line defect could be linked to kinks of the Ag(111) step edges and allow for the structure to extend over step edges like a carpet. For the defect rows, this requires a kink at each step edge, which means that the kinks have the same regularity as the defect rows. This means the porphyrin layer can modify the morphology of the step edges such that the kinks are aligned along the molecular defect rows. Furthermore, molecules in the defect rows are aligned along one of the high symmetry axes of the Ag(111) substrate. Since, the molecular order is most pronounced after Zn deposition on ZnTCNPP this indicates that the deposited Zn preferentially adsorbs at the step edges. Zn is very mobile and thus can be arranged such that the molecular order of regular rows and defect rows is maintained over the step edges. Looking at the intermolecular interaction, the rotation of the molecules in the line defect row breaks the dipole-dipole interactions of the cyano groups between neighboring molecules (see Figure 4.18d). This lost interaction is compensated by forming a N-H bond between a CN-function and a H atom of the neighboring pyrrole group of the macrocycle. This shows how much the molecules prefer adsorption sites at the step edges and that the islands start to grow from there.

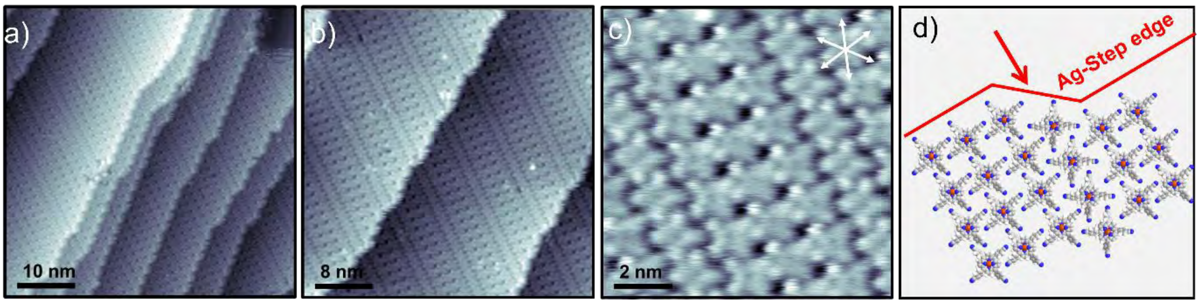

Figure 4.18: a-c) High resolution STM images of ZnTCNPP + Zn. d) Schematic drawing of the correlation between step edge shape and orientation of the rows (red arrow indicates differently orientated row. (a) U_{bias} = -1000 mV, I_{set} = 300 pA; (b) U_{bias} = -441 mV, I_{set} = 300 pA; (c) U_{bias} = -455 mV, I_{set} = 300 pA. Modified image from [P3] with permission.

5 Conclusion

The thesis at hand addresses the adsorption behavior of different tetraphenylporphyrin derivatives (naphthyl and cyano functionalization) on single crystal surfaces at and around RT by scanning tunneling microscopy. It presents a detailed investigation and discussion of intramolecular conformation, diffusion behavior, role of intermolecular interactions in the formation of supramolecular structures, and the interaction and reaction with coadsorbed metal atoms, which sets the stage for the fabrication of functional nanostructures from porphyrins.

The publications [P2 and P4] address the adsorption behavior of the naphthyl-functionalized porphyrins 2HTNP and 2HTNBP. We observe a very peculiar adsorption behavior of 2HTNP molecules on Cu(111): Individual molecules are found to adsorb in the "inverted" conformation with upright standing pyrrole rings at RT, which are orientated along the main crystallographic directions of the substrate. Due to the asymmetry of the naphthyl groups, 16 different surface conformers are possible, 10 of which have a different appearance and could indeed be identified by STM. Interestingly, 2HTNBP molecules adsorb as individual molecules as well. On Cu(111), no island formation of 2HTNBP occurs, which indicates a strong interaction of this porphyrin with the substrate, similar to 2HTPP and 2HTNP. The possible driving forces could be a coordination of the iminic nitrogen atoms of the isoindole groups to Cu substrate atoms, like for 2HTPP and 2HTNP, and the larger footprint of the molecules. The investigation of the diffusion behavior of both molecules shows different mobilities, which can be classified into three categories, that is, low, medium, and high. While for 2HTNBP no information of the naphthyl orientation could be linked to the different mobilities, the mobility of 2HTNP is related to the naphthyl orientation relative to the main axis of the molecule along the iminic nitrogen atoms. Fast diffusing species have 3 or 4 naphthyl groups in τ-orientation (pointing in the direction of the movement, which is aligned with the crystallographic axis). Immobile species have only 0 or 1 naphthyl groups orientated in this direction, which equals 4 or 3 groups in α-orientation (away from the main molecular axis and diffusion direction). This behavior shows that the introduction of asymmetric functional groups in the periphery linked to the macrocycle via single C−C bonds can have a strong influence on the adsorption behavior by yielding a variety of non-chiral and chiral conformers, which behave differently in their diffusion.

To expand our understanding of the influence of the asymmetric naphthyl group on the adsorption behavior of 2HTNP and 2HTNBP, we studied the adsorption behavior on Ag(111) as well. For 2HTNP on Ag(111), we observed a commensurable $\begin{pmatrix} 7 & 0 \\ -2 & 5 \end{pmatrix}$ structure, leading to identical adsorption sites for each molecule on the surface. Upon annealing to 600 K, the commensurability with the substrate is lost and the structure transforms into a denser packed arrangement. Notably, the distance along one unit cell vector remains unchanged; however, it is no longer aligned along one of the surface high symmetry axes, resulting in only every third molecule sitting on the same adsorption site on the surface (within the margin of error). For 2HTNBP, we observed also island formation on Ag(111) at RT in non-commensurable structures, which are stabilized by T-type interactions between the naphthyl-groups of neighboring molecules. Upon annealing to 500 K, the structure converts to a structure with a slightly higher density, which is now stabilized by π-π stacking of neighboring naphthyl groups. Our studies reveal a pronounced difference of the adsorption of the porphyrins on Cu(111) and Ag(111) surfaces, which is maintained when the pyrrole groups are replaced by an isoindole group and the phenyl groups by naphthyl groups. In summary, the flexibility of the naphthyl group allows for the formation of different conformers on the reactive Cu(111), and structural motifs based on repulsive interactions occurring at too close specific adsorption sites or attractive interactions via T-type bonding or π-π stacking arrangements on Ag(111).

The second part of this thesis focusses on the interaction and reaction of cyano-functionalized phenylporphyrins 2H*trans*DCNPP and 2HTCNPP with metal atoms (Co and Zn) and is based on the publications [P1 and P3]. On Ag(111), 2H*trans*DCNPP molecules exhibit a bifunctional behavior toward coadsorbed Co atoms. In a first step, the four N atoms in the macrocycle of the molecules react with Co atoms under the formation of Co*trans*DCNPP (metalation reaction). Cobalt-deposition onto 2H*trans*DCNPPs leads to a rapid and effective metalation reaction at RT. When switching the deposition order, the metalation reaction requires elevated temperatures. As a second step, the peripheral cyano groups can also coordinate with Co atoms. While a 4-fold coordination motif is preferred, also 3-fold, five-fold and six-fold motifs are observable. The metal–organic coordination structures appear at RT, and annealing at 400 K enhances the coordination process.

The metalation reaction of 2HTCNPP with post-deposited Zn atoms to ZnTCNPP on a Ag(111) surface was investigated, and a reaction intermediate (SAT complex) was identified by scanning tunneling microscopy at RT. After Zn deposition onto a 2HTCNPP layer at RT, the formation of three different 2D ordered island types, which coexist on the surface, was observed. Within all three island types, a new species could be identified as a bright protrusion, the amount of which correlates with the amount of post-deposited Zn. This species is attributed to a metastable SAT complex. In this SAT complex, the Zn atom coordinates with the macrocycle while the pyrrolic hydrogen atoms are still bound to the nitrogen atoms. This metastable SAT complex has been previously observed by Shubina *et al.* in the corresponding metalation reaction of the non-cyano-functionalized 2HTPP to ZnTPP, with a characteristic signature in XPS. Upon heating to 500 K, the activation barrier for the subsequent reaction of the intermediate SAT complex to the metalated porphyrin is overcome, yielding ZnTCNPP, and hydrogen desorbs. As an alternative to thermal activation, the barrier for the reaction of the SAT complex to metalated ZnTCNPP can also be overcome by a positive voltage pulse applied to the STM tip. Furthermore, a peculiar long range ordered structure, which covers several terraces of the Ag(111) surface like a carpet, was observed after the deposition of Zn onto a layer of already metalated ZnTCNPP at RT.

In conclusion, the thesis at hand gives valuable insights into the adsorption behavior of porphyrins on single crystal metal surfaces like Cu(111) and Ag(111). The functionalization plays a critical role to tailor the peculiar molecular-substrate or molecule-molecule interactions of porphyrins. The presented and discussed results of the publications [P1-4] indicate different strategies to tailor the adsorption behavior of porphyrins on surfaces, and thus deliver a toolbox for the fabrication of functional molecular architectures.

6 Zusammenfassung

Die vorliegende Arbeit befasst sich mit dem Adsorptionsverhalten verschiedener Tetraphenylporphyrin-Derivate (Naphthyl- und Cyano-Funktionalisierung) auf Einkristall-oberflächen bei und um RT mittels Rastertunnelmikroskopie. Inhalt ist eine detaillierte Untersuchung und Diskussion der intramolekularen Konformation, des Diffusionsverhaltens, der Rolle der intermolekularen Wechselwirkungen bei der Bildung supramolekularer Strukturen und der Wechselwirkung und Reaktion mit koadsorbierten Metallatomen, die die Grundlage für die Herstellung funktioneller Nanostrukturen basierend auf Porphyrinen bildet.

Die Veröffentlichungen [P2 und P4] befassen sich mit dem Adsorptionsverhalten der Naphthyl-funktionalisierten Porphyrine 2HTNP und 2HTNBP. Für 2HTNP wird auf Cu(111) ein sehr außergewöhnliches Adsorptionsverhalten beobachtet: Einzelne Moleküle adsorbieren bei RT in der "inverted" Konformation mit aufrecht stehenden Pyrrolringen, die entlang der kristallographischen Hauptrichtungen des Substrats orientiert sind. Aufgrund der Asymmetrie der Naphthylgruppen sind 16 verschiedene Oberflächen-Konformationen möglich, von denen 10 ein unterschiedliches Aussehen haben und durch STM identifiziert werden konnten. Interessanterweise adsorbiert auch 2HTNBP in Form einzelner Moleküle auf Cu(111), d.h. es kommt zu keiner Inselbildung von 2HTNBP, was auf eine starke Wechselwirkung mit dem Substrat hinweist, ähnlich wie bei 2HTPP und 2HTNP. Die möglichen Triebkräfte könnten eine Koordination der iminischen Stickstoffatome der Isoindolgruppen an Cu-Substratatome sein, wie bei 2HTPP und 2HTNP, sowie die größere Grundfläche der Moleküle. Das Diffusionsverhaltens der beiden Moleküle zeigt unterschiedliche Mobilitäten, die in drei Kategorien eingeteilt werden können, nämlich niedrig, mittel und hoch. Während für 2HTNBP keine Information über die Naphthyl-Orientierung vorliegt, hängt die Mobilität von 2HTNP mit der Naphthyl-Orientierung bezogen auf die Hauptachse des Moleküls entlang der iminischen Stickstoffatome zusammen. Schnell diffundierende Spezies haben 3 oder 4 Naphthylgruppen in τ-Orientierung (die in die Richtung der Diffusion zeigen, die entlang der kristallographischen Achse ausgerichtet ist). Unbewegliche Spezies haben nur 0 oder 1 Naphthylgruppe in dieser Richtung, was 4 oder 3 Gruppen in α-Orientierung (weg von der Hauptmolekülachse und der Diffusionsrichtung) entspricht. Dieses Verhalten zeigt, dass die Einführung asymmetrischer funktioneller Gruppen in der Peripherie, die über einzelne C-C-Bindungen mit dem Makrozyklus verbunden sind, einen starken Einfluss auf das Adsorptionsverhalten haben kann, indem sie eine Vielzahl von nicht-chiralen und chiralen Konformeren hervorbringt, die sich in ihrer Diffusion unterscheiden.

Um unser Verständnis über den Einflusses der asymmetrischen Naphthylgruppe auf das Adsorptionsverhalten von 2HTNP und 2HTNBP zu erweitern, haben wir auch das Adsorptionsverhalten auf Ag(111) untersucht. Für 2HTNP auf Ag(111) beobachteten wir eine kommensurable $\begin{pmatrix} 7 & 0 \\ -2 & 5 \end{pmatrix}$ Struktur, die zu identischen Adsorptionsplätzen für jedes Molekül auf der Oberfläche führte. Nach dem Heizen auf 600 K geht die Kommensurabilität mit dem Substrat verloren, und die Struktur wandelt sich in eine dicht gepackte Anordnung um. Der Abstand entlang des Vektors einer Einheitszelle bleibt unverändert; er ist jedoch nicht mehr entlang einer der hohen Vorzugsrichtungen der Oberfläche orientiert, was dazu führt, dass nur jedes dritte Molekül auf denselben Adsorptionsplatz auf der Oberfläche sitzt (innerhalb der Fehlertoleranz). Für 2HTNBP beobachteten wir bei RT auch eine Inselbildung auf Ag(111) in nicht-kommensurablen Strukturen, die durch T-artige Wechselwirkungen zwischen den Naphthyl-Gruppen benachbarter Moleküle stabilisiert werden. Beim Heizen auf 500 K ändert sich die Dichte der Struktur, die nun durch π-π Stapelung benachbarter Naphthylgruppen stabilisiert wird. Unsere Untersuchungen zeigen einen ausgeprägten Unterschied in der Adsorption der Porphyrine auf Cu(111)- und Ag(111)-Oberflächen, der erhalten bleibt, wenn die Pyrrolgruppen durch eine Isoindolgruppen und die Phenylgruppen durch Naphthylgruppen ersetzt werden. Zusammenfassend lässt sich sagen, dass die Flexibilität der Naphthylgruppe die Bildung verschiedener Konformere auf der reaktiven Cu(111) Oberfläche und struktureller Motive ermöglicht, die auf abstoßenden Wechselwirkungen an zu nahen spezifischen Adsorptionspositionen oder auf anziehenden Wechselwirkungen über T-artige Bindungen oder π-π Stapelung auf Ag(111) beruhen.

Der zweite Teil dieser Arbeit konzentriert sich auf die Wechselwirkung und Reaktion von Cyano-funktionalisierten Phenylporphyrinen 2H*trans*DCNPP und 2HTCNPP mit Metallatomen (Co und Zn) und basiert auf den Veröffentlichungen [P1 und P3]. Auf Ag(111) zeigen die 2H*trans*DCNPP Moleküle ein bifunktionelles Verhalten gegenüber koadsorbierten Co-Atomen. In einem ersten Schritt reagieren die vier N-Atome im Makrozyklus der Moleküle mit Co-Atomen unter Bildung von Co*trans*DCNPP (Metallisierungsreaktion). Die Abscheidung von Kobalt auf 2H*trans*DCNPPs führt zu einer schnellen und effektiven Metallisierungsreaktion bei RT. Wird die Reihenfolge der Co-Abscheidung geändert, erfordert die Metallisierungsreaktion höhere Temperaturen. In einem zweiten Schritt können auch die peripheren Cyanogruppen mit Co-Atomen koordinieren. Während ein 4-faches Koordinationsmotiv bevorzugt wird, sind auch 3-fache, 5-fache und 6-fache Motive zu beobachten. Die metallorganischen Koordinationsstrukturen treten bei RT auf, und ein Heizschritt bei 400 K verstärkt den Koordinationsprozess.

Die Metallisierungsreaktion von 2HTCNPP mit nachträglich abgeschiedenen Zn-Atomen zu ZnTCNPP wurde auf einer Ag(111)-Oberfläche untersucht, und ein Reaktionszwischenprodukt wurde durch Rastertunnelmikroskopie bei RT identifiziert. Nach der Abscheidung von Zn auf einer 2HTCNPP-Schicht bei RT wurde die Bildung von drei verschiedenen geordneten 2D-Inseltypen beobachtet, die nebeneinander auf der Oberfläche existieren. Innerhalb aller drei Inseltypen konnte eine neue Spezies als helle Intensitätsmaxima identifiziert werden, deren Anzahl mit der Menge des nachträglich abgeschiedenen Zn korreliert. Diese Spezies wird einem metastabilen SAT-Komplex ("sitting atop") zugeschrieben. In diesem SAT-Komplex koordiniert das Zn-Atom mit dem Makrozyklus, während die pyrrolischen Wasserstoffatome noch an die Stickstoffatome gebunden sind. Dieser metastabile SAT-Komplex wurde zuvor von Shubina *et al.* bei der entsprechenden Metallisierungsreaktion des nicht-Cyano-funktionalisierten 2HTPP zu ZnTPP beobachtet, mit einer charakteristischen Signatur im XPS. Beim Erhitzen auf 500 K wird die Aktivierungsbarriere für die anschließende Reaktion des intermediären SAT-Komplexes zum Metalloporphyrin überwunden, wobei ZnTCNPP entsteht und Wasserstoff desorbiert. Alternativ zur thermischen Aktivierung kann die Aktivierungsbarriere der Reaktion des SAT-Komplexes zu metallisiertem ZnTCNPP auch durch einen positiven Spannungsimpuls an der STM-Spitze überwunden werden. Darüber hinaus wurde nach der Abscheidung von Zn auf einer Schicht von bereits metallisiertem ZnTCNPP bei RT eine eigentümliche langreichweitig geordnete Struktur beobachtet, die mehrere Terrassen der Ag(111) Oberfläche wie ein Teppich bedeckt.

Zusammenfassend lässt sich sagen, dass die vorliegende Arbeit wertvolle Einblicke in das Adsorptionsverhalten von Porphyrinen auf einkristallinen Metalloberflächen wie Cu(111) und Ag(111) gibt. Die Funktionalisierung spielt eine entscheidende Rolle, um die besonderen Molekül-Substrat- oder Molekül-Molekül-Wechselwirkungen von Porphyrinen zu beeinflussen. Die in den Veröffentlichungen [P1-4] vorgestellten und diskutierten Ergebnisse zeigen verschiedene Strategien zur Anpassung des Adsorptionsverhaltens von Porphyrinen au Oberflächen auf und liefern damit einen Werkzeugkasten für die Herstellung funktioneller molekularer Architekturen.

7 List of Abbreviation

AFM	atomic force microscopy
DFT	density functional theory
fcc	face centered cubic
LDOS	local density of states
LEED	low energy electron diffraction
NEXAFS	near edge X-ray absorption fine structure
NIXSW	normal incidence X-ray standing waves
RT	room temperature
STM	scanning tunneling microscopy
STS	scanning tunneling spectroscopy
TPD	temperature programmed desorption
TPP	tetraphenylporphyrin
UHV	ultra-high vacuum
XPS	X-ray photoelectron spectroscopy

8 References

[1] Barth, J. V.; Costantini, G.; Kern, K., Engineering atomic and molecular nanostructures at surfaces. *Nature* **2005,** *437* (7059), 671-679.

[2] Sosa-Vargas, L.; Kim, E.; Attias, A.-J., Beyond "decorative" 2D supramolecular self-assembly: strategies towards functional surfaces for nanotechnology. *Materials Horizons* **2017,** *4* (4), 570-583.

[3] Whitesides, G. M., Nanoscience, nanotechnology, and chemistry. *Small* **2005,** *1* (2), 172-179.

[4] Moore, G., Cramming more components onto integrated circuits. *Electronics* **1965,** *38*, 114-116.

[5] Marbach, H., Microscopic and Spectromicroscopic Insight and Fabrication of Nanoscaled Structures on Surfaces. *Habilitation Thesis* **2010,** *FAU Erlangen-Nürnberg*.

[6] Barth, J. V., Molecular architectonic on metal surfaces. *Annu Rev Phys Chem* **2007,** *58*, 375-407.

[7] Whitesides, G., Molecular Self-Assembly and Nanochemistry: A Chemical Strategy for the Synthesis of Nanostructures. *Science* **1991,** *254* (5036), 1312-1319.

[8] Jung, T.; Schlittler, R.; Gimzewski, J., Conformational identification of individual adsorbed molecules with the STM. *Nature* **1997,** *386* (6626), 696-698.

[9] De Feyter, S.; De Schryver, F. C., Two-dimensional supramolecular self-assembly probed by scanning tunneling microscopy. *Chem Soc Rev* **2003,** *32* (3), 139-150.

[10] Auwärter, W.; Écija, D.; Klappenberger, F.; Barth, J. V., Porphyrins at interfaces. *Nature chemistry* **2015,** *7* (2), 105-120.

[11] Gottfried, M., Surface chemistry of porphyrins and phthalocyanines. *Surface Science Reports* **2015,** *70* (3), 259-379.

[12] Gottfried, M., Marbach, H., Surface-Confined Coordination Chemistry with Porphyrins and Phtalocyanines: Aspect of Formation, Electronic Straucture, and Reactivity. *Z. Phys. Chem.* **2009,** *223*, 53-74.

[13] Milgrom, L. R.; Warren, M. J., The colours of life: an introduction to the chemistry of porphyrins and related compounds. **1997**.

[14] Grätzel, M., Dye-sensitized solar cells. *Journal of photochemistry and photobiology C: Photochemistry Reviews* **2003,** *4* (2), 145-153.

[15] Carvalho, C. M.; Brocksom, T. J.; de Oliveira, K. T., Tetrabenzoporphyrins: synthetic developments and applications. *Chem Soc Rev* **2013,** *42* (8), 3302-3317.

[16] Rakow, A colorimetric sensor array for odour visualization. *Nature (London)* **2000,** *406*, 710-713.

[17] Baddeley, C. J., Fundamental investigations of enantioselective heterogeneous catalysis. *Topics in Catalysis* **2003,** *25*, 17-28.

[18] Collman, J. P.; Denisevich, P.; Konai, Y.; Marrocco, M.; Koval, C.; Anson, F. C., Electrode catalysis of the four-electron reduction of oxygen to water by dicobalt face-to-face porphyrins. *Journal of the American Chemical Society* **2002,** *102* (19), 6027-6036.

[19] Young, R.; Ward, J.; Scire, F., The topografiner: an instrument for measuring surface microtopography. *Review of Scientific Instruments* **1972,** *43* (7), 999-1011.

[20] Binnig, G.; Rohrer, H.; Ch., G.; E, W., Surface studies by scanning tunneling microscopy. *Phys. Rev. Lett* **1982,** *49* (1), 57-68.

[21] Binnig, G.; Rohrer, H.; Gerber, C.; Weibel, E., 7× 7 reconstruction on Si (111) resolved in real space. *Physical review letters* **1983,** *50* (2), 120-123.

[22] Yao, N.; Wang, Z., Handbook of microscopy for nanotechnology. . *Springer* **2005**.

[23] Wiesendanger, R.; Mulvey, T., Scanning probe microscopy and spectroscopy. *Measurement Science and Technology* **1995,** *6* (5), 600.

[24] Hansma, P. K.; Tersoff, J., Scanning tunneling microscopy. *Journal of Applied Physics* **1987,** *61* (2), R1-R24.

[25] Oura, K.; Lifshits, V.; Saranin, A.; Zotov, A.; Katayama, M., Surface science: an introduction. *Springer Science & Business Media* **2013**.

[26] Besocke, K., An easily operable scanning tunneling microscope. *Surface Science* **1987,** *181* (1-2), 145-153.

[27] Horcas, I.; Fernández, R.; Gomez-Rodriguez, J.; Colchero, J.; Gómez-Herrero, J.; Baro, A., WSXM: a software for scanning probe microscopy and a tool for nanotechnology. *Review of scientific instruments* **2007,** *78* (1), 013705.

[28] Atwood, J. L.; Steed, J. W., Supramolecular chemistry. *John Wiley & Sons* **2009**.

[29] Dixon, H.; Cornish-Bowden, A.; Liebecq, C.; Loening, K.; Moss, G.; Reedijk, J.; Velick, S.; Venetianer, P.; Vliegenthart, J., Nomenclature of tetrapyrroles. *Pure Appl. Chem* **1987,** *59*, 779-832.

[30] Buchner, F.; Comanici, K.; Jux, N.; Steinrück, H.-P.; Marbach, H., Polymorphism of porphyrin molecules on Ag (111) and how to weave a rigid monolayer. *The Journal of Physical Chemistry C* **2007,** *111* (36), 13531-13538.

[31] Moresco, F.; Meyer, G.; Rieder, K.-H.; Ping, J.; Tang, H.; Joachim, C., TBPP molecules on copper surfaces: a low temperature scanning tunneling microscope investigation. *Surface science* **2002,** *499* (1), 94-102.

[32] Ditze, S.; Stark, M.; Buchner, F.; Aichert, A.; Jux, N.; Luckas, N.; Görling, A.; Hieringer, W.; Hornegger, J.; Steinrück, H.-P., On the energetics of conformational switching of molecules at and close to room temperature. *Journal of the American Chemical Society* **2014,** *136* (4), 1609-1616.

[33] Auwärter, W.; Klappenberger, F.; Weber-Bargioni, A.; Schiffrin, A.; Strunskus, T.; Wöll, C.; Pennec, Y.; Riemann, A.; Barth, J. V., Conformational adaptation and selective adatom capturing of tetrapyridyl-porphyrin molecules on a copper (111) surface. *Journal of the American Chemical Society* **2007,** *129* (36), 11279-11285.

[34] Moresco, F.; Meyer, G.; Rieder, K.-H.; Tang, H.; Gourdon, A.; Joachim, C., Conformational changes of single molecules induced by scanning tunneling microscopy manipulation: A route to molecular switching. *Physical Review Letters* **2001,** *86* (4), 672-675.

[35] Brede, J.; Linares, M.; Kuck, S.; Schwöbel, J.; Scarfato, A.; Chang, S.-H.; Hoffmann, G.; Wiesendanger, R.; Lensen, R.; Kouwer, P. H., Dynamics of molecular self-ordering in tetraphenyl porphyrin monolayers on metallic substrates. *Nanotechnology* **2009,** *20* (27), 275602.

[36] Buchner, F.; Kellner, I.; Hieringer, W.; Görling, A.; Steinrück, H.-P.; Marbach, H., Ordering aspects and intramolecular conformation of tetraphenylporphyrins on Ag (111). *Physical Chemistry Chemical Physics* **2010,** *12* (40), 13082-13090.

[37] Jarvis, S. P.; Taylor, S.; Baran, J. D.; Thompson, D.; Saywell, A.; Mangham, B.; Champness, N. R.; Larsson, J.; Moriarty, P., Physisorption controls the conformation and density of states of an adsorbed porphyrin. *The Journal of Physical Chemistry C* **2015,** *119* (50), 27982-27994.

[38] Diller, K.; Klappenberger, F.; Marschall, M.; Hermann, K.; Nefedov, A.; Wöll, C.; Barth, J., Self-metalation of 2H-tetraphenylporphyrin on Cu (111): An x-ray spectroscopy study. *The Journal of chemical physics* **2012,** *136* (1), 014705.

[39] Buchner, F.; Xiao, J.; Zillner, E.; Chen, M.; Röckert, M.; Ditze, S.; Stark, M.; Steinrück, H.-P.; Gottfried, J. M.; Marbach, H., Diffusion, rotation, and surface chemical bond of individual 2 H-tetraphenylporphyrin molecules on Cu (111). *The Journal of Physical Chemistry C* **2011,** *115* (49), 24172-24177.

[40] Xiao, J.; Ditze, S.; Chen, M.; Buchner, F.; Stark, M.; Drost, M.; Steinrück, H.-P.; Gottfried, J. M.; Marbach, H., Temperature-dependent chemical and structural

transformations from 2H-tetraphenylporphyrin to copper (II)-tetraphenylporphyrin on Cu (111). *The Journal of Physical Chemistry C* **2012,** *116* (22), 12275-12282.

[41] Buchner, F., STM Investigation of Molecular Architectures of Porphyrinoids on a Ag (111) Surface: Supramolecular Ordering, Electronic Properties and Reactivity. *Springer Science & Business Media* **2010**.

[42] Ditze, S., On the dynamics of molecular processes: STM investigations of porphyrins on Cu(111). *Ph. D. thesis FAU Erlangen-Nürnberg* **2014**.

[43] Wölfle, T.; Görling, A.; Hieringer, W., Conformational flexibility of metalloporphyrins studied by density-functional calculations. *Phys Chem Chem Phys* **2008,** *10* (37), 5739-5742.

[44] Buchner, F.; Zillner, E.; Röckert, M.; Gläßel, S.; Steinrück, H.-P.; Marbach, H., Substrate-mediated phase separation of two porphyrin derivatives on Cu(111). *Chemistry* **2011,** *17* (37), 10226-10229.

[45] Auwärter, W.; Seufert, K.; Klappenberger, F.; Reichert, J.; Weber-Bargioni, A.; Verdini, A.; Cvetko, D.; Dell'Angela, M.; Floreano, L.; Cossaro, A.; Bavdek, G.; Morgante, A.; Seitsonen, A. P.; Barth, J. V., Site-specific electronic and geometric interface structure of Co-tetraphenyl-porphyrin layers on Ag(111). *Physical Review B* **2010,** *81* (24), 245403.

[46] Weber-Bargioni, A.; Auwärter, W.; Klappenberger, F.; Reichert, J.; Lefrancois, S.; Strunskus, T.; Wöll, C.; Schiffrin, A.; Pennec, Y.; Barth, J. V., Visualizing the frontier orbitals of a conformationally adapted metalloporphyrin. *Chemphyschem* **2008,** *9* (1), 89-94.

[47] Stark, M.; Ditze, S.; Drost, M.; Buchner, F.; Steinrück, H.-P.; Marbach, H., Coverage dependent disorder-order transition of 2H-tetraphenylporphyrin on Cu(111). *Langmuir* **2013,** *29* (12), 4104-4110.

[48] Röckert, M.; Ditze, S.; Stark, M.; Xiao, J.; Steinrück, H.-P.; Marbach, H.; Lytken, O., Abrupt Coverage-Induced Enhancement of the Self-Metalation of Tetraphenylporphyrin with Cu(111). *The Journal of Physical Chemistry C* **2014,** *118* (3), 1661-1667.

[49] Gottfried, M.; Marbach, H., Surface-Confined Coordination Chemistry with Porphyrins and Phthalocyanines: Aspects of Formation, Electronic Structure, and Reactivity. *Zeitschrift für Physikalische Chemie* **2009,** *223* (1-2), 53-74.

[50] Albrecht, F.; Bischoff, F.; Auwärter, W.; Barth, J. V.; Repp, J., Direct identification and determination of conformational response in adsorbed individual non-planar molecular species using non-contact atomic force microscopy. *Nano Letter* **2016,** *16*, 7703-7709.

[51] Lepper, M.; Kobl, J.; Schmitt, T.; Gurrath, M.; de Siervo, A.; Schneider, M. A.; Steinruck, H. P.; Meyer, B.; Marbach, H.; Hieringer, W., "Inverted" porphyrins: a distorted adsorption geometry of free-base porphyrins on Cu(111). *Chem Commun (Camb)* **2017,** *53* (58), 8207-8210.

[52] Ryan, P. T. P.; Lalaguna, P. L.; Haag, F.; Braim, M. M.; Ding, P.; Payne, D. J.; Barth, J. V.; Lee, T. L.; Woodruff, D. P.; Allegretti, F.; Duncan, D. A., Validation of the inverted adsorption structure for free-base tetraphenyl porphyrin on Cu(111). *Chem Commun (Camb)* **2020,** *56* (25), 3681-3684.

[53] Zhang, L.; Lepper, M.; Stark, M.; Menzel, T.; Lungerich, D.; Jux, N.; Hieringer, W.; Steinruck, H. P.; Marbach, H., On the critical role of the substrate: the adsorption behaviour of tetrabenzoporphyrins on different metal surfaces. *Phys Chem Chem Phys* **2017,** *19* (30), 20281-20289.

[54] Buchner, F., STM Investigation of Molecular Architectures of Porphyrinoids on a Ag (111) Surface: Supramolecular Ordering, Electronic Properties and Reactivity. *Springer Science & Business Media* **2010**.

[55] Auwärter, W.; Weber-Bargioni, A.; Riemann, A.; Schiffrin, A.; Gröning, O.; Fasel, R.; Barth, J., Self-assembly and conformation of tetrapyridyl-porphyrin molecules on Ag (111). *The Journal of chemical physics* **2006,** *124* (19), 194708.

[56] Marbach, H., Surface-Mediated in Situ Metalation of Porphyrins at the Solid-Vacuum Interface. *Acc. Chem. Res.* **2015,** *48* (9), 2649-2658.

[57] Diller, K.; Papageorgiou, A. C.; Klappenberger, F.; Allegretti, F.; Barth, J. V.; Auwarter, W., In vacuo interfacial tetrapyrrole metallation. *Chem Soc Rev* **2016,** *45* (6), 1629-1656.

[58] Mochida, K.; Suetsugu, K.; Fujitsu, H.; Takeshita, K., A Kinetic study on Reduction of Nitric Oxide over Coblat Tetraphenylporphyrin Supported on Titanium Dioxide. *Journal of Catalysis* **1982,** *77*, 519-526.

[59] Hieringer, W.; Flechtner, K.; Kretschmann, A.; Seufert, K.; Auwärter, W.; Barth, J. V.; Görling, A.; Steinrück, H.-P.; Gottfried, J. M., The surface trans effect: influence of axial ligands on the surface chemical bonds of adsorbed metalloporphyrins. *J Am Chem Soc* **2011,** *133* (16), 6206-6222.

[60] Gottfried, J. M.; Flechtner, K.; Kretschmann, A.; Lukasczyk, T.; Steinrück, H.-P., Direct Synthesis of a Metalloporphyrin Complex on a Surface. *Journal of the American Chemical Society* **2006,** *128* (17), 5644-5645.

[61] Li, Y.; Xiao, J.; Shubina, T. E.; Chen, M.; Shi, Z.; Schmid, M.; Steinrück, H.-P.; Gottfried, J. M.; Lin, N., Coordination and Metalation Bifunctionality of Cu with 5,10,15,20-Tetra(4-pyridyl)porphyrin: Toward a Mixed-Valence Two-Dimensional Coordination Network. *Journal of the American Chemical Society* **2012,** *134* (14), 6401-6408.

[62] Buchner, F.; Flechtner, K.; Bai, Y.; Zillner, E.; Kellner, I.; Steinrück, H.-P.; Marbach, H.; Gottfried, J. M., Coordination of Iron Atoms by Tetraphenylporphyrin Monolayers and Multilayers on Ag(111) and Formation of Iron-Tetraphenylporphyrin. *The Journal of Physical Chemistry C* **2008,** *112* (39), 15458-15465.

[63] Écija, D.; Trelka, M.; Urban, C.; Mendoza, P. d.; Mateo-Martí, E.; Rogero, C.; Martín-Gago, J. A.; Echavarren, A. M.; Otero, R.; Gallego, J. M.; Miranda, R., Molecular Conformation, Organizational Chirality, and Iron Metalation of meso-Tetramesitylporphyrins on Copper(100). *The Journal of Physical Chemistry C* **2008,** *112* (24), 8988-8994.

[64] Shubina, T. E.; Marbach, H.; Flechtner, K.; Kretschmann, A.; Jux, N.; Buchner, F.; Steinrück, H.-P.; Clark, T.; Gottfried, J. M., Principle and Mechanism of Direct Porphyrin Metalation: Joint Experimental and Theoretical Investigation. *J Am Chem Soc* **2007,** *129*, 9476-9483.

[65] Kretschmann, A.; Walz, M. M.; Flechtner, K.; Steinrück, H.-P.; Gottfried, J. M., Tetraphenylporphyrin picks up zinc atoms from a silver surface. *Chem Commun (Camb)* **2007,** (6), 568-570.

[66] Chen, M.; Feng, X.; Zhang, L.; Ju, H.; Xu, Q.; Zhu, J.; Gottfried, J. M.; Ibrahim, K.; Qian, H.; Wang, J., Direct Synthesis of Nickel(II) Tetraphenylporphyrin and Its Interaction with a Au(111) Surface: A Comprehensive Study. *The Journal of Physical Chemistry C* **2010,** *114* (21), 9908-9916.

[67] Wang, C.; Fan, Q.; Hu, S.; Ju, H.; Feng, X.; Han, Y.; Pan, H.; Zhu, J.; Gottfried, J. M., Coordination reaction between tetraphenylporphyrin and nickel on a TiO2(110) surface. *Chem Commun (Camb)* **2014,** *50* (61), 8291-8294.

[68] Weber-Bargioni, A.; Reichert, J.; Seitsonen, A. P.; Auwärter, W.; Schiffrin, A.; Barth, J. V., Interaction of Cerium Atoms with Surface-Anchored Porphyrin Molecules. *The Journal of Physical Chemistry C* **2008,** *112* (10), 3453-3455.

[69] González-Moreno, R.; Sánchez-Sánchez, C.; Trelka, M.; Otero, R.; Cossaro, A.; Verdini, A.; Floreano, L.; Ruiz-Bermejo, M.; García-Lekue, A.; Martín-Gago, J. Á.;

Rogero, C., Following the Metalation Process of Protoporphyrin IX with Metal Substrate Atoms at Room Temperature. *The Journal of Physical Chemistry C* **2011,** *115* (14), 6849-6854.

[70] Haq, S.; Hanke, F.; Dyer, M. S.; Persson, M.; Iavicoli, P.; Amabilino, D. B.; Raval, R., Clean coupling of unfunctionalized porphyrins at surfaces to give highly oriented organometallic oligomers. *J Am Chem Soc* **2011,** *133* (31), 12031-12039.

[71] Doyle, C. M.; Krasnikov, S. A.; Sergeeva, N. N.; Preobrajenski, A. B.; Vinogradov, N. A.; Sergeeva, Y. N.; Senge, M. O.; Cafolla, A. A., Evidence for the formation of an intermediate complex in the direct metalation of tetra(4-bromophenyl)-porphyrin on the Cu(111) surface. *Chem Commun (Camb)* **2011,** *47* (44), 12134-12136.

[72] Goldoni, A.; Pignedoli, C. A.; Di Santo, G.; Castellarin-Cudia, C.; Magnano, E.; Bondino, F.; Verdini, A.; Passerone, D., Room Temperature Metalation of 2H-TPP Monolayer on Iron and Nickel Surfaces by Picking up Substrate Metal Atoms. *ACS Nano* **2012,** *6*, 10800-10807.

[73] Ditze, S.; Stark, M.; Drost, M.; Buchner, F.; Steinrück, H.-P.; Marbach, H., Activation energy for the self-metalation reaction of 2H-tetraphenylporphyrin on Cu(111). *Angew Chem Int Ed Engl* **2012,** *51* (43), 10898-10901.

[74] Lepper, M.; Köbl, J.; Zhang, L.; Meusel, M.; Hölzel, H.; Lungerich, D.; Jux, N.; de Siervo, A.; Meyer, B.; Steinrück, H.-P.; Marbach, H., Controlling the Self-Metalation Rate of Tetraphenylporphyrins on Cu(111) via Cyano Functionalization. *Angew Chem Int Ed Engl* **2018,** *57* (32), 10074-10079.

[75] Fleischer, E. B.; Wang, J. H., The detection of a type of reaction intermediate in the combination of metal ions with porphyrins. *Journal of the American Chemical Society* **1960,** *82* (14), 3498-3502.

[76] Hsiao, Y.-W.; Ryde, U., Interpretation of EXAFS spectra for sitting-atop complexes with the help of computational methods. *Inorganica chimica acta* **2006,** *359* (4), 1081-1092.

[77] De Luca, G.; Romeo, A.; Scolaro, L. M.; Ricciardi, G.; Rosa, A., Sitting-atop metalloporphyrin complexes: experimental and theoretical investigations on such elusive species. *Inorganic chemistry* **2009,** *48* (17), 8493-8507.

[78] Bischoff, F.; Seufert, K.; Auwärter, W.; Seitsonen, A. P.; Heim, D.; Barth, J. V., Metalation of porphyrins by lanthanide atoms at interfaces: direct observation and stimulation of cerium coordination to 2H-TPP/Ag (111). *The Journal of Physical Chemistry C* **2018,** *122* (9), 5083-5092.

[79] Röckert, M.; Franke, M.; Tariq, Q.; Steinrück, H.-P.; Lytken, O., Evidence for a precursor adcomplex during the metalation of 2HTPP with iron on Ag (1 0 0). *Chemical Physics Letters* **2015,** *635*, 60-62.

[80] Mielke, J.; Hanke, F.; Peters, M. V.; Hecht, S.; Persson, M.; Grill, L., Adatoms underneath single porphyrin molecules on Au (111). *Journal of the American chemical society* **2015,** *137* (5), 1844-1849.

[81] Inami, E.; Yamaguchi, M.; Nemoto, R.; Yorimitsu, H.; Krüger, P.; Yamada, T. K., Direct Imaging of Precursor Adcomplex States during Cryogenic-Temperature On-Surface Metalation: Scanning Tunneling Microscopy Study on Porphyrin Array with Fe Adsorption at 78.5 K. *The Journal of Physical Chemistry C* **2020,** *124* (6), 3621-3631.

[82] Röckert, M.; Franke, M.; Tariq, Q.; Lungerich, D.; Jux, N.; Stark, M.; Kaftan, A.; Ditze, S.; Marbach, H.; Laurin, M., Insights in reaction mechanistics: isotopic exchange during the metalation of deuterated tetraphenyl-21, 23 D-porphyrin on Cu (111). *The Journal of Physical Chemistry C* **2014,** *118* (46), 26729-26736.

[83] He, Y.; Garnica, M.; Bischoff, F.; Ducke, J.; Bocquet, M.-L.; Batzill, M.; Auwärter, W.; Barth, J. V., Fusing tetrapyrroles to graphene edges by surface-assisted covalent coupling. *Nature chemistry* **2017,** *9* (1), 33-38.

[84] Grill, L.; Dyer, M.; Lafferentz, L.; Persson, M.; Peters, M. V.; Hecht, S., Nano-architectures by covalent assembly of molecular building blocks. *Nature nanotechnology* **2007,** *2* (11), 687-691.

[85] Gottardi, S.; Müller, K.; Moreno-López, J. C.; Yildirim, H.; Meinhardt, U.; Kivala, M.; Kara, A.; Stöhr, M., Cyano-Functionalized Triarylamines on Au (111): Competing Intermolecular versus Molecule/Substrate Interactions. *Advanced Materials Interfaces* **2014,** *1* (1), 1300025.

[86] Heim, D.; Ecija, D.; Seufert, K.; Auwarter, W.; Aurisicchio, C.; Fabbro, C.; Bonifazi, D.; Barth, J. V., Self-assembly of flexible one-dimensional coordination polymers on metal surfaces. *Journal of the American Chemical Society* **2010,** *132* (19), 6783-6790.

[87] Lepper, M.; Schmitt, T.; Gurrath, M.; Raschmann, M.; Zhang, L.; Stark, M.; Hölzel, H.; Jux, N.; Meyer, B.; Schneider, M. A., Adsorption behavior of a cyano-functionalized porphyrin on Cu (111) and Ag (111): from molecular wires to ordered supramolecular two-dimensional aggregates. *The Journal of Physical Chemistry C* **2017,** *121* (47), 26361-26371.

[88] Rojas, G.; Chen, X.; Bravo, C.; Kim, J.-H.; Kim, J.-S.; Xiao, J.; Dowben, P. A.; Gao, Y.; Zeng, X. C.; Choe, W., Self-assembly and properties of nonmetalated tetraphenyl-porphyrin on metal substrates. *The Journal of Physical Chemistry C* **2010,** *114* (20), 9408-9415.

[89] Adhikari, R.; Kuliga, J.; Ruppel, M.; Jux, N.; Marbach, H.; Steinrück, H.-P., Self-Assembled 2D-Coordination Kagome, Quadratic, and Close-Packed Hexagonal Lattices Formed from a Cyano-Functionalized Benzoporphyrin on Cu (111). *The Journal of Physical Chemistry C* **2021,** *125* (13), 7204-7212.

[90] Van Vörden, D.; Lange, M.; Schmuck, M.; Schaffert, J.; Cottin, M.; Bobisch, C.; Möller, R., Communication: Substrate induced dehydrogenation: Transformation of octa-ethyl-porphyrin into tetra-benzo-porphyrin. *The Journal of chemical physics* **2013,** *138* (21), 211102.

[91] Lepper, M.; Zhang, L.; Stark, M.; Ditze, S.; Lungerich, D.; Jux, N.; Hieringer, W.; Steinrück, H.-P.; Marbach, H., Role of specific intermolecular interactions for the arrangement of Ni (II)-5, 10, 15, 20-tetraphenyltetrabenzoporphyrin on Cu (111). *The Journal of Physical Chemistry C* **2015,** *119* (34), 19897-19905.

[92] Brede, J.; Linares, M.; Lensen, R.; Rowan, A. E.; Funk, M.; Bröring, M.; Hoffmann, G.; Wiesendanger, R., Adsorption and conformation of porphyrins on metallic surfaces. *Journal of Vacuum Science & Technology B: Microelectronics and Nanometer Structures Processing, Measurement, and Phenomena* **2009,** *27* (2), 799-804.

[93] Urgel, J. I.; Ecija, D.; Auwärter, W.; Stassen, D.; Bonifazi, D.; Barth, J. V., Orthogonal Insertion of Lanthanide and Transition-Metal Atoms in Metal–Organic Networks on Surfaces. *Angewandte Chemie International Edition* **2015,** *54* (21), 6163-6167.

[94] Urgel, J. I.; Schwarz, M.; Garnica, M.; Stassen, D.; Bonifazi, D.; Ecija, D.; Barth, J. V.; Auwärter, W., Controlling coordination reactions and assembly on a Cu (111) supported boron nitride monolayer. *Journal of the American Chemical Society* **2015,** *137* (7), 2420-2423.

[95] Schlickum, U.; Klappenberger, F.; Decker, R.; Zoppellaro, G.; Klyatskaya, S.; Ruben, M.; Kern, K.; Brune, H.; Barth, J., Surface-Confined Metal− Organic Nanostructures from Co-Directed Assembly of Linear Terphenyl-dicarbonitrile Linkers on Ag (111). *The Journal of Physical Chemistry C* **2010,** *114* (37), 15602-15606.

[96] Buchner, F.; Schwald, V.; Comanici, K.; Steinrück, H.-P.; Marbach, H., Microscopic Evidence of the Metalation of a Free-Base Porphyrin Monolayer with Iron. *ChemPhysChem* **2007,** *8* (2), 241-243.

[97] Auwärter, W.; Weber-Bargioni, A.; Brink, S.; Riemann, A.; Schiffrin, A.; Ruben, M.; Barth, J. V., Controlled metalation of self-assembled porphyrin nanoarrays in two dimensions. *ChemPhysChem* **2007,** *8* (2), 250-254.

[98] Bai, Y.; Buchner, F.; Wendahl, M. T.; Kellner, I.; Bayer, A.; Steinrück, H.-P.; Marbach, H.; Gottfried, J. M., Direct metalation of a phthalocyanine monolayer on Ag (111) with coadsorbed iron atoms. *The Journal of Physical Chemistry C* **2008,** *112* (15), 6087-6092.

[99] Ditze, S.; Röckert, M.; Buchner, F.; Zillner, E.; Stark, M.; Steinrück, H.-P.; Marbach, H., Towards the engineering of molecular nanostructures: local anchoring and functionalization of porphyrins on model-templates. *Nanotechnology* **2013,** *24* (11), 115305.

[100] Schlickum, U.; Decker, R.; Klappenberger, F.; Zoppellaro, G.; Klyatskaya, S.; Ruben, M.; Silanes, I.; Arnau, A.; Kern, K.; Brune, H., Metal− organic honeycomb nanomeshes with tunable cavity size. *Nano letters* **2007,** *7* (12), 3813-3817.

[101] Buchner, F.; Warnick, K.-G.; Wölfle, T.; Görling, A.; Steinrück, H.-P.; Hieringer, W.; Marbach, H., Chemical fingerprints of large organic molecules in scanning tunneling microscopy: Imaging adsorbate− substrate coupling of metalloporphyrins. *The Journal of Physical Chemistry C* **2009,** *113* (37), 16450-16457.

[102] Sperl, A.; Kröger, J. r.; Berndt, R., Demetalation of a single organometallic complex. *Journal of the American Chemical Society* **2011,** *133* (29), 11007-11009.

[103] Wang, Y.; Kröger, J. r.; Berndt, R.; Hofer, W. A., Pushing and pulling a Sn ion through an adsorbed phthalocyanine molecule. *Journal of the American Chemical Society* **2009,** *131* (10), 3639-3643.

9 Acknowledgements

I would like to thank and acknowledge all persons who supported me during my scientific time, without their help I would not be where I am today. I want to express my gratitude to:

Professor Hans-Peter Steinrück for giving me the opportunity to do my PhD at his chair and taking over my supervision from PD Dr. Hubertus Marbach. I always enjoyed the outstanding scientific support, excellent mentorship, and the providing of a great social environment.

PD Dr. Hubertus Marbach and Dr. Simon Jaekel for excellent supervision, valuable scientific discussions, and helpful ideas during the time of my PhD.

To my collaboration partners: Professor Abner de Siervo who supervised me during my stay in Campinas. I want to thank him as well as Rodrigo C.C. Ferreira for introducing me to the culture of Brazil and taking care of me during my stay in Campinas. The group of Professor Norbert Jux, especially Dr. Helen Hölzel, Dr. Michael Ruppel and M. Sc. Lampros-Pascal Gazetas for the synthesis of several porphyrins and being always open for discussions.

My colleagues from the STM/EBID lab, Michael Lepper, Rajan Adhikari, Stephen Massicot, Majid Shaker, Christian Preischl, Florian Vollnhals and Elif Bilgilisoy. Special thanks to the rest of the chair of Physical Chemistry II for the great working atmosphere. I always enjoyed our activities like pleasant conversation during coffee, playing soccer in the summer and competing in dart tournaments.

Hans-Peter Bäumler, Bernd Kress, Friedhold Wölfel and all the members of the mechanical workshop for helping me with their technical knowledge and support as well as constructing or repairing various parts of the machine to enable outstanding experimental working conditions.

To Susana Kreß and Andrea Meixner-Wolf for helping me with many little, but important bureaucratic things, so that I could focus mostly on scientific problems.

Special thanks to my friends and family who always supported me and made all my successes possible. No matter how big the setbacks were, you always encouraged me to overcome them. The most important role played my wife by supporting me with patience and encouragement.

10 Appendix

10.1 List of Publications

[P1] **Metalation and coordination reactions of 2H-*meso*-*trans*-di(*p*-cyanophenyl)porphyrin on Ag(111) with coadsorbed cobalt atoms,** J. Kuliga, L. Zhang, M. Lepper, D. Lungerich, H. Hölzel, N. Jux, H.-P. Steinrück, and H. Marbach, *Phys.Chem.Chem.Phys.*, ***20***, 25062-25068 (**2018**); 10.1039/C8CP05255G

[P2] **Conformation Controls Mobility: 2H-Tetranaphthylporphyrins on Cu(111),** J. Kuliga, S. Massicot, R. Adhikari, M. Ruppel, N. Jux, H.-P. Steinrück, and H. Marbach, *ChemPhysChem, **21**,* 423-427 (**2020**); 10.1002/cphc.201901135

[P3] **Metalation of 2HTCNPP on Ag(111) with Zn: Evidence for the Sitting atop Complex at Room Temperature,** J. Kuliga, R. de Campos Ferreirra, R. Adhikari, S. Massicot, M. Lepper, H. Hölzel, N. Jux, H. Marbach, A. de Siervo, and H.-P. Steinrück, *ChemPhysChem, **22**,* 396-403 (**2021**); 10.1002/cphc.202000883

[P4] **On the adsorption of different tetranaphthylporphyrins on Cu(111) and Ag(111),** J. Brox, R. Adhikari, M. Shaker, M. Ruppel, N. Jux, H. Marbach, S. Jaekel, and H.-P. Steinrück, *Surface Science, **720**,* 122047 (**2022**); 10.1016/j.susc.2022.122047

10.1.1 [P1]

Metalation and coordination reactions of 2H-*meso*-*trans*-di(*p*-cyanophenyl)porphyrin on Ag(111) with coadsorbed cobalt atoms

J. Kuliga, L. Zhang, M. Lepper, D. Lungerich, H. Hölzel, N. Jux, H.-P. Steinrück, and H. Marbach, *Phys.Chem.Chem.Phys.*, ***20***, 25062-25068 (**2018**); 10.1039/C8CP05255

PCCP

ROYAL SOCIETY OF CHEMISTRY

PAPER

View Article Online
View Journal | View Issue

Cite this: *Phys. Chem. Chem. Phys.*, 2018, **20**, 25062

Metalation and coordination reactions of 2*H*-*meso*-*trans*-di(*p*-cyanophenyl)porphyrin on Ag(111) with coadsorbed cobalt atoms†

Jan Kuliga,[ab] Liang Zhang,[ab] Michael Lepper,[ab] Dominik Lungerich,[bc] Helen Hölzel,[bc] Norbert Jux,[bc] Hans-Peter Steinrück[ab] and Hubertus Marbach *[ab]

Received 17th August 2018,
Accepted 14th September 2018

DOI: 10.1039/c8cp05255g

rsc.li/pccp

We investigated the metalation and coordination reactions of Co with 2*H*-5,15-bis(*para*-cyanophenyl)-10,20-bisphenylporphyrin (2*Htrans*DCNPP) on a Ag(111) surface by scanning tunneling microscopy. At room temperature (RT), 2*Htrans*DCNPPs self-assemble into a supramolecular structure stabilized by intermolecular hydrogen bonding. The metalation of 2*Htrans*DCNPP is achieved either by depositing Co atoms onto the supramolecular structure at RT, or, alternatively, by depositing the molecules onto a submonolayer Co-precovered Ag(111) surface with a subsequent heating to 500 K. In addition, the molecules coordinate to Co atoms through the N atoms in the peripheral cyano groups with a preference of isolated 4-fold coordination motifs at RT.

Introduction

The investigation of functional molecules on solid surfaces has become a vivid research field in fundamental and applied sciences, with the goal to fabricate novel molecular based devices. The rational design of functional molecular architectures *via* surface-confined coordination chemistry was identified as a promising route to target this goal.[1,2] Such systems represent a new class of functional materials, which promise unique functionalities from unsaturated metal centers and/or the molecular ligands. A particularly promising family of molecular building blocks are porphyrins with functional peripheral substituents.[3–10] Related studies mainly focused on relevant surface reactions such as the direct metalation of the porphyrin macrocycle, coordination of additional ligands and cross-linking *via* surface coordinative bonds.[3–8]

The reaction of porphyrins with coadsorbed metal atoms under ultrahigh vacuum (UHV) conditions is especially interesting for the *in situ* synthesis of reactive metalloporphyrins such as iron(II)-tetraphenylporphyrins. The latter are difficult to handle outside the vacuum, due to their high affinity toward oxygen.[11,12] The metalation is a redox reaction and has been studied for a variety of porphyrins, with different substituents and with different metals, such as Ce,[13] Co,[6,7,14] Cu,[15–20] Fe,[11,12,21] Ni[22,23] and Zn.[14,24] In a combined experimental and theoretical study of this complex reaction, it was initially proposed that the metal atom is first coordinated to the four N atoms of the intact porphyrin, and thereafter, the two aminic hydrogen atoms are successively transferred to the metal center, where they recombine and desorb as molecular hydrogen (H_2).[14] However, for 2*H*-tetraphenylporphyrins (2HTPP) on a Cu(111) surface, it was recently demonstrated by means of temperature-programmed desorption that the hydrogen atoms are not directly released as H_2 into the gas phase, but are first transferred to the substrate and associatively desorb from there.[19] The theoretical studies of this reaction mechanism in a gas phase reaction predict that Fe and Co species react with porphyrin at RT, whereas elevated temperatures are required for Cu and Zn atoms, as confirmed in various experimental studies on adsorbed porphyrins.[6,7,11,12,14,21,24] Besides metalation of porphyrins coadsorbed metal atoms can also be utilized to interlink porphyrins *via* metal–organic bond formation on the surface.[5,8,25–28]

In this work, we report on the self-assembly and reaction of 2*H*-5,15-bis(*para*-cyanophenyl)-10,20-bisphenylporphyrin (2*Htrans*DCNPP) with coadsorbed Co atoms on a Ag(111) surface investigated by scanning tunneling microscopy (STM). We show that deposition of Co atoms on the surface pre-covered with

---

[a] *Lehrstuhl für Physikalische Chemie II, Friedrich-Alexander-Universität Erlangen-Nürnberg, Egerlandstr. 3, 91058 Erlangen, Germany. E-mail: hubertus.marbach@fau.de*

[b] *Interdisciplinary Center for Molecular Materials (ICMM), Friedrich-Alexander-Universität Erlangen-Nürnberg, Nikolaus-Fiebiger-Str. 10, 91058 Erlangen, Germany*

[c] *Lehrstuhl für Organische Chemie II, Friedrich-Alexander-Universität Erlangen-Nürnberg, Nikolaus-Fiebiger-Str. 10, 91058 Erlangen, Germany*

† Electronic supplementary information (ESI) available: Detailed evaluation of molecular arrangement of 2HtransDCNPP on Ag(111). See DOI: 10.1039/c8cp05255g

2*Htrans*DCNPP results in metalation of the molecules at RT. In addition, the metalated porphyrins also coordinate with Co atoms through the N atoms of the cyano groups at RT; annealing at 400 K enhances the process. However, no supramolecular metal–organic coordination network formation is observed.

Experimental

The experiments and sample preparations were performed in a two-chamber ultrahigh vacuum (UHV) system with a base pressure of $\sim 10^{-10}$ mbar. The microscope is an RHK UHV VT STM 300 with RHK SPM 100 electronics. The STM images were acquired at RT in constant current mode with a Pt/Ir tip. The given bias voltages refer to the sample. The STM images were processed with WSxM software and moderate filtering (Gaussian smooth, background subtraction) was applied for noise reduction. The Ag(111) single crystal was prepared by repeated cycles of Ar^+ sputtering (500 eV) and annealing to 850 K. The 2*Htrans*DCNPP molecules were deposited onto the Ag substrate at RT by thermal sublimation from a home-built Knudsen cell at 690 K. The coverage of the 2*Htrans*DCNPP monolayers on the Ag substrate was determined by STM. The molecular models were optimized with the MM2 force field calculation method implemented in Chem & Bio 3D.

Results and discussion

The deposition of 2*Htrans*DCNPP on Ag(111) at RT gives rise to the close-packed and well-ordered supramolecular structure shown in Fig. 1, which reflects a subtle balance between intermolecular and molecule–substrate interactions.[5,11,29] The lattice vectors of the unit cell are a = 1.61 ± 0.04 nm and b = 2.65 ± 0.03 nm, with an enclosed angle γ = 90 ± 3°; see Fig. 1b. This unit cell yields a molecular density of 0.47 molecules per nm^2 which corresponds to a coverage of 0.034 ML, with a ML defined as one adsorbate molecule or atom per substrate surface atom. Notably, about ~85% of the surface is covered with this structure, with the rest of the surface uncovered which results in an effective coverage of ~0.029 ML.

In order to further elucidate the arrangement of 2*Htrans*DCNPPs, the appearance of individual molecules in STM images has to be clarified first. Fig. 1c shows a close-up STM image of one molecule incorporated in a two-dimensional island; the same image is also shown in Fig. 1d with a scaled overlay of a space filling model of 2*Htrans*DCNPP. Similar to the intramolecular conformation of 2HTPP[11,29] and 2*H*-5,10,15,20-tetrakis(*para*-cyanophenyl)porphyrin (2HTCNPP)[25] on Ag(111), 2*Htrans*DCNPP appears as four protrusions in the periphery around a core with a depression in the center. The four protrusions show different lateral size, with two opposite protrusions larger and the other two smaller. From the molecular dimensions we assign the former to the cyano-phenyl groups and the latter to the "bare" phenyl groups. The good agreement between the STM image and the scaled molecular model in Fig. 1d further corroborates this assignment along with a detailed analysis documented in the ESI.†

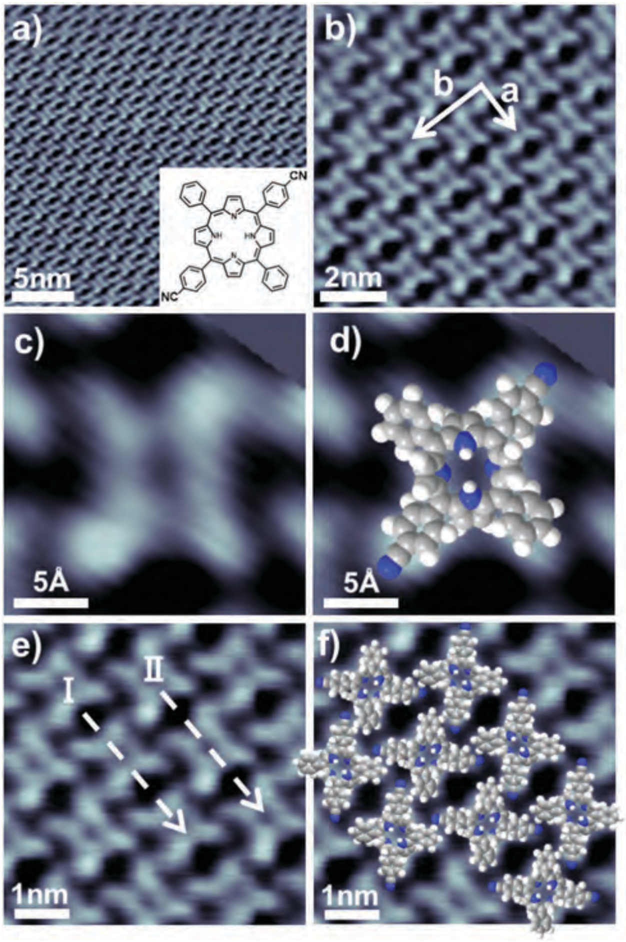

Fig. 1 (a and b) Constant current STM images of the self-assembled 2*Htrans*DCNPP on Ag(111). A unit cell is also overlaid in (b). (c) Close up STM image of one 2*Htrans*DCNPP molecule, and (d) the same image overlaid with the corresponding scaled space filling model. (e) Magnified detail of the center part of (a), and (f) the same image overlaid with the correspondingly scaled molecular models. Tunneling parameters: U = −0.1 V, I = 27 pA.

With the interpretation of the appearance of individual 2*Htrans*DCNPP molecules, the supramolecular arrangement within the islands is analyzed in detail. Fig. 1e shows a high resolution STM image clearly resolving the sub-molecular features in the structure. To facilitate the identification of both supramolecular and intramolecular features, the image is superimposed with scaled models of 2*Htrans*DCNPP (Fig. 1f): all molecules within a row (I) are oriented along the same direction while this azimuthal orientation switches by 90° in the neighboring rows (II). (The orientation of individual molecules is determined by the position of cyano groups.) Consequently, in every second row the molecules have the same molecular orientation. This supramolecular structure is likely to be stabilized by van der Waals interactions and intermolecular hydrogen bonding between terminal nitrogen atoms in the cyano group and hydrogen atoms of pyrrole groups of adjacent molecules in the neighboring rows.[15,30] It should be noted that for 2HTPP on Ag(111), the molecules self-assemble in domains with a square unit cell caused by the T-type intermolecular interactions between the peripheral phenyl substituents of neighboring molecules.[29] This is obviously not the case for 2*Htrans*DCNPP studied here. Closer inspection reveals, that the cyano groups ''avoid'' direct neighborhood, which can be understood by simple electrostatic considerations. In this regard the attachment of the cyano groups is obviously suitable to significantly influence the intermolecular interactions and thus to tailor the resulting supramolecular structure to some extent.

As next step, we deposited 0.012 ± 0.003 ML of Co, which is stoichiometrically roughly one third of the amount required to metalate all porphyrins on the surface (1 ML is defined as one adsorbate per substrate surface atom). Following Co deposition, a fraction of the molecules appear as protrusions in the STM images, while the others remain unchanged, see Fig. 2a. The observed protrusions are in line with an enhanced tunneling contribution through the Co(II) $3d_{z^2}$ orbitals and are a strong indication for metalation of the 2*Htrans*DCNPP molecules with Co to CotransDCNPP.[3,31] The fraction of CotransDCNPP (31%) is in good agreement with the amount of deposited Co.

The STM images of Fig. 2b and c were acquired after the successive deposition of equal amounts of 0.012 ± 0.003 ML Co onto the molecules, yielding 0.024 and 0.036 ML of deposited Co, respectively. The number of protrusions, that is CotransDCNPP molecules, increases roughly proportional to the amount of codeposited Co: the fraction of metalated molecules in Fig. 2 are (a) 31%, (b) 73% and (c) 97%; these numbers have to be compared to the values expected for a stoichiometric reaction which are (a) 41%, (b) 82% and (c) 120%, considering the effective starting coverage of 0.029 ML for 2*Htrans*DCNPP. Comparing these values under consideration of the margin of error (25% of the amount of deposited Co) it becomes immediately clear that the efficiency of the metalation reaction is close to 100%.

Notably, the supramolecular structure is maintained during the described metalation, despite the known affinity of CN groups to Co atoms favoring the formation of metal–organic networks at RT with related linkers.[27,28,32] As the evaporation of Co atoms on the surface is a statistical process, it can be ruled out that all Co atoms directly adsorb at the center of a 2*Htrans*DCNPP molecule. Therefore, at least some of the Co atoms have to diffuse to the corresponding sites and then metalate the molecules.[3] Similar observations were also reported for Co/2HTPP/Ag(111),[6,7] Fe/2HTPP/Ag(111),[11,12] Fe/2*H*-tetrapyridylporphyrin/Ag(111),[33] Fe/2*H*-octaethylporphyrin (2HOEP)/Ag(111),[34] Ni/2HOEP/Cu(111),[35] Co/2*H*-tetra(4-cyanophenyl)phenylporphyrin (2HTPCN)/Ag(111)[27] and Co/2HTPCN/BN/Cu(111).[28]

Further increase of the amount of deposited Co to 0.072 ML, which is stoichiometrically more than double the amount of Co needed for full metalation of the porphyrin layer, leads to a breakup of the supramolecular structure into a variety of disordered intermolecular arrangements, as is shown in Fig. 3a. This process is even more pronounced after annealing at 400 K, after which most molecules have formed disordered clusters or cannot be imaged any more (Fig. 3b). Since the disordered clusters emerge exclusively upon the codeposition of excessive Co, we conclude that they must involve Co atoms. Previous studies of codeposited Co atoms and cyano-functionalized polyphenyl molecules demonstrated the formation of ordered metal–organic networks where each Co atom coordinates to three molecules with an angle of 120° between each other.[26,32] Notably, upon depositing more molecules than required for a saturated honeycomb mesh, 4-, 5- and 6-fold coordination of Co atoms was observed, which goes along with various pore shapes.[32] More relevant are the findings by Urgel *et al.*, who reported that cyano-functionalized porphyrins form 3-fold prevailed metal–organic coordination motifs with codeposited Co atoms on a Ag(111).[27] Based on the overall similarity of the latter system and 2*Htrans*DCNPP, we propose that the disordered clusters found after the deposition of over-stoichiometric Co amounts is due to the formation of Co-CotransDCNPP coordination compounds. Apparently, the stepwise deposition of Co first leads to metalation of the free-base 2*Htrans*DCNPP at RT with high efficiency. Upon increasing the total amount of Co on the surface significantly above the stoichiometrically amount needed to metalate all molecules we propose the formation of Co-coordinated

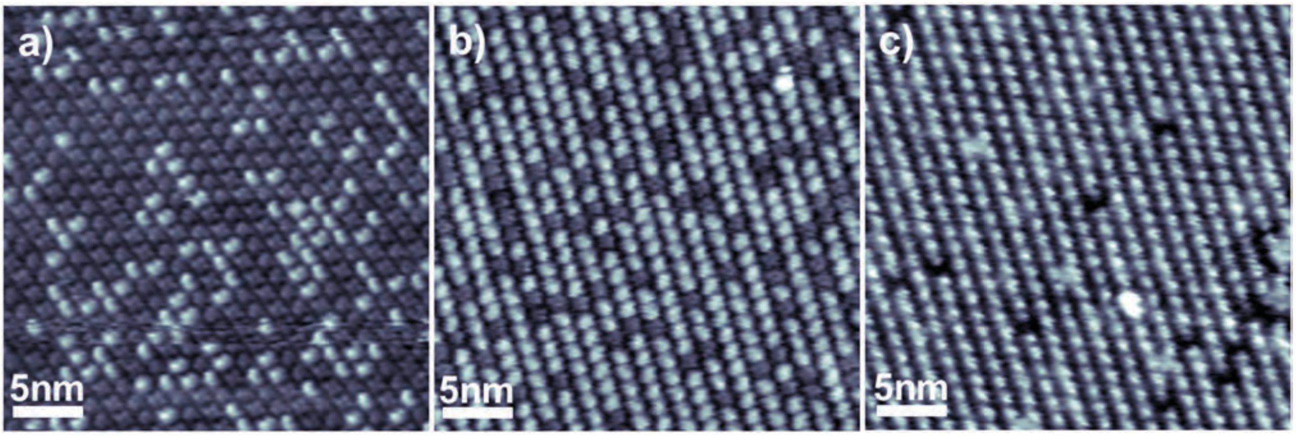

Fig. 2 Constant current STM images of a monolayer of 2*Htrans*DCNPP molecules after the incremental deposition of Co (0.012 ML in each step). Tunneling parameters: U = −1.0 V, I = 29 pA.

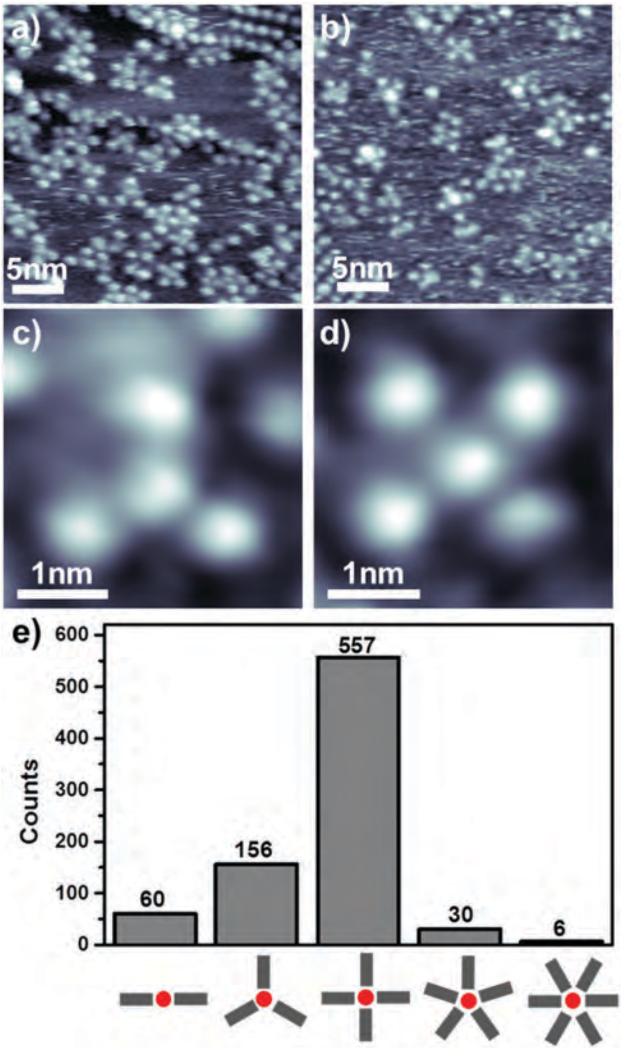

Fig. 3 (a) STM image of amorphous metal–organic structure of metalated 2*Htrans*DCNPP (CotransDCNPP) and Co formed at RT. (b) STM image of the amorphous coordination structure observed after annealing the sample to 400 K. (c and d) STM images of two representative coordination motifs observed in experimental results; (e) distribution of the number of CotransDCNPP molecules coordinating to a Co atom. Tunneling parameters: $U = -1.0$ V, $I = 29$ pA.

CotransDCNPP structures. However, these coordination structures lead to a breaking up of the ordered supramolecular arrangement. While the preceding metalation occurs at RT and without further thermal treatment, the proposed subsequent coordination is promoted by 400 K annealing. One simple way to understand this behavior is that for the metalation the Co atoms can easily diffuse to the porphyrins bound in the supramolecular structure at RT. However, additional thermal energy for the rearrangement of molecules is needed, *e.g.*, to overcome activation barriers for diffusion, to realize the formation of the observed coordination structures.

Fig. 3c and d display the STM images of two representative motifs observed in our study. All observed motifs (see Fig. 3e) have in common that two to six protrusions are arranged around one central protrusion (marked in red in Fig. 3e). The average distance of an ''outer'' protrusion to a central protrusion is 1.0 ± 0.1 nm irrespective of the actual motif.

This estimated distance is much too small to identify all protrusions with CotransDCNPP molecules. This is evident, considering the lattice parameter $a = 1.61 \pm 0.04$ nm estimated for the molecular order discussed in detail above. As discussed above, at the given negative bias voltages, *i.e.*, sensitive to the HOMO of the CotransDCNPP molecules, the appearance of a central round protrusion is fully expected. This can be explained by a strong contribution of an orbital-mediated tunneling process *via* the hybrid Co(d_{z^2})–Ag orbital of the adsorption complex, induced by molecule–substrate interactions.[3,31] We speculate that a Co atom coordinated by two to six nitrogen atoms from cyano groups might exhibit a similar appearance as a Co atom coordinated by four nitrogen atoms in the porphyrin macrocycle. Based on the latter consideration in combination with the short protrusion–protrusion distances we propose that the central protrusions are Co atoms coordinated by the cyano groups of surrounding CotransDCNPP molecules. This interpretation is also supported by a control experiment without deposition of Co, in which only the closed packed arrays of molecules were observed after the corresponding annealing procedure. To verify our interpretation STM images at the same position with both negative and positive bias voltages were acquired. The motivation of this course of action is that at positive bias voltage the corresponding STM images of Co-porphyrins rather reflect the topography of the molecules than the pronounced electronic effect at negative bias. It should be mentioned that the corresponding experiments are extremely demanding, nevertheless we could acquire some conclusive data as depicted in Fig. 4.

In the upper two rows of Fig. 4 two examples of bias switching (first column: negative bias, second column: positive bias) along with the corresponding STM images overlayed with scaled models (third column). Fig. 4a depicts one of the most frequently observed five-protrusion motifs acquired at negative bias voltage. The exact same region of interest is depicted in Fig. 4b, now at positive bias voltage. From this STM image one can clearly identify the four outer protrusions in Fig. 4a as CotransDCNPP molecules, while no porphyrin is observed in Fig. 4b at the position of the central protrusion in Fig. 4a. Instead a rather small protrusion is observed which we assign to Co. The corresponding arrangement is depicted in Fig. 4c with the superimposed scaled molecular models and the Co center indicated as red dot. Again, it should be mentioned that the acquisition of such polarity switching STM images is extremely demanding and time consuming in our instrument. This is probably due to unintended tip modifications due to the bias switching in combination with the existence of mobile material at room temperature. In this regard it should be pointed out, that the observed motif deviates from the vast majority of other five-protrusion motifs, since the characteristic distances in the particular case shown in Fig. 4a–c is with 1.2 ± 0.1 nm somewhat enlarged in comparison to the average value of 1 ± 0.1 nm. The typical distance is resembled by the STM images shown in Fig. 4d–f. However, in that case the central spot is missing at negative bias as depicted in Fig. 4a.

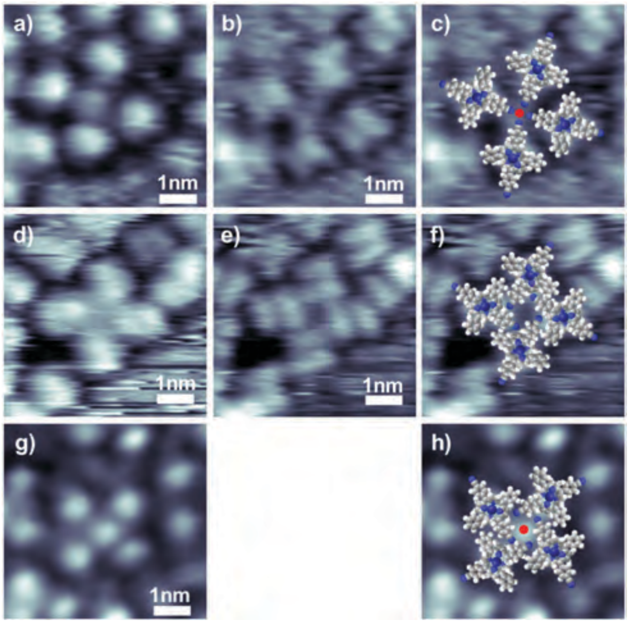

Fig. 4 Bias dependent STM measurements. The first column (a, d and g) presents images measured with negative bias. The second column (b and e) depicts the images measured at the same position but with positive bias. In the third column (c, f and h) the images are presented with overlayed scaled models. Tunneling parameters: (a and d) U = −1.0 V, I = 29 pA. (b and c) U = +1.0 V, I = 29 pA. (e) U = +1.7 V, I = 29 pA. (g and h) U = −0.1 V, I = 30 pA.

This is again referred to a specific tip modification, since all motifs at this measurement appeared without the central protrusion at negative bias, which reappeared on the same preparation after some time and a presumed tip chance. However, in the latter case it was not possible to image at positive bias. Fig. 4g reproduces Fig. 3d in which the four outer protrusions have the same arrangement and measurements. We therefore conclude that the underlying molecular arrangement is also identical. The corresponding conformation is revealed by the STM image acquired at positive bias depicted in Fig. 4e. Here an ''windmill'' arrangement is observed (see Fig. 4f and h). We propose that this arrangement is indeed the dominating motif since it also resembles a distance of the center of the CotransDCNPP molecules to the center of the supramolecular arrangement, *i.e.* the position of the central Co atom of 1 ± 0.1 nm. It should be mentioned that the oxidation state of Co in CotransDCNPP and in coordination nodes might be different.[15,28] Indeed, in analogy to free Co-TPP,[6] an oxidation state of 2+ is assumed for isolated CotransDCNPP, while the Co coordination nodes might maintain the 0 oxidation state of isolated adatoms,[28] which might explain that the central coordinating Co atom is invisible in Fig. 4d. Based on the presented evidence along with a lack of plausible alternative explanations we conclude that the observed features are indeed CotransDCNPP molecules linked *via* Co atoms.

It is interesting to note that these metal–organic coordination motifs do not form extended 2D networks with the metalated CotransDCNPP in our experiments. We speculate that the absence of long-range order as observed here might be related to the symmetry and lattice mismatch between the coordination structure and the hexagonal substrate.[27] Another possibility might be that we did not explore the right preparation parameters, *i.e.*, that the observed coordination motifs are kinetically trapped.[36]

For further insight into the formed organic-metal coordination compounds, a statistical analysis of ∼800 molecules was performed. The distribution of coordination numbers is shown in Fig. 3e. Motifs ranging from 3-fold up to 6-fold coordination can be found, with the 4-fold coordination dominating the scheme. Additional Co clusters found on the terraces exclude the shortage of metal atoms as a possible reason for the diverse coordination structures.[32] We propose that the 4-fold coordination bond is stronger than the other coordination bonds, but the energy difference between them is not sufficient to significantly favor one binding motif (4-fold) over the others (2-, 3-, 5-, 6-fold).[36] Note that metal dimer, trimers, and possibly larger clusters could constitute the coordination nodes, and therefore the coordination number depends on the cluster size.[36–38] However, there is no experimental evidence to support this hypothesis and so far the literature reports unanimously agree that cyano groups coordinate to only one metal center.[26–28,32] Notably, the appearance of 5- and 6-fold lateral coordination is surprising considering steric limitations, and could indicate that the CotransDCNPP molecules in these coordination motifs are not flat-lying but are tilted with respect to the surface due to the repulsion between neighboring molecules or even that involved molecules are actually damaged, *e.g.*, are missing a side group or the likes.

Based on the discussion above, we conclude that the 2*Htrans*DCNPPs are metalated and coordinated by post-deposited Co atoms at the porphyrin core and the peripheral cyano groups, respectively. A next logical step is to explore these reactions by changing the sequence of the deposited materials, that is, to first deposit the metal and then the porphyrins. Fig. 5a and b show the STM images of a Ag(111) surface before and after the deposition of ∼0.1 ML of Co at RT. The result reveals that Co atoms form three-dimensional islands which decorate the atomic steps on the Ag(111) surface.

After the deposition of roughly a closed monolayer 2*Htrans*DCNPP onto the Co precovered Ag(111) at RT, a homogeneous adlayer of 2*Htrans*DCNPP is observed on terraces, in addition to the Co cluster at the steps, (Fig. 5c). The molecules show the same supramolecular structure as on clean Ag(111). The coexistence of Co clusters and the porphyrin molecules in the undisturbed island structure indicates that the metalation reaction at RT is very slow at the given conditions.

Interestingly, heating to 500 K leads to the partial formation of CotransDCNPP, as shown Fig. 5d. The bright species are assigned to CotransDCNPP (43%) and the dim species to 2*Htrans*DCNPP (57%). The required annealing step indicated that in the clusters the Co atoms are relatively strongly bound and consequently heating is necessary to dissolve the Co clusters and make the individual Co atoms available for metalation *via* diffusion to a 2*Htrans*DCNPP molecule. In other words, metalation with pre-deposited Co atoms is kinetically hindered,

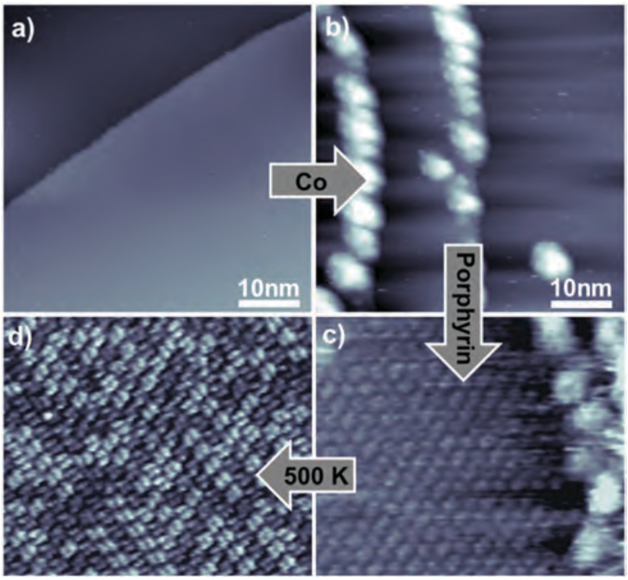

Fig. 5 (a) STM image of the clean Ag(111). (b) STM image showing the nucleation of Co on step edges of Ag(111). (c) 2*Htrans*DCNPP monolayer prepared *via* vapor deposition onto the surface depicted in Fig. 4b. (d) Situation after heating the surface shown in Fig. 4c to 500 K. The bright spots in the image are assigned to CotransDCNPP formed by metalation of 2*Htrans*DCNPP. Tunneling parameters: (a) $U = -1.0$ V, $I = 29$ pA; (b) $U = -1.3$ V, $I = 30$ pA; (c and d) $U = 1.0$ V, $I = 30$ pA.

and heating is necessary to overcome the kinetic hindrance.[3,11,24] At higher heating temperatures, the supramolecular ordering is totally degraded, and the uniform shape of the molecules is no longer present (not shown). This is most likely due to the decomposition of the molecules. As a consequence, no metal–organic coordination structures are observed.

Conclusions

We have demonstrated that 2*Htrans*DCNPP molecules on Ag(111) exhibit a bifunctional behavior toward coadsorbed Co atoms. In a first step, the molecules react with Co atoms through the four N atoms in the macrocycle under formation of CotransDCNPP. If Co is deposited onto 2*Htrans*DCNPPs, the reaction proceeds rapidly and efficiently at RT; if Co is deposited first, the metalation reaction requires elevated temperatures. As a second step, the peripheral cyano groups can also coordinate with Co atoms with a preferred 4-fold coordination motif, but also 3-fold, five-fold and six-fold motifs. The metal–organic coordination structures appear at RT and annealing at 400 K enhances the coordination process.

Conflicts of interest

There are no conflicts to declare.

Acknowledgements

The authors gratefully acknowledge the funding by the German Research Council (DFG) through research unit FOR 1878/funCOS, the Cluster of Excellence 'Engineering of Advanced Materials' (http://www.eam.uni-erlangen.de) and by the Collaborative Research Center SFB 953 at the Friedrich-Alexander-Universität Erlangen-Nürnberg. L. Z. thanks the Alexander von Humboldt Foundation for a research fellowship. M. L. and D. L. thank the Graduate School Molecular Science (GSMS) for financial support.

Notes and references

1 J. V. Barth, G. Costantini and K. Kern, *Nature*, 2005, **437**, 671–679.

2 L. Bartels, *Nat. Chem.*, 2010, **2**, 87–95.

3 H. Marbach, *Acc. Chem. Res.*, 2015, **48**, 2649–2658.

4 H. Marbach and H.-P. Steinrück, *Chem. Commun.*, 2014, **50**, 9034.

5 J. M. Gottfried, *Surf. Sci. Rep.*, 2015, **70**, 259–379.

6 J. M. Gottfried, K. Flechtner, A. Kretschmann, T. Lukasczyk and H.-P. Steinrück, *J. Am. Chem. Soc.*, 2006, **128**, 5644–5645.

7 J. M. Gottfried and H. Marbach, *Z. Phys. Chem.*, 2009, **223**, 53–74.

8 W. Auwärter, D. Écija, F. Klappenberger and J. V. Barth, *Nat. Chem.*, 2015, **7**, 105–120.

9 L. Zhang, M. Lepper, M. Stark, D. Lungerich, N. Jux, W. Hieringer, H.-P. Steinrück and H. Marbach, *Phys. Chem. Chem. Phys.*, 2015, **17**, 13066–13073.

10 M. Lepper, L. Zhang, M. Stark, S. Ditze, D. Lungerich, N. Jux, W. Hieringer, H.-P. Steinrück and H. Marbach, *J. Phys. Chem. C*, 2015, **119**, 19897–19905.

11 F. Buchner, K. Flechtner, Y. Bai, E. Zillner, I. Kellner, H.-P. Steinrück, H. Marbach and J. M. Gottfried, *J. Phys. Chem. C*, 2008, **112**, 15458–15465.

12 F. Buchner, V. Schwald, K. Comanici, H.-P. Steinrück and H. Marbach, *ChemPhysChem*, 2007, **8**, 241–243.

13 A. Weber-Bargioni, J. Reichert, A. Seitsonen, W. Auwärter, A. Schiffrin and J. Barth, *J. Phys. Chem. C*, 2008, **112**, 3453–3455.

14 T. E. Shubina, H. Marbach, K. Flechtner, A. Kretschmann, N. Jux, F. Buchner, H.-P. Steinrück, T. Clark and J. M. Gottfried, *J. Am. Chem. Soc.*, 2007, **129**, 9476–9483.

15 Y. Li, J. Xiao, T. E. Shubina, M. Chen, Z. L. Shi, M. Schmid, H.-P. Steinrück, J. M. Gottfried and N. Lin, *J. Am. Chem. Soc.*, 2012, **134**, 6401–6408.

16 M. Stark, S. Ditze, M. Lepper, L. Zhang, H. Schlott, F. Buchner, M. Röckert, M. Chen, O. Lytken and H.-P. Steinrück, *Chem. Commun.*, 2014, **50**, 10225–10228.

17 L. Zhang, M. Lepper, M. Stark, R. Schuster, D. Lungerich, N. Jux, H.-P. Steinrück and H. Marbach, *Chem. – Eur. J.*, 2016, 3347–3354.

18 K. Diller, F. Klappenberger, M. Marschall, K. Hermann, A. Nefedov, C. Wöll and J. V. Barth, *J. Chem. Phys.*, 2012, **136**, 014705.

19 M. Röckert, M. Franke, Q. Tariq, D. Lungerich, N. Jux, M. Stark, A. Kaftan, S. Ditze, H. Marbach, M. Laurin, J. Libuda, H.-P. Steinrück and O. Lytken, *J. Phys. Chem. C*, 2014, **118**, 26729–26736.

20 S. Ditze, M. Stark, M. Drost, F. Buchner, H.-P. Steinrück and H. Marbach, *Angew. Chem., Int. Ed.*, 2012, **51**, 10898–10901.

21 D. Ecija, M. Trelka, C. Urban, P. D. Mendoza, E. Mateo-Martí, C. Rogero, J. A. Martín-Gago, A. M. Echavarren, R. Otero and J. M. Gallego, *J. Phys. Chem. C*, 2008, **112**, 8988–8994.

22 M. Chen, X. F. Feng, L. Zhang, H. X. Ju, Q. Xu, J. F. Zhu, J. M. Gottfried, K. Ibrahim, H. J. Qian and J. O. Wang, *J. Phys. Chem. C*, 2010, **114**, 9908–9916.

23 C. Wang, Q. Fan, S. Hu, H. Ju, X. Feng, Y. Han, H. Pan, J. Zhu and J. M. Gottfried, *Chem. Commun.*, 2014, **50**, 8291–8294.

24 A. Kretschmann, M. M. Walz, K. Flechtner, H.-P. Steinrück and J. M. Gottfried, *Chem. Commun.*, 2007, 568–570.

25 M. Lepper, T. Schmitt, M. Gurrath, M. Raschmann, L. Zhang, M. Stark, H. Hölzel, N. Jux, B. Meyer, M. A. Schneider, H.-P. Steinrück and H. Marbach, *J. Phys. Chem. C*, 2017, **121**, 26361–26371.

26 U. Schlickum, R. Decker, F. Klappenberger, G. Zoppellaro, S. Klyatskaya, M. Ruben, I. Silanes, A. Arnau, K. Kern and H. Brune, *Nano Lett.*, 2007, **7**, 3813–3817.

27 J. I. Urgel, D. Ecija, W. Auwärter, D. Stassen, D. Bonifazi and J. V. Barth, *Angew. Chem., Int. Ed.*, 2015, **54**, 6163–6167.

28 J. I. Urgel, M. Schwarz, M. Garnica, D. Stassen, D. Bonifazi, D. Ecija, J. V. Barth and W. Auwärter, *J. Am. Chem. Soc.*, 2015, **137**, 2420–2423.

29 F. Buchner, I. Kellner, W. Hieringer, A. Görling, H.-P. Steinrück and H. Marbach, *Phys. Chem. Chem. Phys.*, 2010, **12**, 13082–13090.

30 W. Auwärter, A. Weber-Bargioni, A. Riemann, A. Schiffrin, O. Gröning, R. Fasel and J. V. Barth, *J. Chem. Phys.*, 2006, **124**, 194708.

31 F. Buchner, K. G. Warnick, T. Wölfle, A. Görling, H.-P. Steinrück, W. Hieringer and H. Marbach, *J. Phys. Chem. C*, 2009, **113**, 16450–16457.

32 U. Schlickum, F. Klappenberger, R. Decker, G. Zoppellaro, S. Klyatskaya, M. Ruben, K. Kern, H. Brune and J. Barth, *J. Phys. Chem. C*, 2010, **114**, 15602–15606.

33 W. Auwärter, A. Weber-Bargioni, S. Brink, A. Riemann, A. Schiffrin, M. Ruben and J. V. Barth, *ChemPhysChem*, 2007, **8**, 250–254.

34 Y. Bai, F. Buchner, M. T. Wendahl, I. Kellner, A. Bayer, H.-P. Steinrück, H. Marbach and J. M. Gottfried, *J. Phys. Chem. C*, 2008, **112**, 6087–6092.

35 S. Ditze, M. Röckert, F. Buchner, E. Zillner, M. Stark, H.-P. Steinrück and H. Marbach, *Nanotechnology*, 2013, **24**, 115305.

36 S. Krotzky, C. Morchutt, V. S. Vyas, B. V. Lotsch, R. Gutzler and K. Kern, *J. Phys. Chem. C*, 2016, **120**, 4403–4409.

37 S. Stepanow, M. Lingenfelder, A. Dmitriev, H. Spillmann, E. Delvigne, N. Lin, X. Deng, C. Cai, J. V. Barth and K. Kern, *Nat. Mater.*, 2004, **3**, 229–233.

38 F. Bebensee, K. Svane, C. Bombis, F. Masini, S. Klyatskaya, F. Besenbacher, M. Ruben, B. Hammer and T. R. Linderoth, *Angew. Chem., Int. Ed.*, 2014, **53**, 12955–12959.

Electronic Supplementary Material (ESI) for Physical Chemistry Chemical Physics.
This journal is © the Owner Societies 2018

Supplementary Information to:

Metalation and coordination reactions of 2H-meso-trans-di(p-cyanophenyl)porphyrin on Ag(111) with coadsorbed cobalt atoms

Jan Kuliga,[a,b] Liang Zhang,[a,b] Michael Lepper,[a, b] Dominik Lungerich,[b,c] Helen Hölzel,[b,c] Norbert Jux,[b,c]
Hans-Peter Steinrück,[a,b] and Hubertus Marbach [a,b*]

a. Lehrstuhl für Physikalische Chemie II, Friedrich-Alexander-Universität Erlangen-Nürnberg, Egerlandstr. 3, 91058 Erlangen, Germany.

b. Interdisciplinary Center for Molecular Materials (ICMM), Friedrich-Alexander-Universität Erlangen-Nürnberg, Nikolaus-Fiebiger-Str. 10, 91058 Erlangen, Germany.

c. Lehrstuhl für Organische Chemie II, Friedrich-Alexander-Universität Erlangen-Nürnberg, Nikolaus-Fiebiger-Str. 10, 91058 Erlangen, Germany.

Closer Inspection of molecular arrangement of 2HtransDCNPP on Ag(111)

To further elucidate the molecular order in particular the peculiar orientational arrangement of the 2HtransDCNPP molecules on Ag(111) we did measurements of the relevant molecular axes as documented in Fig. SI1 and Table SI1. The values clearly show alternating behavior (…larger value-smaller value-larger value-smaller value….) along the horizontal and vertical directions as expected from the proposed model (c.f. Fig. 1 in main manuscript). However in a few cases (indicated with red background in Table SI1) the ratio of the axes was either wrong or not clear (ratio of 1). This triggered a closer inspection of the STM image and the correspondingly measured values. Since the slow scanning direction of the depicted micrograph was the vertical direction one might expect distortions in that direction due to thermal drift. Indeed we found by averaging the blue values separated by the directions in Table SI1 (8 times each molecular orientation) that the average of the "green" values was 1.52 nm while the corresponding value for the "red" direction amounts to 1.85 nm. This finding indicates a compression (probably due to thermal drift) in the vertical direction with a factor or 1.12. We therefore calculated the corrected values (column C Table SI1) and found that indeed with the comprehensible correction all values are in perfect agreement with the proposed molecular orientations of the 2HtransDCNPP molecules.

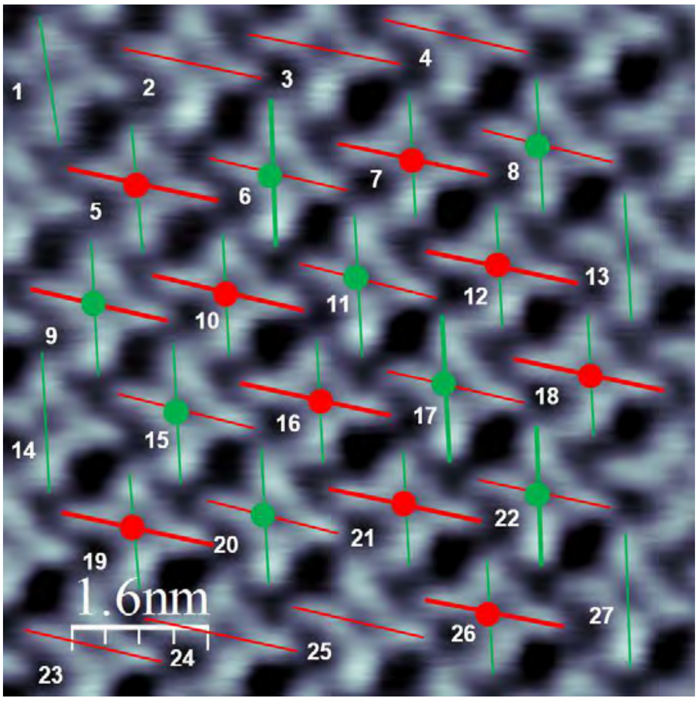

Figure SI1 *Constant current STM images of the self-assembled 2HtransDCNPP on Ag(111) as shown in Fig. 1 b in the original paper. The characteristic molecular axes were measured as indicated by the red (close to horizontal direction) and green (close to vertical direction) lines. The corresponding values are documented in Table SI 1. The individual 2HtransDCNPP are labelled with white numbers left of the molecules. Thicker lines within one molecule indicate which axis is longer for the actual molecule (if both are thin the length is equal). The green and red dots indicate which axis of the corresponding molecule is longer after correcting (drift correction) the vertical length as indicated in text. Tunneling parameters: U = -0.1 V, I = 27 pA.*

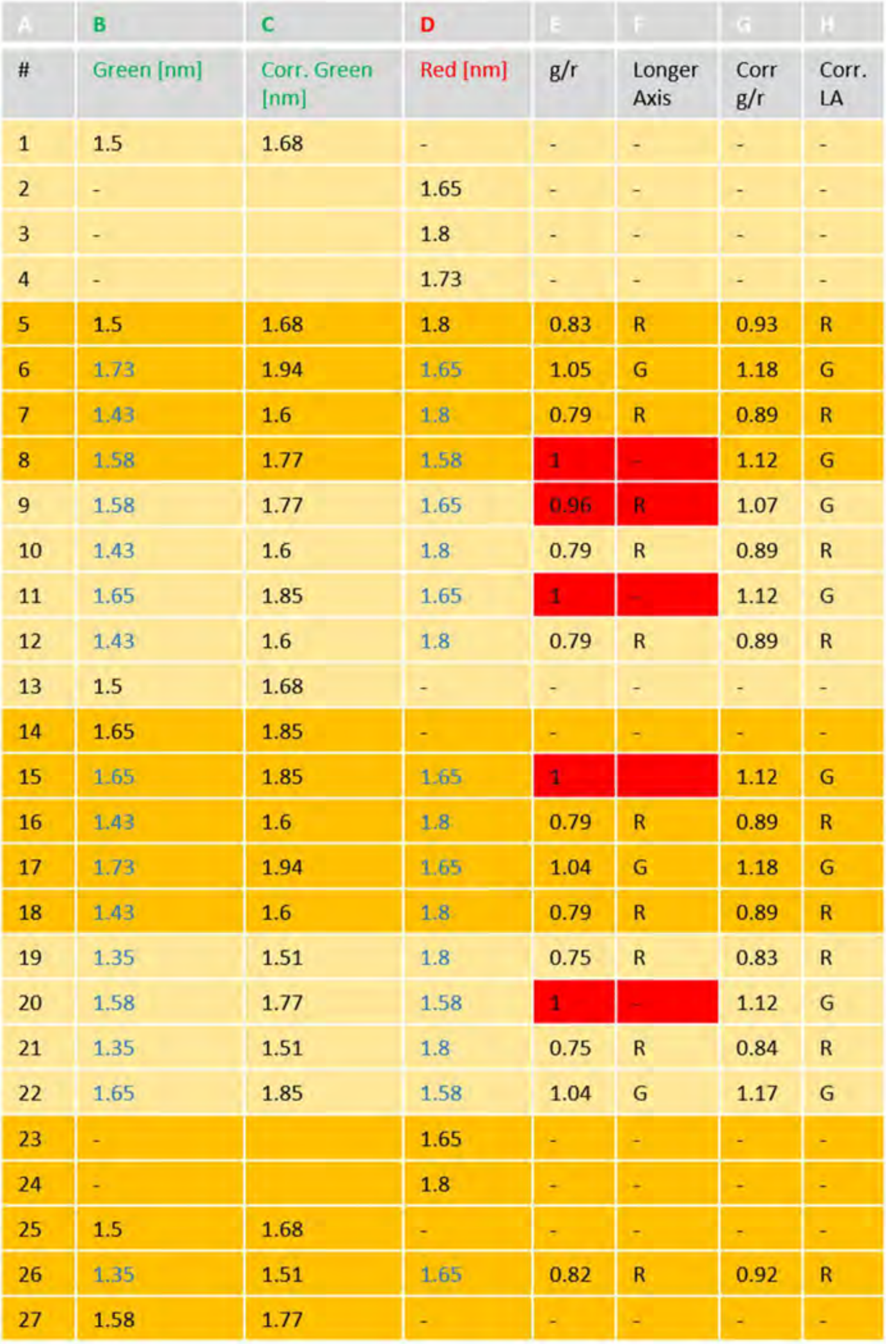

A	B	C	D	E	F	G	H
#	Green [nm]	Corr. Green [nm]	Red [nm]	g/r	Longer Axis	Corr g/r	Corr. LA
1	1.5	1.68	-	-	-	-	-
2	-		1.65	-	-	-	-
3	-		1.8	-	-	-	-
4	-		1.73	-	-	-	-
5	1.5	1.68	1.8	0.83	R	0.93	R
6	1.73	1.94	1.65	1.05	G	1.18	G
7	1.43	1.6	1.8	0.79	R	0.89	R
8	1.58	1.77	1.58	1	-	1.12	G
9	1.58	1.77	1.65	0.96	R	1.07	G
10	1.43	1.6	1.8	0.79	R	0.89	R
11	1.65	1.85	1.65	1	-	1.12	G
12	1.43	1.6	1.8	0.79	R	0.89	R
13	1.5	1.68	-	-	-	-	-
14	1.65	1.85	-	-	-	-	-
15	1.65	1.85	1.65	1		1.12	G
16	1.43	1.6	1.8	0.79	R	0.89	R
17	1.73	1.94	1.65	1.04	G	1.18	G
18	1.43	1.6	1.8	0.79	R	0.89	R
19	1.35	1.51	1.8	0.75	R	0.83	R
20	1.58	1.77	1.58	1	-	1.12	G
21	1.35	1.51	1.8	0.75	R	0.84	R
22	1.65	1.85	1.58	1.04	G	1.17	G
23	-		1.65	-	-	-	-
24	-		1.8	-	-	-	-
25	1.5	1.68	-	-	-	-	-
26	1.35	1.51	1.65	0.82	R	0.92	R
27	1.58	1.77	-	-	-	-	-

Table SI1 *Measured and processed values from Figure SI1. The following values are documented in the corresponding columns:* ***A*** *molecular labels;* ***B*** *measured values in nanometer along green lines as indicated in Fig. SI1;* ***C*** *drift corrected (see text) values from A;* ***D*** *correspondingly measured values for red lines;* ***E*** *ratio of axes within one molecule (length of green direction divided by red direction);* ***F*** *colour of longer axes (G:= green, R:= red);* ***G*** *ratio of axes with corrected values from column C analoge to column E;* ***H F*** *colour of longer axes with corrected values from C. The yellow and orange blocks indicate molecules within one "horizontal line". The red background indicate deviations from the proposed molecular order.*

10.1.2 [P2]

Conformation Controls Mobility: 2H-Tetranaphthylporphyrins on Cu(111)

J. Kuliga, S. Massicot, R. Adhikari, M. Ruppel, N. Jux, H.-P. Steinrück, and H. Marbach, *ChemPhysChem*, ***21***, 423-427 (**2020**); 10.1002/cphc.201901135

ChemPubSoc Europe

DOI: 10.1002/cphc.201901135

CHEMPHYSCHEM
Articles

Conformation Controls Mobility: 2H-Tetranaphthylporphyrins on Cu(111)

Jan Kuliga,[a, b] Stephen Massicot,[a, b] Rajan Adhikari,[a, b] Michael Ruppel,[b, c] Norbert Jux,[b, c] Hans-Peter Steinrück,[a, b] and Hubertus Marbach*[a, b]

The adsorption behavior and the mobility of 2H-Tetranaphthylporphyrin (2HTNP) on Cu(111) was investigated by scanning tunneling microscopy (STM) at room temperature (RT). The molecules adsorb, like the structurally related 2HTPP, in the "inverted" structure with the naphthyl plane restricted to an orientation parallel to the Cu surface. The orientation of the four naphthyl groups yields altogether 16 possible conformations. Due to the existence of rotamer pairs, 10 different appearances are expected on the surface, and all of them are identified by STM at RT. Most interestingly, the orientation of the naphthyl groups significantly influences the diffusion behavior of the molecules on Cu(111). We identify three different groups of conformers, which are either immobile, medium or fast diffusing at RT. The mobility seems to decrease with increasing size of the footprint of the conformers on the surface.

1. Introduction

The design and construction of functional architectures on the nanoscale is a very active research topic due to the growing demand for the miniaturization of devices.[1] A most promising approach is the bottom-up route, where complex organic molecules adsorb and eventually self-assemble on well-defined surfaces.[2] The choice of functional groups and molecular as well as substrate symmetry have a major impact on the adsorption behavior of the organic building blocks, and can even induce surface chirality.[3–8] In particular, the mobility of the molecules on the surface is of great importance, as it is a prerequisite for the formation of molecular networks. Different functional groups, orientation to the surface and shape can contribute to the diffusion behavior and mobility of large organic molecules.[9–11] Identifying the correlation of specific functional groups with this surface mobility thus is of very high interest.

Porphyrins are a most promising class of functional organic molecules, since they combine an intrinsic functionality governed by the coordination of different metal atoms at the center of the macrocycle, with their conformational flexibility. The latter leads to a large variety of supramolecular structures on surfaces.[12–14] Scanning tunneling microscopy (STM) has been proven as a powerful tool to investigate such arrangements, their intramolecular conformation and their electronic structure.[13,15] Extensive studies[2] have shown that the conformation and supramolecular arrangement strongly depend on the substrate,[16,17] molecular coverage,[18] presence and nature of a coordinated metal atom,[19,20] heat treatments[13,21] and functional side groups.[22] In this regard, 2H-tetraphenylporphyrin (2HTPP) has become a well-understood reference system.[23–27] On Cu(111), the strong chemical interaction between the iminic nitrogen atoms and the Cu substrate atoms leads to a peculiar intramolecular conformation, the so called "inverted" structure.[28,29] Based on the detailed knowledge of this structure, we herein now tackle the changes that occur when replacing the phenyl group by a naphthyl group to introduce a rotation axis in the molecular plane. For 2HTNP on Cu(111), assuming flat adsorption of the naphthyl groups, 16 different surface conformations are expected, including chiral and non-chiral species. Our systematic study by STM at room temperature documents that these different adsorption conformers can indeed be observed and, most interestingly, that their surface mobility strongly depends on the specific conformation.

2. Results and Discussion

As a first step, we describe and discuss the general adsorption behavior of 2HTNP on Cu(111). All STM images shown in this section were acquired at RT. Figure 1a depicts an STM image for a coverage of 0.0012 ML (1 ML refers to the one adsorbate molecule per substrate atom); this coverage corresponds to ~2–3% of a closed first layer of flat lying molecules. 2HTNPs adsorb as isolated molecules, which are aligned along one of

---

[a] *J. Kuliga, S. Massicot, R. Adhikari, Prof. Dr. H.-P. Steinrück, Dr. H. Marbach*
Lehrstuhl für Physikalische Chemie II
Universität Erlangen-Nürnberg
Egerlandstr. 3, 91058 Erlangen, Germany
E-mail: hubertus.marbach@fau.de

[b] *J. Kuliga, S. Massicot, R. Adhikari, M. Ruppel, Prof. Dr. N. Jux, Prof. Dr. H.-P. Steinrück, Dr. H. Marbach*
Interdisciplinary Center for Molecular Materials (ICMM)
Universität Erlangen-Nürnberg
Henkestr. 42, 91054 Erlangen, Germany

[c] *M. Ruppel, Prof. Dr. N. Jux*
Lehrstuhl für Organische Chemie II
Universität Erlangen-Nürnberg
Henkestr. 42, 91054 Erlangen, Germany

Supporting information for this article is available on the WWW under https://doi.org/10.1002/cphc.201901135

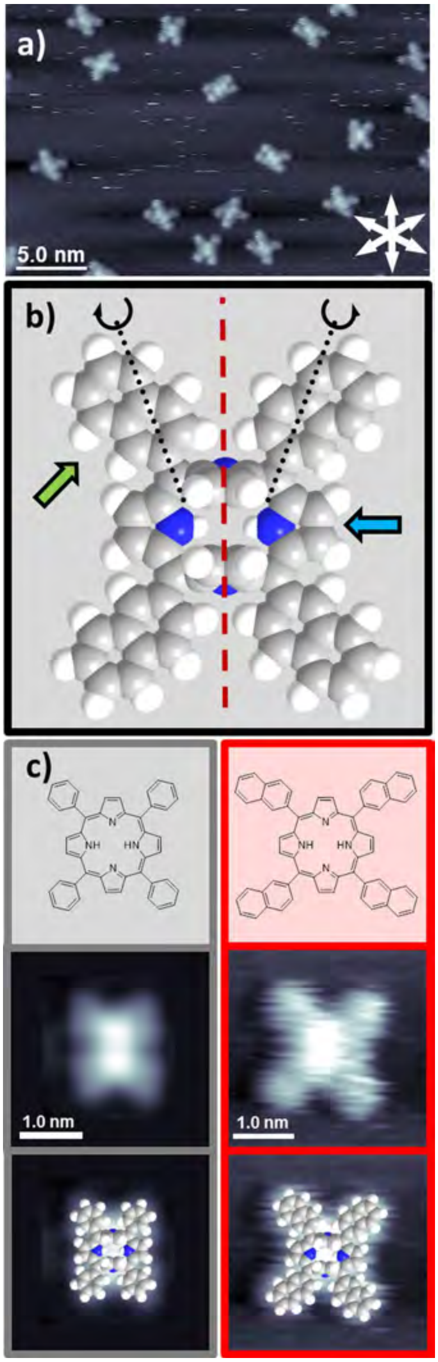

Figure 1. a) Constant-current STM image of a low coverage of 2HTNP, prepared and measured at RT. b) Top view of a space-filling model of the "inverted" structure of 2HTNP: Each naphthyl substituent (indicated by a green arrow) can be oriented away (α) or towards (τ) the main axis of the molecule through the iminic pyrrole groups (dashed red line); also shown is the tilt angle of the iminic (═N–) pyrrole group; the aminic pyrrole group is indicated by the blue arrow. c) Chemical structure, high-resolution STM image, and structural overlay of inverted space-filling models of 2HTPP (left) and 2HTNP (right) for comparison.

the three main crystallographic directions of Cu(111). High resolution STM images of individual molecules exhibit two (sometimes merged to one) elongated parallel protrusions in the center of the molecule, which are surrounded by four dimmer protrusions in the periphery. This adsorption behavior is very similar to the well-investigated 2HTPP, which adsorbs as isolated molecules on Cu(111) at low to medium coverages.[23] This specific molecular appearance is due to strong molecule-substrate interactions via the iminic nitrogen atoms of the porphyrin macrocycle. As a result, the iminic pyrrole groups are rotated slightly more than 90° out of the macrocycle plane, that is, their plane is oriented almost perpendicular to the surface. This structure is referred to as "inverted" and exhibits two protrusions, which are aligned along one of the three main crystallographic directions of Cu(111) (Figure 1c).[28] The strong similarity of the adsorption behavior and appearance of 2HTNP on Cu(111) to that of 2HTPP gives sufficient evidence to safely conclude that 2HTNP also adsorbs in the "inverted" structure. The four dimmer protrusions per molecule in Figure 1a resemble the flat lying naphthyl groups.

A molecular model of the "inverted" 2HTNP is depicted in Figure 1b. The iminic pyrrole groups are rotated upwards, while the aminic pyrrole groups (blue arrow) are parallel to the surface. For 2HTPP, the phenyl groups are parallel to the surface as well, and rotation of the phenyl group around the linking C–C bond by 180° leaves the symmetry of the molecule unchanged; see Figure 1c. In contrast, for 2HTNP, rotation of the flat-lying naphthyl groups (green arrow) around the linking C–C-bond (black dotted line) by 180° changes the symmetry of the molecule, which leads to a variety of possible conformations, including surface chiral and non surface chiral ones. In order to describe them, we introduce the α/τ -notation. In the α-orientation, the naphthyl group points away from the main molecular axis through the iminic pyrrole groups (red dashed vertical line in Figure 1b), while in the τ-orientation it points towards this axis. By indicating the orientations of the four groups clockwise, starting in the left upper corner of the molecule, we obtain 16 possible conformations.

Figure 2a shows three STM images, which contain altogether 10 different conformations of 2HTNP on Cu(111). A common feature is that the molecules are orientated with their main axis along one of the three main symmetry-equivalent crystallographic substrate directions. The fact that we did not observe 16 different conformations can be explained, if we consider that some molecules are rotamer pairs, that is, rotation by 180° does not lead to a new appearance (see below). In such cases, one appearance has to be attributed to two different α/τ-notations, which are obtained by switching the first two labels with the last two, e.g., $\alpha\alpha\tau\tau$ equals $\tau\tau\alpha\alpha$ (see Figure 3). This observation also indicates that the C_{3v} symmetry of the substrate can be neglected in the point group considerations of the different adsorbed conformers below.

In the following, all observed conformations are discussed according to their appearance, α/τ-notation, symmetry elements and point group. Selected STM images along with the categorization of the observed conformations are depicted in Figure 2. Starting with the X-shape conformation, the elongated central protrusion is surrounded by four dimmer protrusions in a symmetrical fashion. The molecule almost forms a square, with the apparent length and width values of 2.12 and 2.19 nm, respectively. According to the α/τ-notation, the conformation is

Figure 2. a) Three constant-current STM images showing the 10 surface conformations of 2HTNP highlighted by differently colored boxes. b) Name, α/τ -notation, chemical structure, high resolution STM image of a single molecule, STM image overlaid by a scaled space-filling model, point group, and mobility ranking (red: immobile, yellow: medium, green: fast) for all possible conformations. In case of equivalent rotamers, two α/τ -notations are denoted.

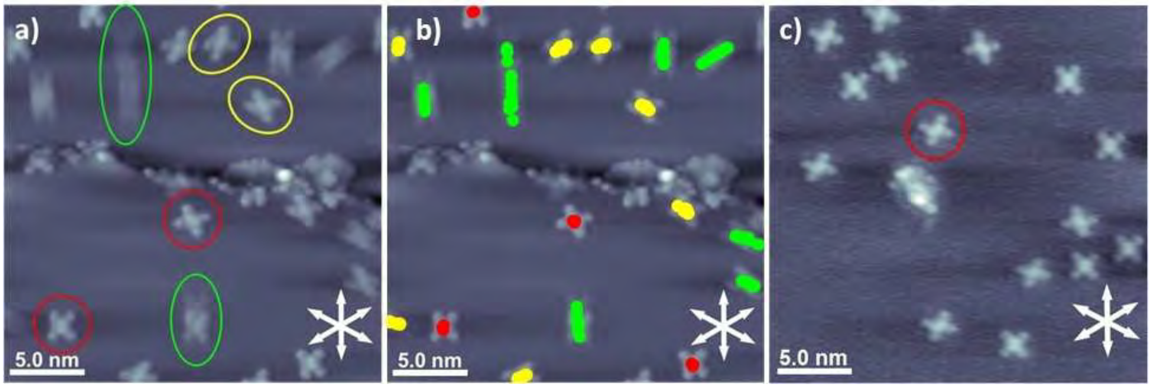

Figure 3. a) Average frames of STM movies of 2HTNP on Cu(111) at RT; $U=-1.15$ V, $I=30$ pA. b) Same image with the positions of the molecules color-coded in each single STM image, according to the observed mobility (red: immobile, yellow: medium, green: fast), and then superimposed over the corresponding STM average frames. c) Average frames of STM movies of 2HTNP on Cu(111) measured at RT after annealing to 400 K for 1 h; all molecules are immobile, as exemplarily indicated for one molecules; $U=-1.10$ V, $I=30$ pA.

$\alpha\alpha\alpha\alpha$. The molecule with two mirror planes belongs to the C_{2v} point group. For the I-shape, the central protrusion is again surrounded in a symmetric way by four dimmer protrusions, but it displays a rectangular shape with apparent length and width values of 2.25 and 1.48 nm, respectively. The conformation is $\tau\tau\tau\tau$, and the point group is again C_{2v}.

The next two shapes, K and T, are a mixture of the first two (X and I), and belong to the C_s point group. The K-shape has one mirror plane perpendicular to the main axis of the molecule. The two protrusions on the left side resemble the elongated protrusions of the I-shape, while the two protrusions on the right side mimic the X-shape. The notations of the corresponding rotamer conformations are $\tau\alpha\alpha\tau$ and $\alpha\tau\tau\alpha$. For the T-shape, the mirror plane is along the molecular axis. It has the two upper protrusions oriented like in the X-shape and the two lower ones are like in the I-shape (or vice versa). The notations of the corresponding rotamers are $\alpha\alpha\tau\tau$ and $\tau\tau\alpha\alpha$.

All conformations discussed so far are achiral adsorption motives. The remaining conformations are surface chiral, that is, they represent three enantiomeric pairs. In order to simplify the description, only one conformation of the pair is described and for its enantiomeric counterpart only the α/τ-notation is given. The first enantiomeric pair is the windmill shapes L and R, where all naphthyl-groups have the alternating α/τ orientation. Thereby, the $\alpha\tau\alpha\tau$ conformer has a counterclockwise orientation (L) and the $\tau\alpha\tau\alpha$ conformer a clockwise orientation of the naphthyl groups (R). Both belong to the C_2 point group with the rotation axis in the center of the macrocycle.

The Y-shape is very similar to the I-shape, with one of the dimmer protrusions pointing away from the main molecular axis. The naphthyl-groups are either orientated $\alpha\tau\tau\tau$ (L) or $\tau\alpha\tau\tau$ (R) for this enantiomeric pair, or $\tau\tau\alpha\tau$ or $\tau\tau\tau\alpha$ for their rotamers, respectively. The opposite of the Y-shape is the λ-shape, in which three naphthyl-groups are pointing away from the main molecular axis and only one protrusion is aligned towards the main molecular axis. This corresponds to $\alpha\tau\alpha\alpha$ (L) and $\tau\alpha\alpha\alpha$ (R) conformers, with $\alpha\alpha\alpha\tau$ and $\alpha\alpha\tau\alpha$ being the corresponding rotamers, respectively. The Y-shape and the λ-shape both have no symmetry element, and thus belong to the C_1 point group.

When evaluating the data and searching for the different conformers, it was very difficult to find the windmill conformers, while the rest was observed quite frequently. It is also important to note that we never observed a switching of the orientations of the naphthyl groups and thus a change in molecular conformation at RT. Therefore, we conclude that the observed conformations are stable at RT.

Next, we address the dynamic behavior of the different 2HTNP conformers. For 2HTPP, it is known that it readily diffuses along the main crystallographic axis at RT.[30] Herein, we therefore investigate the influence of the naphthyl groups compared to the phenyl groups, and the impact of their orientation on their mobility. By evaluating STM movies (see Figure S1 in the Supporting Information) and motion-pathway-plots (superposition of subsequently measured STM images), we find that the diffusion behavior of the different 2HTNP conformers is quite different. This is evident from Figure 3a and 3b, where motion-pathway-plots within a given timeframe are shown. The ten conformers could be classified into three groups, which are indicated in different colors in Figure 3 and also Figure 2 (bottom row). Immobile conformers are indicated in red, conformers with medium mobility in yellow and fast diffusing conformers in green. The X- and both λ-shapes both are immobile; they are practically confined to their position and are hardly moving at all. For the K-, T- and both windmill shapes, the mobility is slightly larger and the molecules diffuse short distances along a crystallographic axis in the time interval of the superimposed STM images. Y- and I-conformers are very mobile and diffuse the longest distances along a crystallographic axis.

From these observations, it is obvious that the intramolecular conformation of adsorbed 2HTNP significantly influence the mobility, that is, its diffusion behavior. The detailed analysis of the different conformations shows a systematics behind our observations. Conformations with 4 (I) or 3 (Y) naphthyl groups in τ-orientation, that is, molecules with the smallest footprint, have a higher mobility and diffuse larger distances (green). Molecules with 2 naphthyl groups in τ-orientation (K, T, windmill) behave intermediate (yellow). Finally, conformations with only 1 (λ) or 0 (X) naphthyl groups in τ-orientation, that is, molecules with the largest footprint, are immobile (red). As one possible explanation, one could imagine that for the molecules with all naphthyl groups in α-orientation, that is, for the larger footprint, the interaction potential has a larger corrugation, and thus the whole molecule is immobilized. Interestingly, chirality seems not play any role, as chiral conformers belong to all 3 mobility categories.

As a final step, the behavior of the molecules was investigated after annealing at 400 K for 1 h. Thereafter, only three of the 10 conformations are observed. The X-shape is the by far dominant conformer, and rarely λ(L)- or λ(R)-shape enantiomers were observed (Figure 3c). Notably, these conformers show no mobility before and after the annealing step. From its lack of mobility and the fact that the other molecules are converted to this conformation upon providing thermal energy, we conclude that the X-shape is the thermodynamically most favorable conformation, i.e. poses an energetic minimum.

3. Conclusions

In summary, we observe a very peculiar adsorption behavior of 2HTNP on Cu(111). At RT, individual molecules are observed by high-resolution STM, which are orientated along the main crystallographic directions. The molecules have an inverted structure with upstanding iminic pyrrole groups, similar to 2HTPP on the same substrate. Due to the asymmetry of the naphthyl groups, 16 different surface conformers are possible, 10 of which have a different appearance in STM. The complete set could indeed be identified. While all conformers are stable at RT, the investigation of their diffusional behavior shows different mobilities, which can be classified into three categories, that is, low, medium and high. Interestingly, the mobility is related to the naphthyl orientation relative to the main axis of the molecule along the iminic nitrogen atoms. Fast diffusing species have 3 or 4 naphthyl groups pointing in the direction of the movement (aligned with the crystallographic axis), immobile species have only 0 or 1 naphthyl groups orientated in this direction (which equals 4 or 3 groups oriented away from the main molecular axis). This behavior shows that the introduction of asymmetric functional groups in the periphery linked to the macrocycle via single C–C bonds can have a strong influence on the adsorption behavior by yielding a variety of non-chiral and chiral conformers, which behave differently in their diffusion. This is an important observation, which could be used to tailor the diffusion properties, e.g., by introduction of rigid bonds to the macrocycle or groups that cannot rotate due to steric hindering.

Acknowledgements

The authors gratefully acknowledge the funding by the German Research Council (DFG) through research unit FOR 1878/funCOS (project Ma4246/2-2), and by the Collaborative Research Center SFB 953 at the Friedrich-Alexander-Universität Erlangen-Nürnberg. Open access funding enabled and organized by Projekt DEAL.

Conflict of Interest

The authors declare no conflict of interest.

Keywords: chirality · diffusion behavior · porphyrinoids · scanning tunneling microscopy · surface chemistry

[1] J. V. Barth, G. Costantini, K. Kern, *Nature* **2005**, *437*, 671–679.
[2] W. Auwärter, D. Écija, F. Klappenberger, J. V. Barth, *Nat. Chem.* **2015**, *7*, 105–120.
[3] K. H. Ernst, *Phys. Status Solidi B* **2012**, *249*, 2057–2088.
[4] K. H. Ernst, Y. Kuster, R. Fasel, M. Müller, U. Ellerbeck, *Chirality* **2001**, *13*, 675–678.
[5] R. Raval, *Chem. Soc. Rev.* **2009**, *38*, 707–721.
[6] U. Schlickum, R. Decker, F. Klappenberger, G. Zoppellaro, S. Klyatskaya, W. Auwärter, S. Neppl, K. Kern, H. Brune, M. Ruben, *J. Am. Chem. Soc.* **2008**, *130*, 11778–11782.
[7] P. Iavicoli, S. Haq, D. B. Amabilino, R. Raval, *Chem. Commun.* **2008**, 1536–1538.
[8] A. Mugarza, N. Lorente, P. Ordejón, C. Krull, S. Stepanow, M.-L. Bocquet, J. Fraxedas, G. Ceballos, P. Gambardella, *Phys. Rev. Lett.* **2010**, *105*, 115702.
[9] M. Schunack, T. R. Linderoth, F. Rosei, E. Laegsgaard, I. Stensgaard, F. Besenbacher, *Phys. Rev. Lett.* **2002**, *88*, 156102.
[10] R. Otero, F. Hümmelink, F. Sato, S. B. Legoas, P. Thostrup, E. Laegsgaard, I. Stensgaard, D. S. Galvao, F. Besenbacher, *Nat. Mater.* **2004**, *3*, 779–782.
[11] C. Nacci, M. Baroncini, A. Credi, L. Grill, *Angew. Chem. Int. Ed. Engl.* **2018**, *57*, 15034–15039.
[12] T. Jung, R. Schlittler, J. Gimzewski, *Nature* **1997**, *386*, 696.
[13] H. Marbach, H. P. Steinrück, *Chem. Commun.* **2014**, *50*, 9034–9048.
[14] J. M. Gottfried, *Surf. Sci. Rep.* **2015**, *70*, 259–379.
[15] F. Klappenberger, *Prog. Surf. Sci.* **2014**, *89*, 1–55.
[16] M. P. de Jong, R. Friedlein, S. Sorensen, G. Öhrwall, W. Osikowicz, C. Tengsted, S. Jönsson, M. Fahlman, W. R. Salaneck, *Phys. Rev. B* **2005**, *72*, 035448.
[17] P. Donovan, A. Robin, M. S. Dyer, M. Persson, R. Raval, *Chem. Eur. J.* **2010**, *16*, 11641–11652.
[18] M. Stark, S. Ditze, M. Drost, F. Buchner, H.-P. Steinrück, H. Marbach, *Langmuir* **2013**, *29*, 4104–4110.
[19] K. Diller, F. Klappenberger, F. Allegretti, A. Papageorgiou, S. Fischer, A. Wiengarten, S. Joshi, K. Seufert, D. Écija, W. Auwärter, *J. Chem. Phys.* **2013**, *138*, 154710.
[20] J. Kuliga, L. Zhang, M. Lepper, D. Lungerich, H. Holzel, N. Jux, H. P. Steinrück, H. Marbach, *Phys. Chem. Chem. Phys.* **2018**, *20*, 25062–25068.
[21] M. Stark, S. Ditze, M. Lepper, L. Zhang, H. Schlott, F. Buchner, M. Röckert, M. Chen, O. Lytken, H.-P. Steinrück, *Chem. Commun.* **2014**, *50*, 10225–10228.
[22] M. Lepper, T. Schmitt, M. Gurrath, M. Raschmann, L. Zhang, M. Stark, H. Hölzel, N. Jux, B. Meyer, M. A. Schneider, *J. Phys. Chem. C* **2017**, *121*, 26361–26371.
[23] S. Ditze, M. Stark, M. Drost, F. Buchner, H. P. Steinrück, H. Marbach, *Angew. Chem. Int. Ed.* **2012**, *51*, 10898–10901; *Angew. Chem.* **2012**, *124*, 11056–11059.
[24] F. Buchner, K. Flechtner, Y. Bai, E. Zillner, I. Kellner, H.-P. Steinrück, H. Marbach, J. M. Gottfried, *J. Phys. Chem. C* **2008**, *112*, 15458–15465.
[25] T. E. Shubina, H. Marbach, K. Flechtner, A. Kretschmann, N. Jux, F. Buchner, H.-P. Steinrück, T. Clark, J. M. Gottfried, *J. Am. Chem. Soc.* **2007**, *129*, 9476–9483.
[26] K. Diller, F. Klappenberger, M. Marschall, K. Hermann, A. Nefedov, C. Wöll, J. Barth, *J. Chem. Phys.* **2012**, *136*, 014705.
[27] G. Rojas, X. Chen, C. Bravo, J.-H. Kim, J.-S. Kim, J. Xiao, P. A. Dowben, Y. Gao, X. C. Zeng, W. Choe, *J. Phys. Chem. C* **2010**, *114*, 9408–9415.
[28] M. Lepper, J. Köbl, T. Schmitt, M. Gurrath, A. de Siervo, M. A. Schneider, H. P. Steinrück, B. Meyer, H. Marbach, W. Hieringer, *Chem. Commun.* **2017**, *53*, 8207–8210.
[29] F. Albrecht, F. Bischoff, W. Auwärter, J. V. Barth, J. Repp, *Nano Lett.* **2016**, *16*, 7703–7709.
[30] F. Buchner, J. Xiao, E. Zillner, M. Chen, M. Röckert, S. Ditze, M. Stark, H.-P. Steinrück, J. M. Gottfried, H. Marbach, *J. Phys. Chem. C* **2011**, *115*, 24172–24177.

Manuscript received: November 29, 2019
Accepted manuscript online: December 6, 2019
Version of record online: February 17, 2020

CHEMPHYSCHEM

Supporting Information

Conformation Controls Mobility: 2H-Tetranaphthylporphyrins on Cu(111)

Jan Kuliga, Stephen Massicot, Rajan Adhikari, Michael Ruppel, Norbert Jux, Hans-Peter Steinrück, and Hubertus Marbach*

Supporting information

Experimental section

The experiments and sample preparations were performed in a two-chamber ultrahigh vacuum (UHV) system at a background pressure in the low 10^{-10} mbar regime. The variable temperature scanning tunneling microscope (STM) is an RHK UHV VT STM 300 with RHK SPM 1000 electronics. All STM images were acquired at room temperature (RT) in constant current mode with a Pt/Ir tip and the bias was applied to the sample. The STM images were processed with WSxM software[1] and moderate filtering (Gaussian smoothing, background subtraction) was applied for noise reduction. The preparation of the clean Cu(111) surface was done by repeated cycles of Ar^+ sputtering (600 eV) and annealing to 850 K. The 2HTNP molecules were deposited onto the metal substrates held at RT, by thermal sublimation from a home-built Knudsen cell at 350 °C.

Tunneling parameters for the STM images shown in the manuscript:

Figure 1: a) U_{bias} = -1.15 V, I_{set} = 30 pA; c) U_{bias} = -1.40 V, I_{set} = 37 pA

Figure 2: a-c) U_{bias} = -1.15 V, I_{set} = 30 pA

Figure 3: a,b) U_{bias} = -1.15 V, I_{set} = 30 pA; c) U_{bias} = -1.10 V, I_{set} = 30 pA

STM movies were acquired to study the diffusion behavior of the 2HTNP. Figure S1 shows nine consecutive STM frames of such a movie. The frames were used to create a motion-pathway-plot by marking each individual molecule with a dot and superimposing all frames on top of each other. The center of the macrocycle with the two inverted pyrrole groups was used as a center of the dot. According to their mobility three different colors were used to emphasize the different mobility of the conformers. Green resembles fast, yellow medium diffusing molecules and red static conformers.

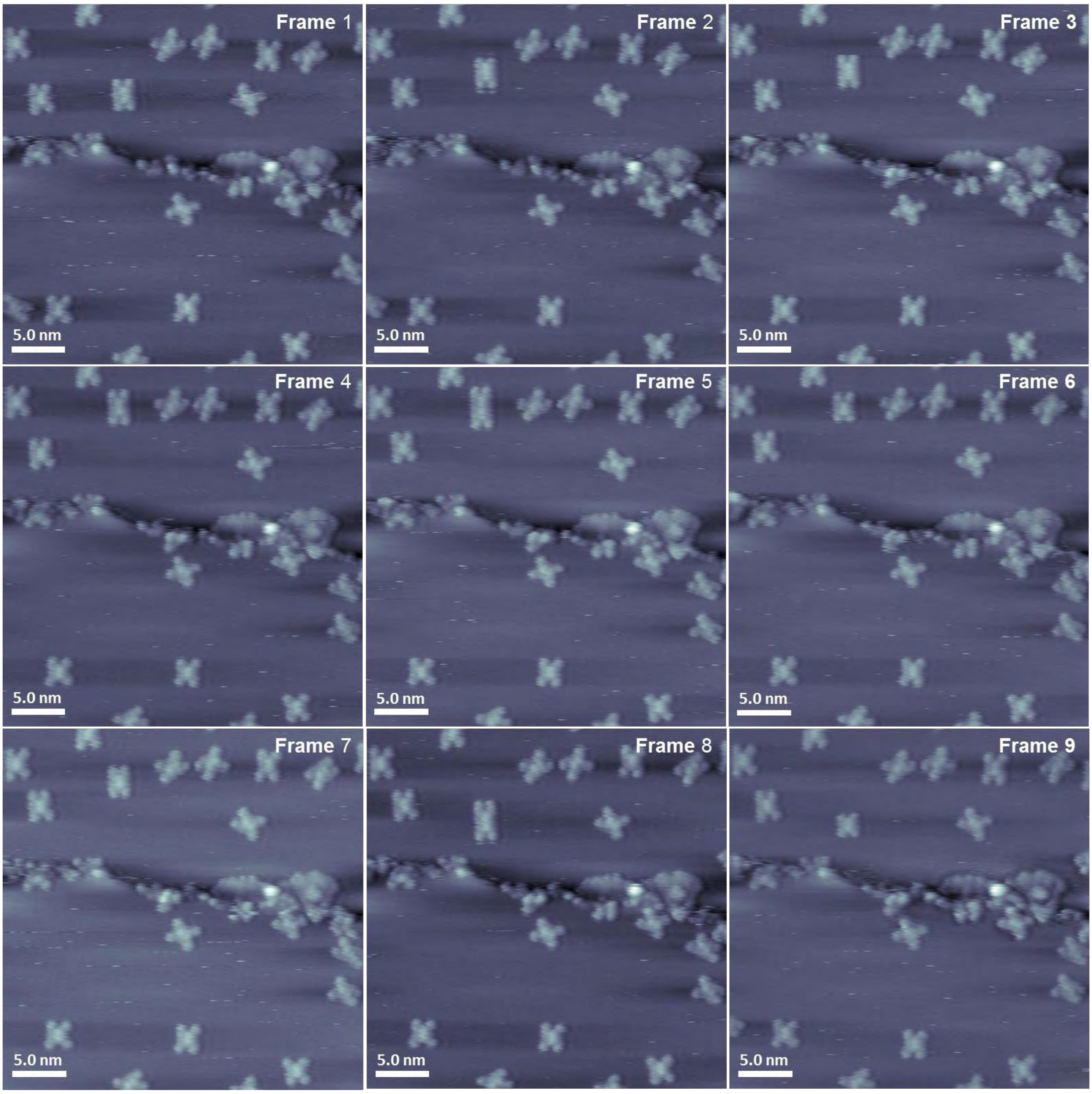

Figure S1: *Subsequent STM images taken to acquire an STM movie and to create a motion-pathway-plots of 2HNTP.*

Synthesis

All chemicals were purchased from Sigma-Aldrich®, Acros Organics®, Fluka®, Fisher Scientific® or Alfa Aesar® and used without further purification. Pyrrole and solvents for chromatography were distilled prior to usage. Dichloromethane was distilled from K_2CO_3. Thin layer chromatography (TLC) was performed on Merck silica gel 60 F524, detected by UV-light (254nm, 366nm). Column chromatography was performed on Macherey-Nagel silica gel 60 M (230-400 mesh, 0.04–0.063 mm). NMR spectroscopy was performed on a Bruker Avance 400 (^{1}H: 400 MHz, ^{13}C: 100 MHz). Deuterated solvents were purchased from

Sigma Aldrich and used as received. ^{1}H NMR and ^{13}C NMR chemical shifts δ are given in parts per million [ppm] and are referenced to residual protic impurities in the solvent ($CHDCl_2$: ^{1}H: 5.32 ppm), or to the deuterated solvent itself (CD_2Cl_2: ^{13}C: 53.8 ppm). The resonance multiplicities are indicated as "s" (singlet), "d" (doublet), "t" (triplet), "q" (quartet) and "m" (multiplet). Signals referred to as "bs" (broad singlet) are not clearly resolved or significantly broadened. LDI/MALDI-ToF (nitrogen UV-laser, 337 nm) mass spectra were obtained by using a Bruker ultrafleXreme spectrometer with 2,5-dihydroxybenzoic acid (DHB) or (*E*)-2-(3-(4-(*tert*-butyl)phenyl)-2-methylallylidene)malononitrile (dctb) as matrices. ESI/APPI-ToF mass spectrometry was carried out on a Bruker maXis 4G UHR TOF MS/MS-spectrometer or a Bruker micrOTOF II focus TOF MS-spectrometer. UV/vis spectroscopy was carried out on a Varian Cary 5000 UV-Vis-NIR spectrometer. Spectra were recorded at room temperature using quartz cuvettes with a path length of 1 cm. Fluorescence spectra were recorded on a Shimadzu RF–5301PC spectrofluorophotometer.

2*H*-tetrakis-(β-naphthyl)-porphyrin (**2HTNP**)

Pyrrole (692 µL, 671 mg, 10.0 mmol) and β-naphthylaldehyde (1.56 g, 10.0 mmol) were dissolved in CH_2Cl_2 (1 L), and degassed by passing nitrogen through the solution for 15 min. Then BF_3 diehtyl etherate (407 µL, 468 mg, 3.30 mmol) was added, and the mixture was stirred under light exclusion for 2 h at room temperature. After the addition of DDQ (1.70 g, 7.50 mmol), the mixture was stirred for additional 2 h at room temperature. The solvent was removed, and the resulting residue was filtered over silica gel (CH_2Cl_2, diameter: 4.0 cm, length: 15 cm). The purple band was collected and concentrated. Precipitation with methanol yielding the product as purple solid.

Yields: 24% (493 mg, 605 µmol).

^{1}H NMR (400 MHz, CDCl3, rt): δ [ppm] = 8.89 (s, 8H), 8.70 (bs, 4H), 8.41 (d, 4H, ^3J = 8.1 Hz), 8.21–8.17 (m, 8H), 8.10–8.08 (m, 4H), 7.73–7.68 (m, 8H), -2.59 (bs, 2H).

^{13}C NMR (100 MHz, CDCl3, rt): δ [ppm] = 139.9, 134.1, 133.2, 133.0, 132.6, 131.8, 128.8, 128.3, 127.3, 127.0, 126.2, 120.6.

HRMS (APPI): m/z calc. for $C_{60}H_{38}N_4$ [M$^+$]: 814.309099; found: 814.308261.

UV/Vis (CH_2Cl_2 + 1% NEt_3) λ [nm] (ε [M^{-1}cm^{-1}]) 424 (29000), 462 (513000), 518 (20000), 555 (11100), 593 (6500), 649 (4900).

Fluorescence (CH_2Cl_2 + 1% NEt_3, λ_{exc} = 424 nm) λ [nm] 655, 718.

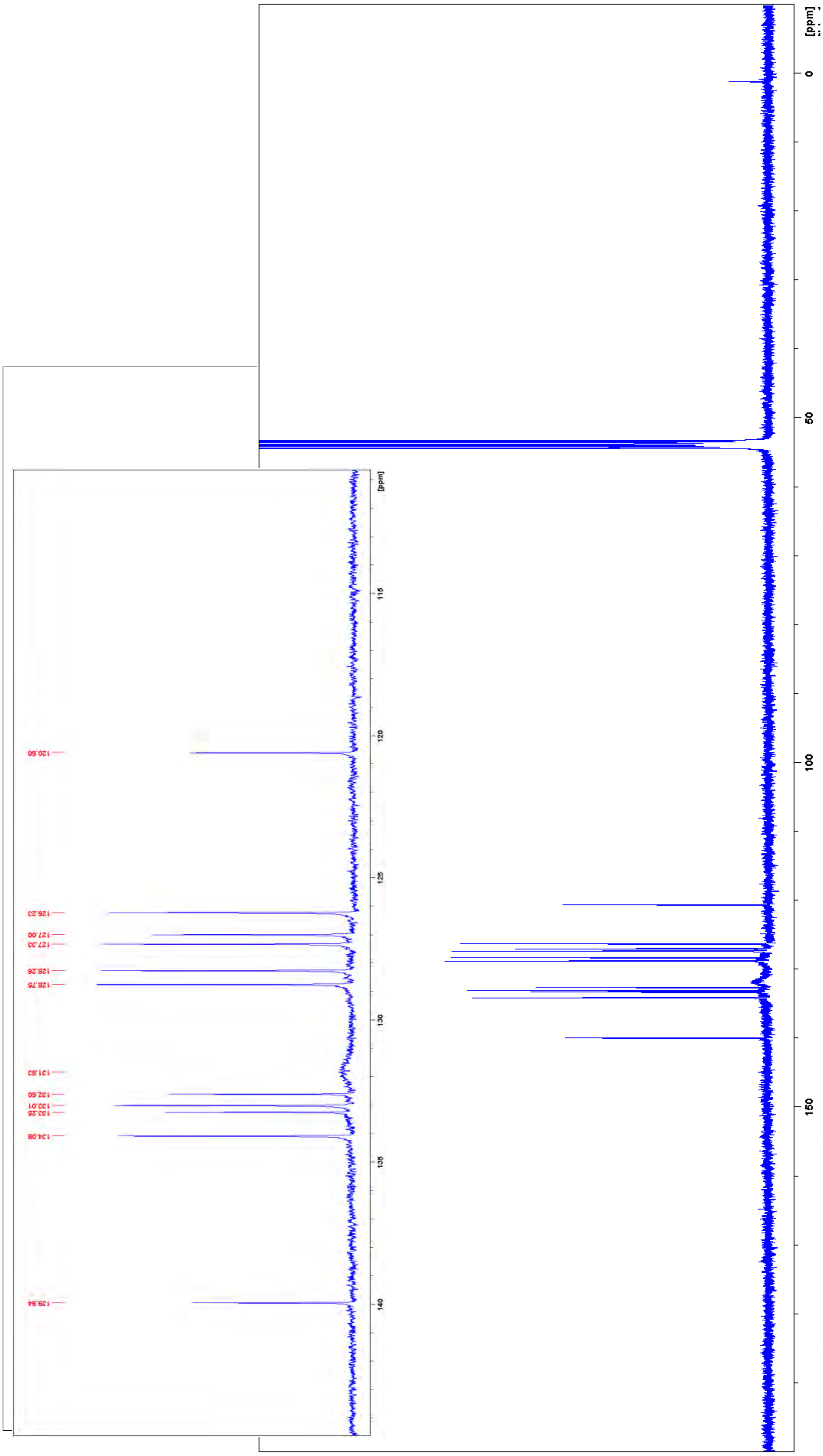

FFigure S3: ^{13}C NMR of **2HTNP**.

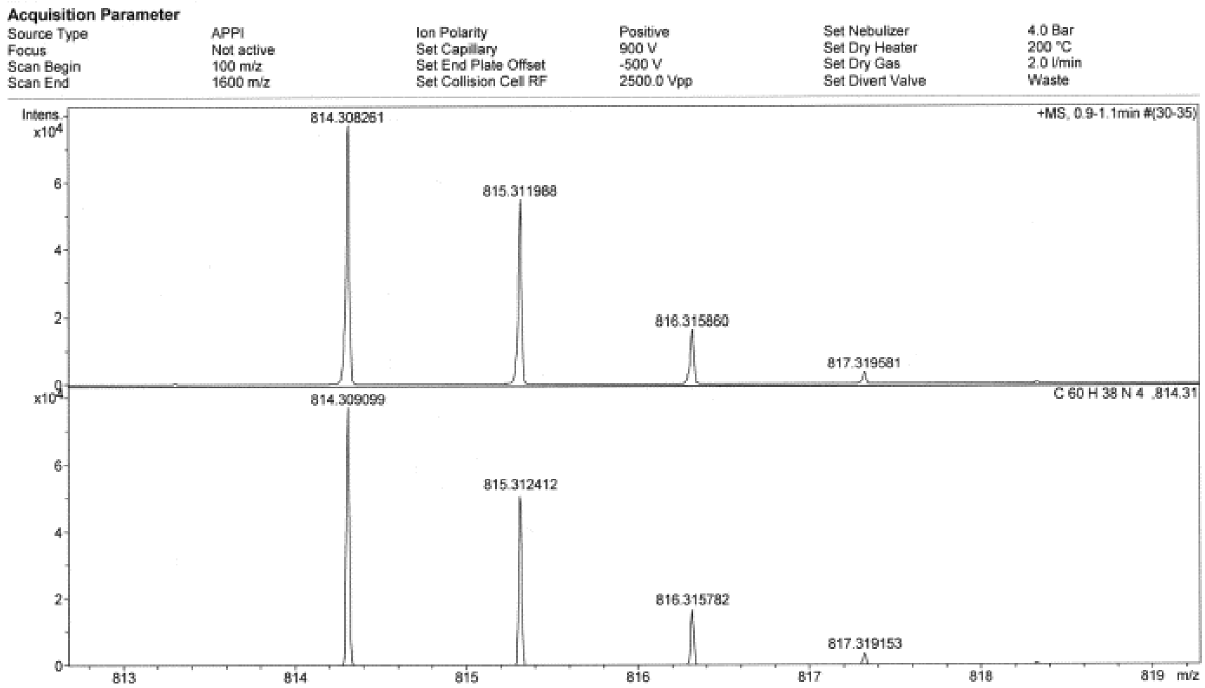

Acquisition Parameter

Source Type	APPI	Ion Polarity	Positive	Set Nebulizer	4.0 Bar
Focus	Not active	Set Capillary	900 V	Set Dry Heater	200 °C
Scan Begin	100 m/z	Set End Plate Offset	-500 V	Set Dry Gas	2.0 l/min
Scan End	1600 m/z	Set Collision Cell RF	2500.0 Vpp	Set Divert Valve	Waste

Figure S4: *HRMS (APPI, toluene) of **2HTNP**.*

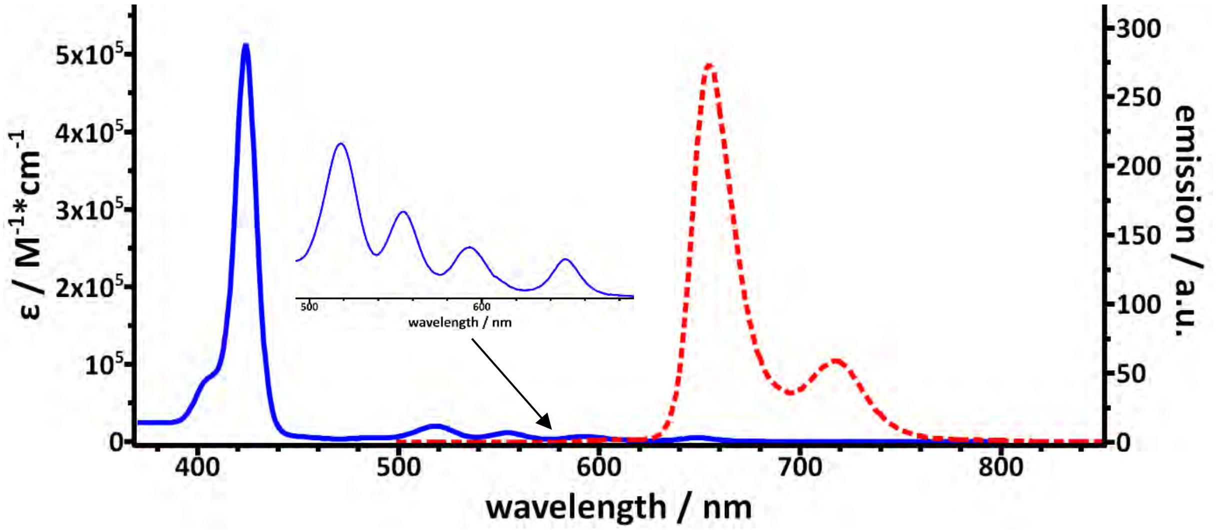

Figure S5: *Absorption (blue line) and emission spectrum of **2HTNP** (dashed red line; excitation at 424 nm) measured in* CH_2Cl_2 *+ 1%* NEt_3 *at RT.*

References

1. I. Horcas, R. Fernández, J. Gomez-Rodriguez, J. Colchero, J. Gómez-Herrero and A. Baro, *Rev. Sci. Instrum.* **2007**, 78, 013705.

10.1.3 [P3]

Metalation of 2HTCNPP on Ag(111) with Zn: Evidence for the Sitting atop Complex at Room Temperature

J. Kuliga, R. de Campos Ferreirra, R. Adhikari, S. Massicot, M. Lepper, H. Hölzel, N. Jux, H. Marbach, A. de Siervo, and H.-P. Steinrück, *ChemPhysChem,* ***22,*** 396-403 (**2021**); 10.1002/cphc.202000883

ChemPhysChem

Articles
doi.org/10.1002/cphc.202000883

Chemistry Europe
European Chemical
Societies Publishing

Very Important Paper

Special Collection

Metalation of 2HTCNPP on Ag(111) with Zn: Evidence for the Sitting atop Complex at Room Temperature

Jan Kuliga,[a] Rodrigo Cezar de Campos Ferreirra,[b] Rajan Adhikari,[a] Stephen Massicot,[a] Michael Lepper,[a] Helen Hölzel,[c] Norbert Jux,[c] Hubertus Marbach,[a] Abner de Siervo,*[b] and Hans-Peter Steinrück*[a]

We study the interaction and metalation reaction of a free base 5,10,15,20-terakis(4-cyanophenyl)porphyrin (2HTCNPP) with post-deposited Zn atoms and the targeted reaction product Zn-5,10,15,20-terakis(4-cyanophenyl)porphyrin (ZnTCNPP) on a Ag(111) surface. The investigations are performed with scanning tunneling microscopy at room temperature after Zn deposition and subsequent heating. The goal is to obtain further insights in the metalation reaction and the influence of the cyanogroups on this reaction. The interaction of 2HTCNPP with post-deposited Zn leads to the formation of three different 2D ordered island types that coexist on the surface. All contain a new species with a bright appearance, which increases with the amount of post-deposited Zn. We attribute this to metastable SAT ("sitting atop") complexes formed by Zn and the macrocycle, that is, an intermediate in the metalation reaction to ZnTCNPP, which occurs upon heating to 500 K. Interestingly, the activation barrier for the successive reaction of the SAT complex to the metalated ZnTCNPP species can also be overcome by a voltage pulse applied to the STM tip.

1. Introduction

The fabrication of functional nanoscale materials by a bottom-up approach has become a major topic in science during the past years. This growing demand of miniaturization is present in areas such as catalysis, energy storage and conversion, electronic and photonic devices.[1,2] The adsorption of functional organic molecules on metal surfaces has proven to be a suitable method for the construction of devices at the nanoscale.[1,3,4] In this context, porphyrins are promising candidates since they offer interesting properties like a conformationally flexible macrocycle with a reactive coordination center and the possibility for functionalization at the periphery. Heme (Fe-porphyrin) and chlorophyll (Mg-porphyrin) are particularly important molecules in nature, which offer different functionalities according to their metal center. While heme is responsible for oxygen transport in mammals, chlorophyll is involved in the photosynthesis of plants. The porphyrin core is known to coordinate a variety of different metal atoms.[5] The most common oxidation state of the metal ions is 2+, e.g. for Cu and Zn, while Co, Ni and Fe can form 2+ and 3+.[6] This huge variety in functionality due to a different metal core offers great potential for a variety of applications.[7–10] In particular for functional nanomaterials the understanding of the metalation reaction of porphyrins on surfaces thereby is of utmost importance.

The metalation reaction on surfaces takes place with either pre- or post-deposited metal atoms.[6] For Fe and Co, it occurs already at room temperature (RT) while moderate annealing is required for metals like Cu and Zn.[11–13] This observation indicates different activation energies for different metal atoms. Additionally, porphyrins are known to undergo a so-called self-metalation reaction on reactive single crystal surfaces like Cu, Fe and Ni, in which the macrocycle reacts directly with metal atoms present on the surface.[14–17] The mechanism of this very complex surface reaction has been topic of several previous studies, and the question arose whether it is a one-step reaction or intermediate states exist like the "sitting atop" (SAT), which has been proposed for metalation in solution,[18–20] as well as at the solid-vacuum interface.[21–23] In this adcomplex, the metal ion coordinates with the macrocycle while the pyrrolic hydrogen atoms are still bound to the nitrogen atoms. Shubina et al. investigated the metalation of 2HTPP with bare Zn atoms on a Ag(111) with XPS and compared it to DFT calculations of the gas-phase reaction.[24] They found a similar complex with Zn weakly bound to the nitrogen atoms of the macrocycle and the

---

[a] J. Kuliga, R. Adhikari, S. Massicot, Dr. M. Lepper, Dr. H. Marbach, Prof. Dr. H.-P. Steinrück
Lehrstuhl für Physikalische Chemie II
Friedrich-Alexander-Universität Erlangen-Nürnberg
Egerlandstr. 3
91058 Erlangen, Germany
E-mail: hans-peter.steinrueck@fau.de

[b] R. C. de Campos Ferreirra, Prof. Dr. A. de Siervo
Instituto de Física "Gleb Wataghin"
Universidade Estadual de Campinas
Campinas, 13083-859, SP, Brazil
E-mail: asiervo@ifi.unicamp.br

[c] H. Hölzel, Prof. Dr. N. Jux
Lehrstuhl für Organische Chemie II
Friedrich-Alexander-Universität Erlangen-Nürnberg
Nikolaus-Fiebiger-Str. 10
91058 Erlangen, Germany

Supporting information for this article is available on the WWW under https://doi.org/10.1002/cphc.202000883

An invited contribution to a Special Collection on Interface Phenomena.

two hydrogen atoms still attached to the two pyrrolic nitrogen atoms. The rate limiting step for metalation is the transfer of the first hydrogen to the metal atom. This step varies for different metal centers. For Zn, evidence for the formation of the adcomplex was found upon heating a coadsorbed Zn and 2HTPP layer on Ag(111) to 300 K, while metalation only occurred upon heating to 500 K. For coadsorbed Fe and 2HTPP on Ag(111), the adcomplex could be identified already at 100 K, as concluded from a shift of the iminic N 1s peak by 0.6 eV to higher binding energies compared to 2HTPP.[22] Metalation was completed already at 350 K, indicating a much lower activation energy as compared to Zn, in line with the calculations by Shubina et al.[24] Yamada et al. were able to image these three different states of the metalation reaction of 2HTPP with low-temperature STM for Fe on Ag(111) at 78.5 K. The original 2HTPP, a 2HTPP precursor adcomplex "α" state (Fe atom on top), and a 2HTPP precursor adcomplex "γ" state (Fe atom inside) were identified by DFT calculations, STM topography and scanning tunneling spectroscopy (STS).[25] One interesting question in this context is, whether for a metal with a higher activation energy for metalation, such as Zn, the adcomplex can also be observed at room temperature, which is closer to operating conditions of real devices.

Another important topic in the context of metalation is the question, whether the activation energy can be influenced by different ligands attached to the macrocycle. Recently, Lepper et al. were able to show that the self-metalation rate of 2HTPP on Cu(111) can be modified by cyano-groups attached to the phenyl ligands.[26] They observed the metalation rate to decrease significantly with increasing number of cyanophenyl ligands. In these studies, no information of reaction intermediates such as the adcomplex is available.

Herein, we report a comprehensive study of the interaction and reaction of a free base 5,10,15,20-terakis(4-cyanophenyl) porphyrin (2HTCNPP) with deposited Zn atoms on a Ag(111) surface. As a reference, we also investigated the targeted reaction product, that is, Zn-5,10,15,20-terakis(4-cyanophenyl) porphyrin (ZnTCNPP). Both molecules and their interaction with Zn are studied with a scanning tunneling microscope at RT with the goal to get further insights in the metalation reaction, and the influence of the cyano groups on this reaction.

2. Results and Discussion

In order to study possible chemical reactions of 2HTCNPP with post-deposited Zn on Ag(111), we first separately studied the adsorption of 2HTCNPP and the potential reaction product ZnTCNPP at RT; the corresponding STM images are shown in Figure 1. At low coverages, individual 2HTCNPP molecules are exclusively found on the step edges. On the terraces, only streaky features are observed, which are attributed to a 2D gas of fast diffusing molecules (see Figure S1 in the Supporting Information). Upon increasing the surface coverage, a long-range-ordered 2D supramolecular structure is found.[27] The individual molecules are clearly resolved with submolecular resolution, as is evident from Figure 1 (left panel). A slight depression marks the center of the bright macrocycle, and the four cyanophenyl groups at periphery of the molecule can be identified. The molecules adsorb in the so-called "saddle shape" conformation and assemble in a square arrangement with lattice vectors of $a = 1.49 \pm 0.04$ nm and $b = 1.45 \pm 0.04$ nm, with an enclosed angle of $\alpha = 87° \pm 5°$, which is in good agreement with the reported literature values.[27] Notably, the individual molecules are rotated relative to unit cell vectors *a/b* of the superstructure by 11°/22°, but are aligned along the substrate high symmetry directions (indicated by white arrows in the Figure 1).

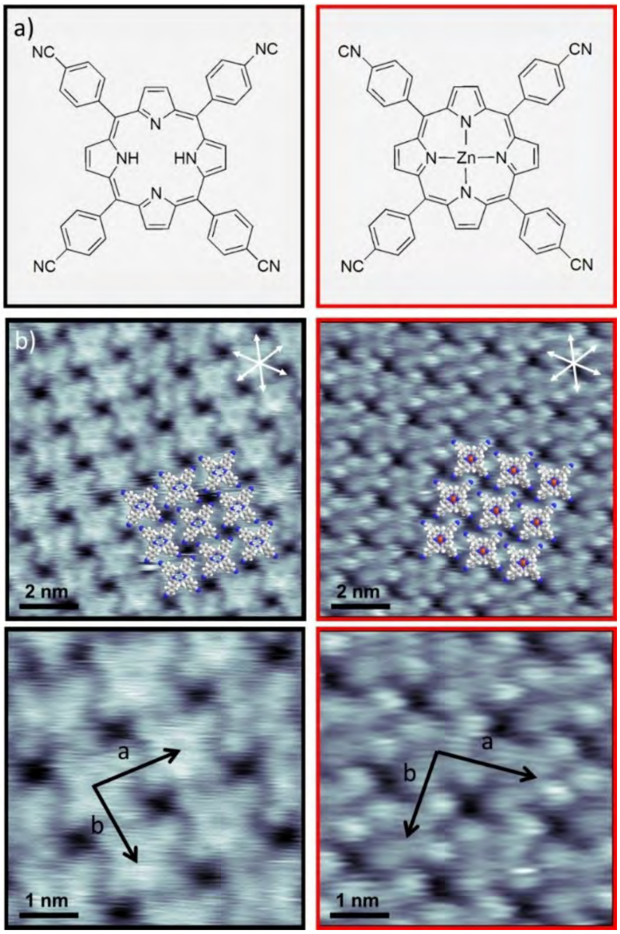

Figure 1. a) Chemical structure of 2HTCNPP (black) and ZnTCNPP (red). b) Constant-current STM images of an island of 2HTCNPP (black, $U = -850$ mV, $I = 19$ pA) and ZnTCNPP (red, $U = -190$ mV, $I = 30$ pA) on Ag(111) at RT and higher resolution of the respective unit cells. Overlaid molecular models indicate the structure of the ordered 2HTCNPP and ZnTCNPP layers; the central Zn atom in ZnTCNPP is depicted in red.

The corresponding metalloporphyrin, ZnTCNPP, shows an overall very similar behavior. At low coverages (not shown) a 2D gas of fast diffusing molecules is identified from streaky features in the STM images, with some molecules adsorbed to step edges at RT. An increase in molecular coverage leads to the formation of long-range ordered 2D supramolecular islands; see Figure 1 (right panel). The appearance within the islands is slightly different to that of 2HTCNPP. It is dominated by four bright protrusions due to the cyanophenyl groups at the periphery of the molecule, with the macrocycle being less bright and no obvious depression in its center. The central Zn atom is not visible at the applied tunneling conditions, since the 4s and 3d orbitals are completely occupied. Within the margins of error, the unit cell vectors $a = 1.51 \pm 0.04$ nm and $b = 1.49 \pm 0.04$ nm and the enclosed angle of $\alpha = 85° \pm 5°$ are the same as for 2HTCNPP. This behavior is expected due to the stabilization via attractive intermolecular interactions (hydrogen bonds between cyano groups and neighboring H atoms of phenyl groups), which are not affected by the Zn atom in the center of the molecule.

After post-deposition of Zn atoms onto the 2HTCNPP islands at room temperature a drastic change is observed. The interaction with post-deposited Zn leads to the formation of three different new island types, A, B and C, which coexist on the surface, as is evident from Figure 2b (for further images see Figure S2 in the SI). Notably, in all three the molecularly resolved structure of some molecules changes towards a bright appearance, with a central double protrusion (depending on scan direction and tunneling conditions sometimes only a single broad protrusion is seen). The rest of molecules still exhibit the features characteristic of 2HTCNPP. The bright appearance of this new species is remarkably similar in the different island types. The number of bright species increases approximately proportional with the amount of deposited Zn (this is demonstrated by subsequent Zn deposition, which is shown in SI Figure S3). The bright appearance clearly differs from that of ZnTCNPP, which is dominated by the four protrusions from the cyanophenyl groups; see Figure 1 (right). This observation rules out a metalation reaction at this stage. Furthermore, the bright protrusions are not stationary and occasionally hop to a different molecule between STM frames (see Figure S4 in the SI). This behavior suggests a loosely bound, mobile Zn adatom. Indeed, in earlier DFT calculations Shubina et al. proposed the formation of a so called "SAT" (sitting atop) complex for 2HTPP plus Zn, in which the Zn atom coordinates the macrocycle without the release of hydrogen.[24] This complex, which can also be denoted as 2H-SAT complex (as both pyrrolic hydrogens are still in place), is the first intermediate in the metalation reaction of 2HTPP to ZnTPP. In order to progress in the reaction pathway to form ZnTPP an activation barrier of 32.6 $\mathrm{kcal\,mol^{-1}}$ is needed to overcome.[24] This correlates with experiments performed by Kretschmann et al., who showed that an annealing step to 550 K is required for the metalation of 2HTPP with Zn.[13] We propose a similar reaction pathway also for deposition of Zn onto a 2HTCNPP layer on Ag(111). Within this interpretation, we assign the bright protrusions seen in the three new structures in Figure 2 to metastable SAT complexes formed by Zn and the macrocycle, prior to the metalation reaction to ZnTCNPP and the release of hydrogen.

The first and dominant island type, A, is shown in Figure 2c, which shows a square ordered 2D island ($a = 1.52 \pm 0.04$ nm, $b = 1.48 \pm 0.04$ nm, $\alpha = 85° \pm 5°$). Notably, both the bright SAT complexes and the remaining 2HTCNPP molecules are rotated against the lattice vectors of the island structures (best seen for molecules with double protrusion appearance), but are aligned along the high directions axis of the Ag(111) substrate. This arrangement is similar to that seen for pure 2HTCNPP in Figure 2a and Figure 1. It indicates that island-type A results

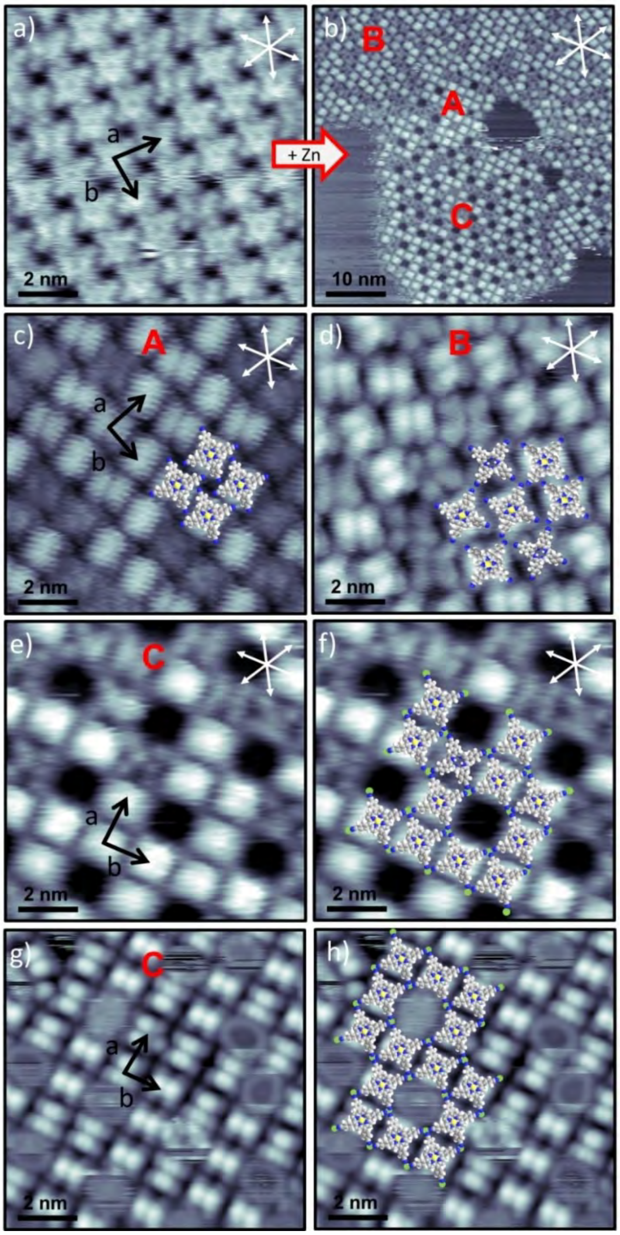

Figure 2. a) High resolution STM image of 2HTCNPP ($U = -850$ mV, $I = 19$ pA). b) The addition of Zn forms the three structures seen in the right overview ($U = -1660$ mV, $I = 30$ pA). c) High-resolution STM image of structure A ($U = -810$ mV, $I = 34$ pA). d) High resolution STM image of structure B, where each molecule has on average six neighbors ($U = -1660$ mV, $I = 30$ pA). e,f) High resolution STM image of structure C with regular missing molecules within the structure ($U = -1660$ mV, $I = 30$ pA). g,h) High resolution STM image of structure C (different contrast; measured in Campinas/Brazil) with circular features within the holes of the structure ($U = -1488$ mV, $I = 13$ pA). Overlaid molecular models indicate the structure of the different layers. The central Zn adatom in the SAT complex is depicted in yellow, and the coordinating Ag adatoms in green.

from the adsorption of Zn onto 2HTCNPP in the square islands without a rearrangement of the porphyrin molecule.

The second island type, B, (Figure 2d) has a densely packed, but disordered structure, with each molecule surrounded by six other molecules. This disorder makes it impossible to give a unit cell. The overall interaction theme within the structure is that three CN-groups of neighboring molecules point towards each other. The double protrusions are predominantly orientated parallel to Ag(111) high symmetry directions.

The third island type, C, is a regular porous 2D structure built by pores, which are surrounded by eight molecules each (Figure 2e). Alternatively, one can describe this structure as an arrangement of two alternating types of rows: in the first, each site along the row is occupied and in the second only every second site occupied. The structure has quite a number of defects by occasional filling of the pores by a molecule and a break of the alternating row symmetry. Figure 2g shows the same structure in a better resolution measured with a different STM (see Experimental Section). Under these conditions, circular bright features are observed within the pores. We attribute these features to fast diffusing Zn metal atoms, which diffuse between the different cyano groups of the molecules. The alternative interpretation as molecules sitting slightly above the pore in a very mobile state, which do not fit in the pores, appears unlikely, since the apparent height is lower than that of neighboring molecules. The molecules are oriented again along the high symmetry direction of the substrate but now also along the rows. The overall lattice is again close to quadratic ($a = 1.66 \pm 0.08$ nm, $b = 1.50 \pm 0.07$ nm, $\alpha = 88^\circ \pm 5^\circ$). However, in contrast to 2HTCNPP, ZnTCNPP and structure A, the lattice vectors are now aligned along the substrate high symmetry directions and are not rotated by 11°/22°. Notably, the different lattice sites are occupied by either a non-metalated 2HTCNPP, a SAT complex or an empty pore, which makes a non-homogeneous structure.

As binding motif of this structure, we tentatively propose a cyano-metal-cyano coordination. The cyano groups of three molecules are pointing towards each other, which implies a metal coordination center with a +3 oxidation state, assuming that only one metal atom is coordinated (Figure 2e and h). For Zn, a +3 oxidation state is highly unlikely, due to its electronic structure. Alternatively, we propose that Ag adatoms, which are present on the surface, serve as coordination centers. Comparable Au-coordination structures formed by cyano-functionalized triarylamines have indeed been observed on a Au(111) surface,[28] where similar to our observations, pores are surrounded by molecules forming long-range-ordered structures. These molecules have a threefold symmetry which results a hexagonal structure, while in our case the fourfold symmetry of the porphyrin core yields a square structure.

The absence of this type of coordination prior to Zn evaporation onto 2HTCNPP indicates that the presence of Zn is needed for the formation of the peculiar structure of island type C. From the fact this structure is not observed upon Zn deposition onto ZnTCNPP (see below), we conclude that Zn must play an active role for the formation of this structure. We tentatively propose that the geometric/electronic structure of the SAT complex is modified, as compared to 2HTCNPP and also ZnTCNPP, such that the formation of the coordination network becomes energetically favorable. In addition, increasing the deposition of Zn could also lead to an increase of the amount of Ag adatoms due to the filling of vacancies/defects in the underlying Ag surface layer by Zn. Especially upon heating Ag is known to dissolve Zn up to 40 atomic percent at 550 K.[29]

Analyzing the differences between the three island types, it appears that types A and B represent two subsequent steps towards type C upon deposition of Zn onto 2HTCNPP. In the first step Zn forms a SAT complex with 2HTCNPP, but in type A the long-range structure remains unchanged. In a next step the molecule tends to arrange towards type C, that is, a quadratic lattice with holes, where the unit cell vectors are aligned along the substrate high symmetry direction. As driving force, we propose the formation of the Ag-coordinated network, with three molecules coordinated to one Ag adatom. Type B has a disordered intermediate structure during this reorganization, in which three neighboring molecules are already coordinated, but the differently oriented quadratic lattice is not yet formed. The coexistence of structures A, B and C indicates that the energetic differences are small. Otherwise, exclusively type C islands would be expected.

As mentioned above, we do not observe the formation of the pore structure upon deposition of Zn onto a pre-adsorbed ZnTCNPP layer directly after deposition, and also not after annealing to temperatures up to 500 K. Considering the fact that the peripheries of 2HTCNPP and ZnTCNPP are identical, this observation further indicates that Zn-adatoms are not coordinating the pore network, further supporting the idea of CN–Ag–CN bonds.

Interestingly, after Zn deposition onto ZnTCNPP a different highly ordered pattern is very frequently observed. This phenomenon is also present for 2HTCNPP and 2HTCNPP+Zn (see SI, Figure S5), but is particularly pronounced for ZnTCNPP (Figure 3a–c). For ZnTCNPP+Zn, we observe an outstandingly pronounced long range order, which extends across substrate step edges. The long-range order is characterized by extended parallel rows of molecules with identical orientation, which form a square lattice (see Figure 3a). Occasionally, the periodicity perpendicular to the rows is broken by single rows of molecules with different azimuthal orientation (see Figure 3a and enlarged image in Figure 3b), which represents a “line defect” in the long range ordered structure. The distance between the defects can vary (with e.g. 3 to 8 regular rows in between – see Figure 3a), or can also be periodic (with e.g. 3 regular rows in between – see Figure 3c). This break of symmetry is not attributed to a domain boundary, but rather to a line defect since the island orientation remains the same after the row of different orientation. The two islands left and right of the line defect row are shifted by half a molecule. Interestingly, this line defect (that is, the single row with molecules of different orientation), always starts at a kink of a Ag(111) step edge and extends over step edges like a carpet. In other words, the island grows in a regular fashion along straight step edges. Starting at kinks, one row of molecules is tilted against the molecules in the regular islands; the molecules in

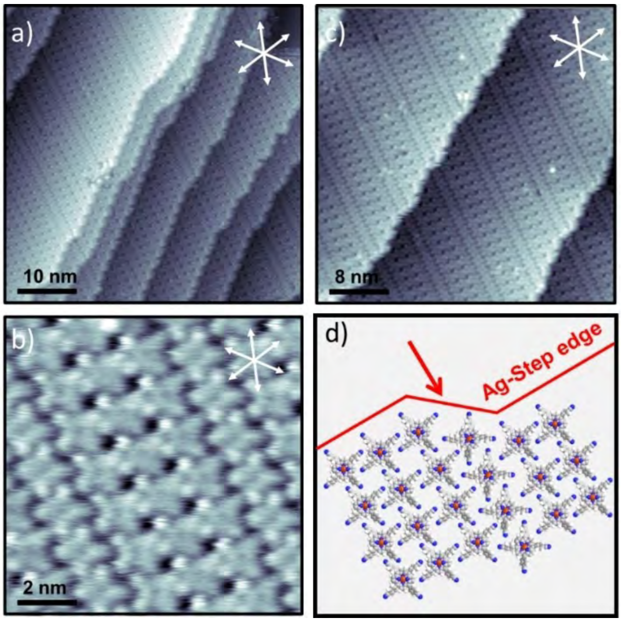

Figure 3. a–c) High resolution STM images (Erlangen) of ZnTCNPP + Zn ($U_a = -1000$ mV, $I = 30$ pA; $U_c = -455$ mV, $I = 30$ pA; $U_c = -441$ mV, $I = 30$ pA). d) Schematic drawing of the correlation between step edge shape and orientation of the rows (red arrow indicates differently orientated row).

this row are aligned along one of the high symmetry axis of the Ag(111) substrate. Looking at the images in Figure 3a and 3c, we observe that the molecular order of the regular rows and also the defect rows extend over many step edges. For the defect rows, this requires (or indicates) a kink at each step edge, which means that the kinks have the same regularity as the defect rows. Considering the fact that one expects no correlation of the kinks between neighboring step edges, one has to conclude that the porphyrin layer is able to modify the morphology of the step edges such that the kinks are aligned along the molecular defect rows. The fact that this type of molecular order is most pronounced after Zn deposition on ZnTCNPP (where no Zn is needed for the formation the SAT complex), could indicate that the deposited Zn preferentially adsorbs the step edges. At the step edge, Zn has a high mobility and thus can be arranged such that the molecular order of regular rows and defect rows is maintained over the step edges.

Notably, the observed structure is quite similar to a highly ordered striped [2 + 1] structure of ZnTPP on Ag(100) observed by Rangan et al.[30] In this structure, one double row of 2 identically oriented molecules is separated by 1 row of molecules, which are azimuthally rotated relative to the molecules in the double rows. This specific structure also extends over step edges and is assigned to a metastable ordered phase which can be transformed to a quadratic phase of equally oriented molecules by heating to 500 K. Furthermore, a similar effect with alternating rows was seen for the supramolecular ordering of a chlorophenyl porphyrin on Ag(111).[31]

For the ZnTCNPP + Zn system studied here, the rotation of the molecules in the line defect row breaks the dipole-dipole interactions of the cyano groups between neighboring molecules (see Figure 3d). This lost interaction is compensated by forming a N–H bond between a CN-group and a H atom of the neighboring pyrrole group of the macrocycle. This shows how much the molecules prefer adsorption sites at the step edges and that the islands start to grow from there.

In a next step, the 2HTCNPP + Zn layer (island types A, B and C; Figure 2) was annealed to check whether the metastable SAT complexes can be metalated, as was the case for 2HTPP plus Zn.[13,24] In Figure 4, we compare high resolution STM images of directly deposited ZnTCNPP (a) and of 2HTCNPP + Zn after annealing to 500 K (b). The molecular appearances in both images are virtually identical, with the four bright protrusions resembling the cyanophenyl groups, and the Zn atom in the center of the macrocycle invisible. Also, the unit cell of the 500 K-annealed 2HTCNPP + Zn layer ($a = 1.54 \pm 0.04$ nm, $b = 1.46 \pm 0.04$ nm, $\alpha = 85° \pm 5°$) matches that of ZnTCNPP ($a = 1.51 \pm 0.04$ nm, $b = 1.49 \pm 0.04$ nm, $\alpha = 85° \pm 5°$), within the margin of error. This similarity is taken as strong evidence that metalation is indeed possible by annealing and further corroborates our interpretation of the SAT complex as a metastable intermediate in the metalation reaction. The uni-

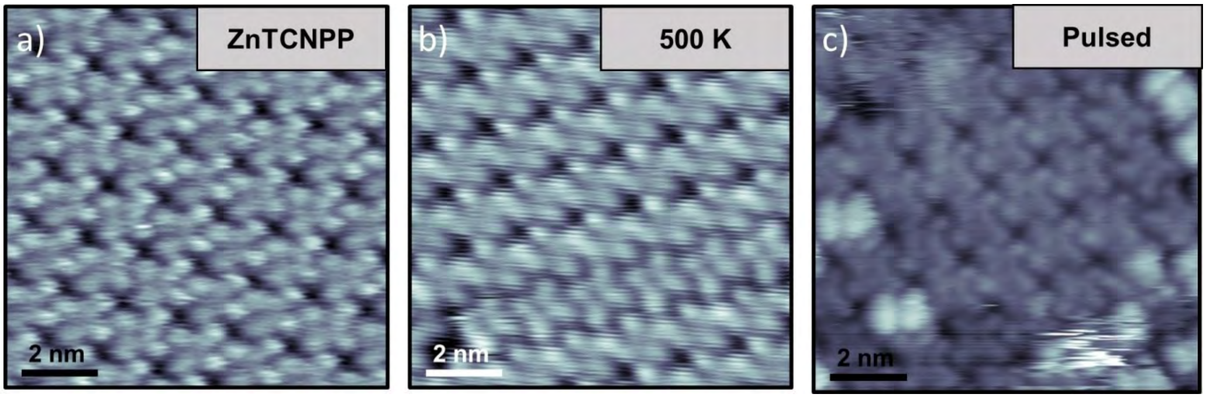

Figure 4. a) High resolution STM images (Erlangen) of ZnTCNPP ($U_a = -190$ mV, $I = 30$ pA), b) High resolution STM images (Erlangen) of 2HTCNPP + Zn + 500 K ($U_b = -1000$ mV, $I = 22$ pA), c) High resolution STM images (Erlangen) of 2HTCNPP + Zn + pulse(+2.73 V) ($U_c = -1660$ mV, $I = 30$ pA).

form appearance of the STM image after heating to 500 K indicates that the bright protrusions which were observed for all three coexisting island types after Zn deposition at RT all transform into the same quadratic structure (with some disordered regions) after metalation, which does not show any sign of a Ag coordinated network. Notably, after the metalation, the molecular rows, and thus the unit cell vectors of all porphyrins are rotated relative to the high symmetry directions of the substrate.

Most interestingly, temperature is not the only possible option to overcome the energy barrier to induce a conformational change or metalation reaction. During the course of our experiments, we observed a peculiar behavior of the SAT complex species after a tip pulse. After applying a positive voltage pulse of 1.5 to 4 V (referred to the sample), the molecular appearance of a small area within the island changed. Higher voltages could not be studied, since the contrast of the overall image changed or the tip drifted, and negative voltage pulses did not induce such a change. Since the appearance of the molecules around the switched species remains unchanged, we attribute our observation to a voltage-induced change of the molecule and not a change in overall contrast (e.g. due to a tip change). To get further insights into this phenomenon, we measured "STM movies" of the same spot: In Figure 5, we show ten successive frames, each measured within 10 sec, which resembles a total of 100 s monitored during the movie (the full movie is provided as Movie M1 in the SI). In the middle of frame 3 a pulse (2.73 V) was applied, and the change of the structure was observed afterwards. This behavior was observed for the bright protrusions in all three island types (see Figure S6 and also the corresponding Movie M2 in the SI). Remarkably, the structural change did not occur instantaneous, but happened over time by switching of 4 to 7 molecules in between frames. Looking at the molecular appearance and comparing it to 2HTCNPP and ZnTCNPP, the four cyanophenyl groups are clearly observable and the bright protrusion of the SAT complex vanishes. While a bias-induced transfer of the coordinated metal atom to the tip has been observed, e.g., for lead-phthalocyanine molecules,[32] we rule out such a process here for two reasons: *(i)* it is hard to imagine that subsequent demetalation of neighboring molecules would occur on the timescale of seconds, and *(ii)* metalation can be also induced thermally (see above).

One can envisage two possible voltage-induced reactions pathways of the SAT complex. The first would be the back reaction to 2HTCNPP under the release of the Zn atom, and the second is the formation of ZnTCNPP under the release of hydrogen. Comparing the appearance of the switched molecules with 2HTCNPP, we do not observe the bright macrocycle characteristic for the free base species. Moreover, there is no evidence of released Zn atoms or fast diffusing species, or Zn diffusion of SAT complexes to neighboring 2HTCNPP. We thus conclude that the SAT complex reacts towards ZnTCNPP. The newly formed species arrange into a regular patterns of ~20 molecules (e.g. 4 times 5) with a quadratic lattice ($a = 1.54 \pm 0.04$ nm, $b = 1.46 \pm 0.04$ nm, $\alpha = 86° \pm 5°$), like that of ZnTCNPP or 2HTCNPP. The question now arises, why the switching occurs not only at the time of the pulse but continues afterwards on the time scale of seconds. One possibility is that the hydrogen released in the course of the reaction of the SAT complex to ZnTCNPP adsorbs as atomic hydrogen on the surface, thereby modifying the local electronic properties such that the activation barrier for the metalation reaction of neighboring SAT complexes is lowered. The fact the metalation happens only with positive bias is difficult to address without calculation. As one possible explanation, we suggest that upon applying a positive voltage pulse, one populates some specific molecular states in the LUMO which induce deprotonation and as a consequence metalation. In the metalated porphyrin probably the central Zn atom interacts with the surface, and thus a reversible switching by applying negative voltage was also not observed. Wang et al. have studied the reversibility metalation/

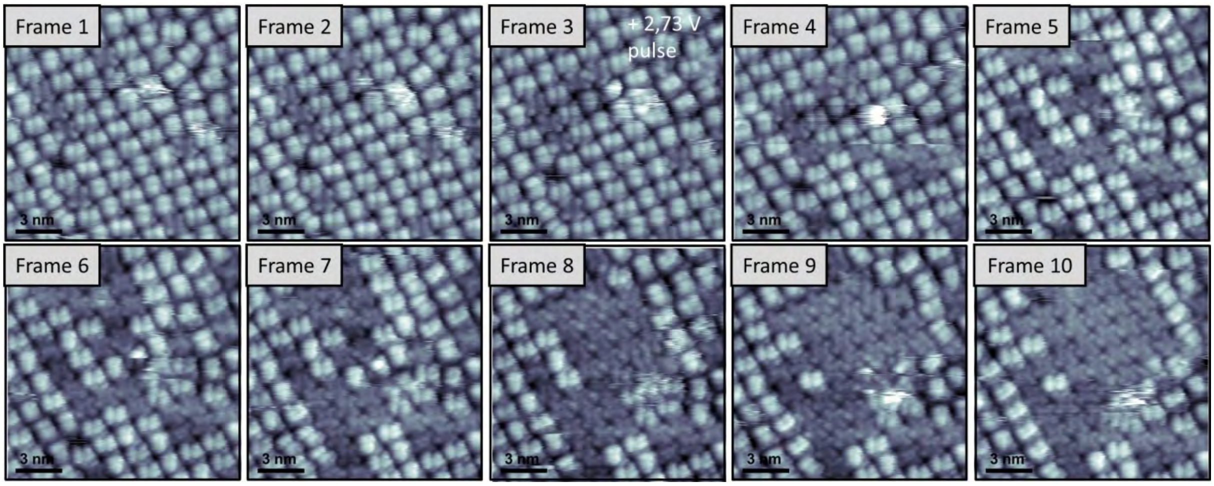

Figure 5. Consecutive STM frames of an 2HTCNPP island (structure A) covered with Zn ($U_c = -1660$ mV, $I = 30$ pA). During Frame 3, a +2.73 V tip pulse was executed, which leads to a change in molecular conformation and supramolecular ordering (compare frames 9 and 10). Complementary data for structures B and C are shown in Figure S6 in the SI.

demetalation of the Sn atom in SnPc.[33] They have found that the injection of electrons in the LUMO+1 gives rise to a negatively charged and thus transiently reduced molecule. Upon leaving the molecule, the electron may deposit energy to vibrational degrees and thus initiate the molecular switching. However, for molecules with a stronger contact to metal surface rapid transfer of the attached electron may suppress switching, as is observed here.

3. Conclusions

The goal of this study was to investigate the metalation reaction of the tetracyanophenyl-functionalized free base porphyrin 2HTCNPP with post-deposited Zn atoms to the metalloporphyrin ZnTCNPP on a Ag(111) surface, and to identify possible reaction intermediates by scanning tunneling microscopy at RT. The study was performed using two different experimental setups, one in Erlangen/Germany and one in Campinas/Brazil, with both studies yielding identical results. After Zn deposition onto a preadsorbed 2HTCNPP layer at RT, we observe the formation of three different 2D ordered island types that coexist on the surface. For all three of them, we find a new species with a bright appearance, the amount of which increases with the amount of post-deposited Zn. We attribute this species to metastable SAT ("sitting atop") complexes. In this SAT complex, the metal ion coordinates with the macrocycle while the pyrrolic hydrogen atoms are still bound to the nitrogen atoms. This metastable SAT complex has been previously observed by Shubina et al. in the corresponding metalation reaction of the non-cyano-functionalized 2HTPP to ZnTPP, with a characteristic signature in XPS.[24] Upon heating to 500 K, the activation barrier for the subsequent reaction of the intermediate SAT complex to the metalated porphyrin is overcome, yielding ZnTCNPP and gaseous dihydrogen. Interestingly, the activation barrier for the successive reaction of the SAT complex to the metalated ZnTCNPP species can also be overcome by a voltage pulse applied to the STM tip.

One additional interesting observation is the mentioned formation of three characteristic adlayer structures after the deposition of Zn at RT. While two of the structures (A and B) can easily by interpreted as modifications of the initial structure of 2HTCNPP induced by the post-deposited Zn atoms, yielding the SAT complex, the third structure (C) has a very characteristic appearance with regular unoccupied sites (holes). We propose this structure to be a coordination network, where three cyanophenyl groups coordinate to Ag adatoms from the substrate. Notably, the formation of this structure seems to require adsorbed SAT complexes, since it is not observed upon post-deposition of Zn onto a ZnTCNPP. When performing this experiment, however, we find the formation of an extremely long-range ordered quadratic phase, which extends over step-edges. This phase contains line defects, which are related to kinks in the steps. The fact that the defect lines extend over the step edges is taken as indication that the porphyrin layer is able to modify the morphology of the step edges such that the kinks are aligned along the molecular defect rows.

Experimental Section

The study was performed using two different experimental setups, one in Erlangen/Germany and one in Campinas/Brazil, with both studies yielding identical results.

The experiments and sample preparations in Erlangen were performed in a two-chamber ultrahigh vacuum (UHV) system at a background pressure in the low 10^{-10} mbar regime. The variable temperature scanning tunneling microscope (STM) is an RHK UHV VT STM 300 with RHK SPM 1000 electronics. All STM images were acquired at room temperature (RT) in constant current mode with a Pt/Ir tip and the bias was applied to the sample. The STM images were processed with WSxM software[34] and moderate filtering (Gaussian smoothing, background subtraction) was applied for noise reduction. The preparation of the clean Ag(111) surface was done by repeated cycles of Ar^+ sputtering (600 eV) and annealing to 850 K. The 2HTCNPP molecules were deposited onto the metal substrates held at RT, by thermal sublimation from a home-built Knudsen cell (nominal temperature: 430 °C).

In Campinas, the experiments were performed in a two interconnected UHV chambers (sample preparation and STM) running with a base pressure in the low 10^{-10} mbar range. The variable temperature STM is a SPECS Aarhus 150 STM operated with a SPECS SPC 260 controller. The STM measurements were performed in a constant current mode with a W tip cleaned in situ by Ar^+ sputtering. STM bias voltages are applied to the sample. The images were analyzed using the WSxM and Gwyddion softwares.[34,35] The Ag(111) crystal was prepared by sequential Ar^+ sputtering cycles at 600 V @ 5 $\mu A\,cm^{-2}$ for 30 min followed by annealing at ~790 K for 10 min. The 2HTCNPP molecules were sublimated using a home-made Knudsen cell with a quartz crucible (nominal temperature: 350 °C) while the Ag(111) sample was held at room temperature (RT). Zn atoms were post-deposited on 2HTCNPP/Ag(111) from ultrapure Zn shots (Alfa Aesar, 99.999 %) inserted in a well degassed Mo crucible in a FOCUS-Omicron EFM3 e-beam evaporator.

Acknowledgements

The authors gratefully acknowledge funding by the German Research Foundation (DFG) through Research Unit FOR 1878 (funCOS), the Collaborative Research Center SFB 953 (project number 182849149) at the Friedrich-Alexander-Universität Erlangen-Nürnberg and São Paulo Research Foundation (FAPESP) through project numbers 2007/54829-5 and 2007/08244-5. M.L., J.K. and H.M are grateful for travel grants from DAAD. R.C.C.F. and A.S. are grateful for travel grants from CAPES (Brazil) under the Brazilian-German collaborative project PROBRAL (1925/2016). Open access funding enabled and organized by Projekt DEAL.

Conflict of Interest

The authors declare no conflict of interest.

Keywords: metalation · porphyrinoids · SAT complex · scanning tunneling microscopy · surface chemistry

[1] J. V. Barth, G. Costantini, K. Kern, *Nature* **2005**, *437*, 671–679.
[2] L. Sosa-Vargas, E. Kim, A.-J. Attias, *Mater. Horiz.* **2017**, *4*, 570–583.
[3] T. Jung, R. Schlittler, J. Gimzewski, *Nature* **1997**, *386*, 696.
[4] S. De Feyter, F. C. De Schryver, *Chem. Soc. Rev.* **2003**, *32*, 139–150.
[5] H. Marbach, *Acc. Chem. Res.* **2015**, *48*, 2649–2658.
[6] J. M. Gottfried, *Surf. Sci. Rep.* **2015**, *70*, 259–379.
[7] L. Wang, H. Li, J. Deng, D. Cao, *Curr. Org. Chem.* **2013**, *17*, 3078–3091.
[8] C. Gutiérrez-Cerón, M. A. Páez, J. H. Zagal, *J. Solid State Electrochem.* **2016**, *20*, 3199–3208.
[9] M. G. Walter, A. B. Rudine, C. C. Wamser, *J. Porphyrins Phthalocyanines* **2010**, *14*, 759–792.
[10] M. Jurow, A. E. Schuckman, J. D. Batteas, C. M. Drain, *Coord. Chem. Rev.* **2010**, *254*, 2297–2310.
[11] J. M. Gottfried, K. Flechtner, A. Kretschmann, T. Lukasczyk, H.-P. Steinrück, *J. Am. Chem. Soc.* **2006**, *128*, 5644–5645.
[12] F. Buchner, V. Schwald, K. Comanici, H. P. Steinruck, H. Marbach, *ChemPhysChem* **2007**, *8*, 241–243.
[13] A. Kretschmann, M. M. Walz, K. Flechtner, H. P. Steinruck, J. M. Gottfried, *Chem. Commun. (Camb.)* **2007**, 568–570.
[14] R. González-Moreno, C. Sánchez-Sánchez, M. Trelka, R. Otero, A. Cossaro, A. Verdini, L. Floreano, M. Ruiz-Bermejo, A. García-Lekue, J. Á. Martín-Gago, *J. Phys. Chem. C* **2011**, *115*, 6849–6854.
[15] C. M. Doyle, S. A. Krasnikov, N. N. Sergeeva, A. B. Preobrajenski, N. A. Vinogradov, Y. N. Sergeeva, M. O. Senge, A. A. Cafolla, *Chem. Commun.* **2011**, *47*, 12134–12136.
[16] K. Diller, F. Klappenberger, M. Marschall, K. Hermann, A. Nefedov, C. Wöll, J. Barth, *J. Chem. Phys.* **2012**, *136*, 014705.
[17] A. Goldoni, C. A. Pignedoli, G. Di Santo, C. Castellarin-Cudia, E. Magnano, F. Bondino, A. Verdini, D. Passerone, *ACS Nano* **2012**, *6*, 10800–10807.
[18] E. B. Fleischer, J. H. Wang, *J. Am. Chem. Soc.* **1960**, *82*, 3498–3502.
[19] Y.-W. Hsiao, U. Ryde, *Inorg. Chim. Acta* **2006**, *359*, 1081–1092.
[20] G. De Luca, A. Romeo, L. M. Scolaro, G. Ricciardi, A. Rosa, *Inorg. Chem.* **2009**, *48*, 8493–8507.
[21] F. Bischoff, K. Seufert, W. Auwärter, A. P. Seitsonen, D. Heim, J. V. Barth, *J. Phys. Chem. C* **2018**, *122*, 5083–5092.
[22] M. Röckert, M. Franke, Q. Tariq, H.-P. Steinrück, O. Lytken, *Chem. Phys. Lett.* **2015**, *635*, 60–62.
[23] J. Mielke, F. Hanke, M. V. Peters, S. Hecht, M. Persson, L. Grill, *J. Am. Chem. Soc.* **2015**, *137*, 1844–1849.
[24] T. E. Shubina, H. Marbach, K. Flechtner, A. Kretschmann, N. Jux, F. Buchner, H.-P. Steinrück, T. Clark, J. M. Gottfried, *J. Am. Chem. Soc.* **2007**, *129*, 9476–9483.
[25] E. Inami, M. Yamaguchi, R. Nemoto, H. Yorimitsu, P. Krüger, T. K. Yamada, *J. Phys. Chem. C* **2020**, *124*, 3621–3631.
[26] M. Lepper, J. Köbl, L. Zhang, M. Meusel, H. Holzel, D. Lungerich, N. Jux, A. de Siervo, B. Meyer, H. P. Steinruck, H. Marbach, *Angew. Chem. Int. Ed.* **2018**, *57*, 10074–10079; *Angew. Chem.* **2018**, *130*, 10230–10236.
[27] M. Lepper, T. Schmitt, M. Gurrath, M. Raschmann, L. Zhang, M. Stark, H. Hölzel, N. Jux, B. Meyer, M. A. Schneider, H.-P. Steinrück, H. Marbach, *J. Phys. Chem. C* **2017**, *121*, 26361–26371.
[28] S. Gottardi, K. Müller, J. C. Moreno-López, H. Yildirim, U. Meinhardt, M. Kivala, A. Kara, M. Stöhr, *Adv. Mater. Interfaces* **2014**, *1*, 1300025.
[29] M. Hansen, K. Anderko, in *'Constitution of binary alloys'*, McGraw-Hill, **1965**.
[30] S. Rangan, P. Kim, C. Ruggieri, S. Whitelam, R. A. Bartynski, *Phys. Rev. B* **2019**, *100*.
[31] R. C. de Campos Ferreira, A. Perez Paz, D. J. Mowbray, J.-Y. Roulet, R. Landers, A. de Siervo, *J. Phys. Chem. C* **2020**.
[32] A. Sperl, J. Kröger, R. Berndt, *J. Am. Chem. Soc.* **2011**, *133*, 11007–11009.
[33] Y. Wang, J. Kröger, R. Berndt, W. A. Hofer, *J. Am. Chem. Soc.* **2009**, *131*, 3639–3643.
[34] I. Horcas, R. Fernández, J. Gomez-Rodriguez, J. Colchero, J. Gómez-Herrero, A. Baro, *Rev. Sci. Instrum.* **2007**, *78*, 013705.
[35] D. Nečas, P. Klapetek, *Open Phys.* **2012**, *10*, 181–188.

Manuscript received: October 23, 2020
Revised manuscript received: December 4, 2020
Accepted manuscript online: December 7, 2020
Version of record online: January 15, 2021

ChemPhysChem

Supporting Information

Metalation of 2HTCNPP on Ag(111) with Zn: Evidence for the Sitting atop Complex at Room Temperature

Jan Kuliga, Rodrigo Cezar de Campos Ferreirra, Rajan Adhikari, Stephen Massicot, Michael Lepper, Helen Hölzel, Norbert Jux, Hubertus Marbach, Abner de Siervo,* and Hans-Peter Steinrück*

Supporting information

The supporting material provides additional information demonstrating:

- The adsorption of molecules at step edges at low coverage, and evidence for a mobile 2D gas phase (**Figure S1**).
- Additional STM images showing the coexistence of island structures A, B and C, complementing the data shown in Figure 2 in the manuscript (**Figure S2**).
- STM images of 2HTCNPP with different amounts of post-deposited Zn, verifying the number of bright protrusions increase with increasing amount of deposited Zn (**Figure S3**).
- Consecutive STM images documenting the diffusion of two Zn protrusions to other 2HTCNPP molecules (**Figure S4**).
- STM images of 2HTCNPP, 2HTCNPP + Zn, and ZnTCNPP + Zn, to highlight the formation of extended long-range ordered phases for ZnTCNPP + Zn (**Figure S5**).
- STM images of 2HTCNPP + Zn islands of structure B (top) and C (down) before and after a positive voltage tip pulse, complementing to the data for structure A in Figure 5 of the main manuscript to demonstrate that switching occurs independent of the island type (**Figure S6**).
- STM movies of 2HTCNPP + Zn islands during and after appyling voltage pulses, measured in Erlangen (**Movie M1**) and Campinas (**Movie M2**).

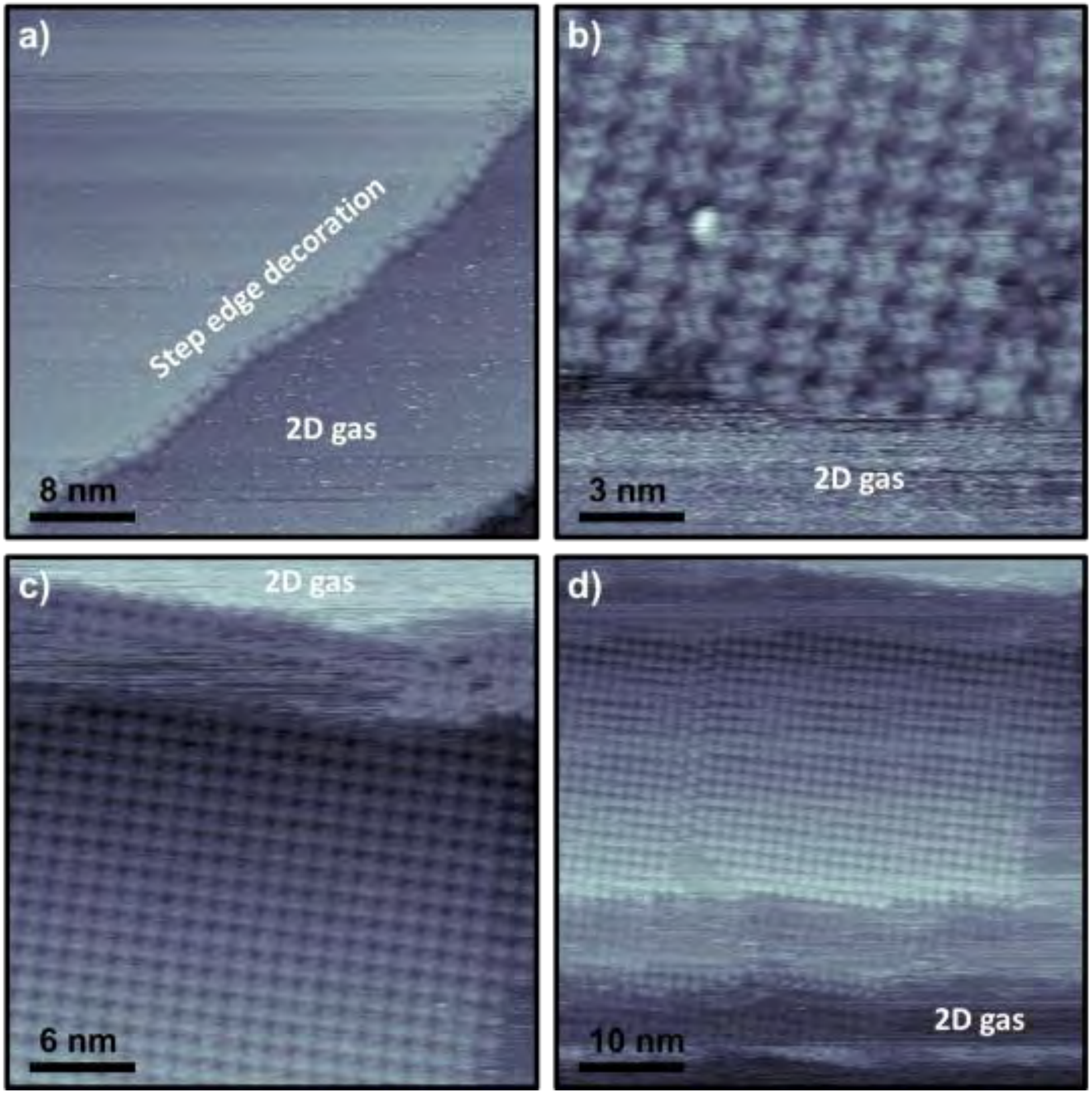

Figure S1: a) Step edges of Ag(111) are covered with 2HTCNP molecules at low coverages. The stripy features on the terraces are 2D gas (STM Erlangen, U= -1260 mV, I = 29 pA). b-d) At higher coverages the molecules start to build larger 2D structures with individual fast diffusing molecules are still present as a 2D gas phase (stripy features). Image b (U= -1250 mV, I = 26 pA) was measured with the STM in Erlangen, while c (U= -670 mV, I = 15 pA) and d (U= -670 mV, I = 14 pA) with the STM in Campinas.

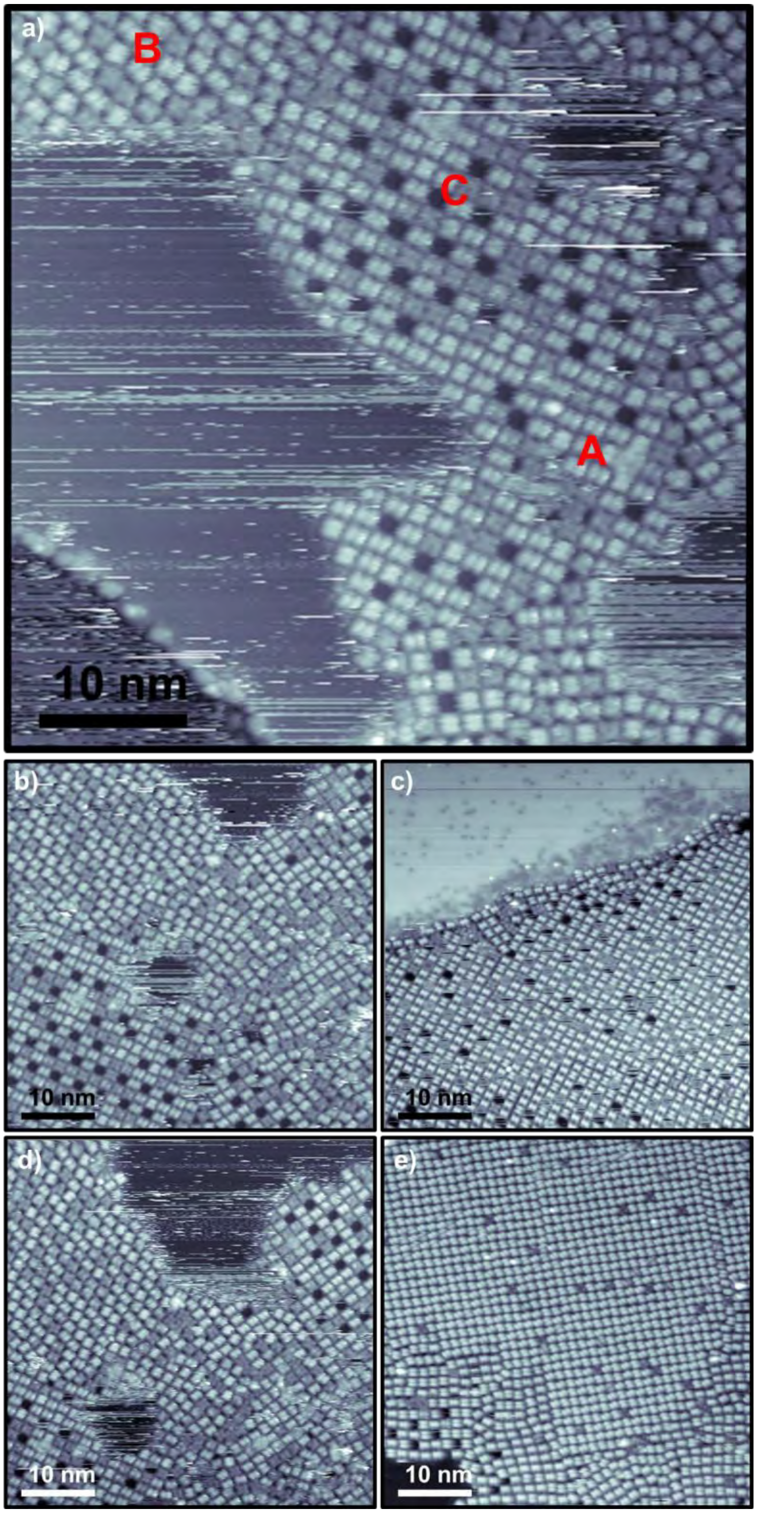

Figure S2: Different STM images showing the coexistence of island structures A, B and C, measured with the STM in Erlangen (a, b and d; U= -1666 mV, I = 29 pA) and Campinas (c and e; U= -1490 mV, I = 12 pA; U= -1444 mV, I = 10 pA).

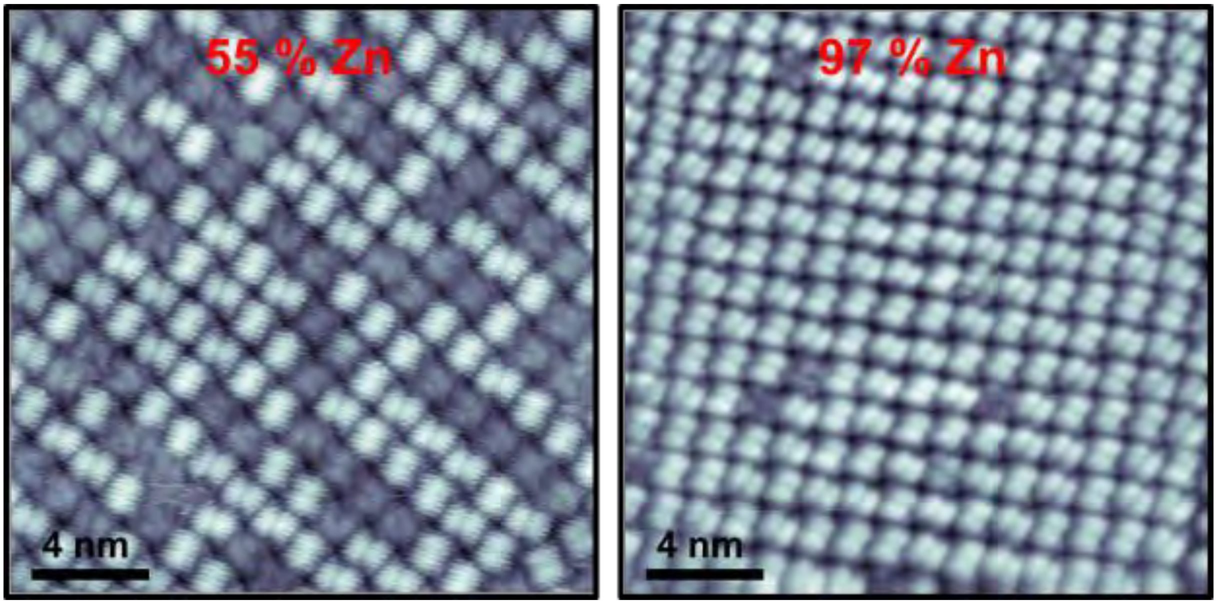

Figure S3: Two STM images of 2HTCNPP with different amount of post-deposited Zn (STM Erlangen, U= -810 mV, I = 34 pA, U= -800 mV, I = 30 pA). A evaporation time of 2 min yielded a Zn interaction with 55 % of the molecules (left image), while 5 min Zn evaporation yielded 97 %.

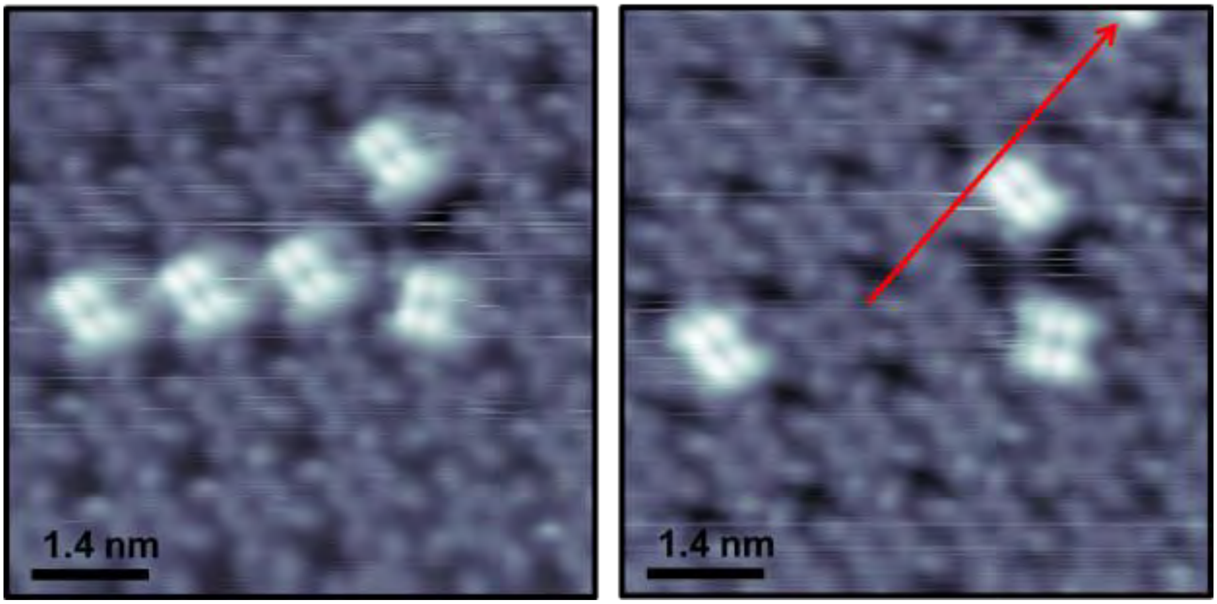

Figure S4: Consecutive STM images after the diffusion of two Zn protrusions to other 2HTCNPP molecules indicated by red arrow (STM Campinas, U= -1200 mV, I = 17 pA).

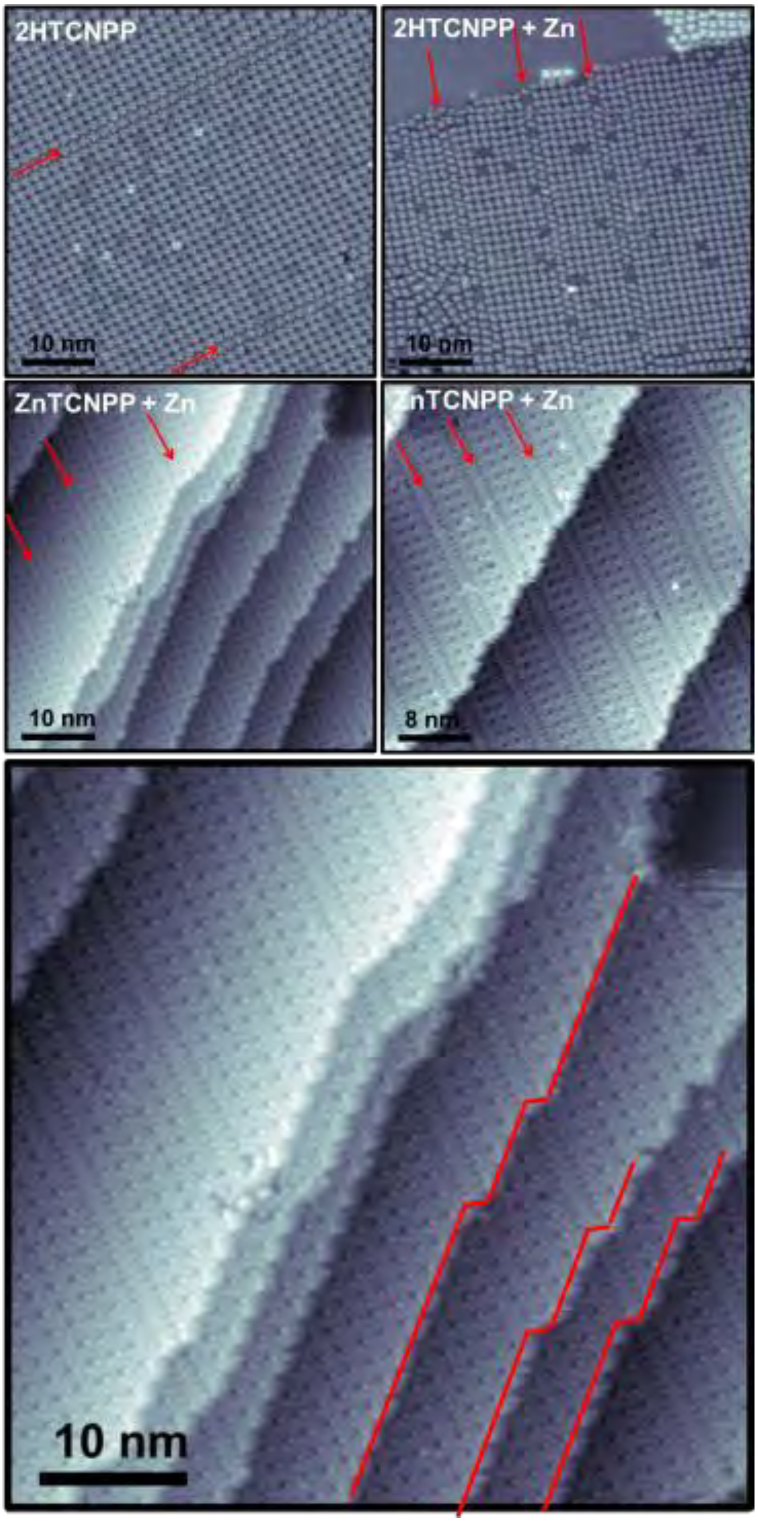

Figure S5: STM images of 2HTCNPP (STM Erlangen, U= -850 mV, I = 19 pA), 2HTCNPP + Zn (STM Campinas, U= -1444 mV, I = 15 pA) and ZnTCNPP + Zn (STM Erlangen, U= -1000 mV, I = 30 pA; U= -455 mV, I = 30 pA) showing molecular rows with a different azimuthal orientation (red arrows point along the different orientated rows). Enlarged image shows the red highlighted the shape of the step edges (STM Erlangen, U= -1000 mV, I = 30 pA).

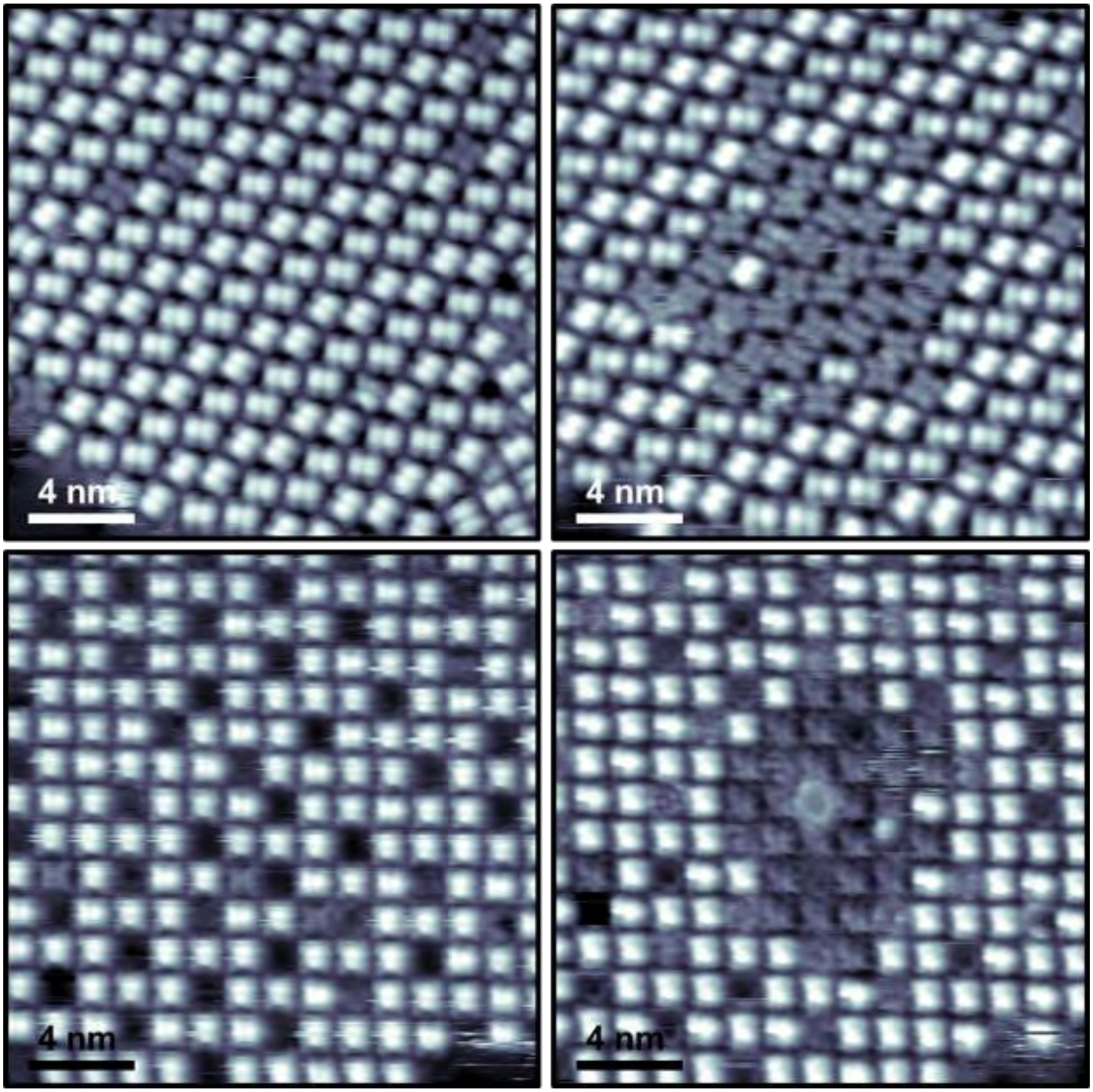

Figure S6: STM images of 2HTCNPP + Zn islands of structure B (top) and C (down) before and after a positive voltage tip pulse (STM Campinas, top row U= -1030 mV, I = 12 pA, U= -1030 mV, I = 19 pA; down row U= -1400 mV, I = 10 pA, U= -1400 mV, I = 7 pA).

Movie M1: STM movie (5 fps) of 10 consecutive taken STM images of an 2HTCNPP island (structure A) covered with Zn. A positive voltage tip pulse of + 2.73 V was applied in the middle of frame 3 (STM Erlangen, U= -1660 mV, I = 30 pA); see separate file.

Movie M2: STM movie (5 fps) of 13 consecutive taken STM images of an 2HTCNPP island (structure B) covered with Zn. A positive voltage tip pulse of + 2.5 V was applied in the middle of frame 2 (STM Campinas, U= -1030 mV, I = 12-19 pA); see separate file.

10.1.4[P4]

On the adsorption of different tetranaphthylporphyrins on Cu(111) and Ag(111)

J. Brox, R. Adhikari, M. Shaker, M. Ruppel, N. Jux, H. Marbach, S. Jaekel, and H.-P. Steinrück, *Surface Science*, ***720***, 122047 (**2022**); 10.1016/j.susc.2022.122047

Surface Science 720 (2022) 122047

Contents lists available at ScienceDirect

Surface Science

journal homepage: www.elsevier.com/locate/susc

On the adsorption of different tetranaphthylporphyrins on Cu(111) and Ag (111)

Jan Brox [a], Rajan Adhikari [a], Majid Shaker [a], Michael Ruppel [b], Norbert Jux [b], Hubertus Marbach [a], Simon Jaekel [a], Hans-Peter Steinrück [a,*]

[a] *Lehrstuhl für Physikalische Chemie II, Friedrich-Alexander-Universität Erlangen-Nürnberg, Egerlandstr. 3, Erlangen 91058, Germany*
[b] *Lehrstuhl für Organische Chemie II, Friedrich-Alexander-Universität Erlangen-Nürnberg, Nikolaus-Fiebiger-Str. 10, Erlangen 91058, Germany*

ARTICLE INFO

Keywords:
STM
Porphyrins
Self-assembly
Naphthyl functionalization
Commensurability

ABSTRACT

We address the adsorption of 2H-tetranaphthylporphyrin (2HTNP) and 2H-tetranaphthylbenzoporphyrin (2HTNBP) on Cu(111) and Ag(111). The difference between the two molecules is that for 2HTNBP the pyrrole groups are replaced by isoindole groups. We were interested in the resulting differences in the adsorption behavior on the two surfaces, in particular the role of the naphthyl groups. The investigations are performed with scanning tunneling microscopy at room temperature (RT) and after heating treatments (500 and 600 K). On Ag (111), 2HTNP forms a commensurable superstructure at RT, which transforms to a denser packed, non-commensurable structure upon annealing. For 2HTNBP, individual molecules are observed on Cu(111) at RT, which exhibit different mobility. In contrast, on Ag(111) the formation of ordered 2HTNBP islands occurs, which are stabilized by T-type interactions. After heating to 500 K, these islands undergo a structural change to a denser packed structure, which is stabilized by π-π stacking of neighboring naphthyl groups.

1. Introduction

Over the past years the design and fabrication of functional materials at the nanoscale has become a major topic in science [1]. One of the most promising approaches to address the growing demand of miniaturization in areas like catalysis, energy storage and conversion, electronic and photonic devices is the bottom-up route [1, 2]. In this method, functional building blocks adsorb and self-assemble on well-defined surfaces [3]. The adsorption of functional organic molecules on metal surfaces has proven to be a suitable method for the construction of such architectures at the nanoscale [1, 4, 5]. Among the wide variety of functional organic molecules, porphyrins are particularly promising building blocks for the fabrication of nanostructures for various reasons. Porphyrins are omnipresent as main functional groups in nature, e.g. in heme, chlorophyll and vitamin B [6, 7]. Their conformational and structural flexibility yields a large variety of supramolecular structures on surfaces [4, 8, 9]. Zinc-metalated porphyrin derivatives are used in solar cells or gas sensing applications, while Co-porphyrins are used for the reduction of oxygen to water [10–12].

In order to obtain a fundamental understanding of the formation of nano-scale materials on surfaces, their structure has to be characterized in detail. In particular, scanning tunneling microscopy (STM) has been proven as a powerful tool to investigate the adsorption behavior of porphyrins at the nanoscale by identifying the intramolecular conformation, electronic structure and intermolecular interaction motifs [8, 13]. Their adsorption behavior can be tuned by their ability to coordinate different metal centers at the macrocycle (Ce [14], Fe [15, 16], Cu [17, 18], Co [19]…) or the functionalization of the periphery with different side groups [9, 20-27]. Furthermore, extensive studies [3, 28] have correlated the influence of the chemical nature of substrate [29, 30], molecular coverage [31], and thermal treatments [8, 32] to the observed adsorption conformation and supramolecular arrangement of the different porphyrins.

Due to its symmetry and structural simplicity, 2H-tetraphenylporphyrin (2HTPP) was established as a well-understood reference system [17, 33, 34]. Replacing the symmetric phenyl- with asymmetric naphthyl groups (with respect to rotation around the C—C bond to the macrocycle) resulted in the presence of ten surface conformers (including chiral and non-chiral species) on Cu(111) at RT [35]. In addition, the mobility strongly depends on the specific conformation and could be linked to the footprint of the molecules. Besides the introduction of rotational symmetry axis, steric effects can have an

---

* Corresponding author.
E-mail address: hans-peter.steinrueck@fau.de (H.-P. Steinrück).

https://doi.org/10.1016/j.susc.2022.122047
Received 23 December 2021; Received in revised form 27 January 2022; Accepted 3 February 2022

influence on the adsorption conformation. Ditze et al. showed that the addition of di-tert-butyl groups to the phenyl legs of 2HTPP resulted in two thermal switchable surface conformers [24]. Replacing one of the di-tert-butylphenyl legs with methoxycarbonylphenyl and metalating the porphyrin with platinum allowed Mishra et al. for building a supramolecular motor based on a chiral directional switch on the surface [36]. Another interesting class of porphyrins with steric bulky side groups are tetrabenzoporphyrins, which received a lot of scientific attention, due to their importance in several applications in fields like catalysis, medicine and material science [37].

Herein, we expand our studies on the influence of the naphthyl group on the adsorption behavior of 2HTNP on Ag(111) and 2H-tetranaphthylbenzoporphyrin (2HTNBP) on Cu(111) and Ag(111). Most interestingly, we observed the individual adsorption of 2HTNBP molecules on Cu (111). Our systematic study by STM at RT and different heat treatments reveal the flexibility of the naphthyl group to undergo different intermolecular interactions. The interaction motifs range from repulsive interactions occurring at too close specific adsorption sites to attractive T-type bonding and π-π stacking arrangements.

2. Experimental section

The experiments and sample preparations were performed in a two-chamber ultrahigh vacuum (UHV) system at a background pressure in the low 10^{-10} mbar regime. The variable temperature scanning tunneling microscope (STM) is an RHK UHV VT STM 300 instrument with RHK SPM 1000 electronics. All STM images were acquired at and slightly below room temperature (RT and −52 °C) in constant current mode with a Pt/Ir tip, and the bias applied to the sample. The STM images were processed with WSxM software [38] and moderate filtering (Gaussian smoothing, background subtraction) was applied for noise reduction. The preparation of the clean Ag(111) and Cu(111) surfaces was done by repeated cycles of Ar^+ sputtering (600 eV) and annealing to 850 K. The 2HTNP and 2HTNBP molecules were deposited onto the metal substrates held at RT, by thermal sublimation from a home-built Knudsen cell, at nominal temperatures of 430 °C and 510 °C, respectively.

3. Results and discussion

We study the influence of naphthyl groups on the adsorption behavior of porphyrins on single crystal surfaces by investigating 2HTNBP on Cu(111) and Ag(111). For the same molecule without the isoindole groups, that is, 2HTNP, we previously demonstrated the simultaneous presence of ten different surface conformers [35]. These different conformers result from the rotation of the naphthyl group around the single C—C bond to the porphyrin macrocycle, which can occur independently for the four naphthyl groups. In order to obtain a systematic understanding, we also studied the influence of this group on the adsorption behavior of 2HTNP on Ag(111), that is, for a less reactive substrate. The chemical structure and space filling ball models of 2HTNP and 2HTBNP are depicted in Fig. 1. The difference between the two molecules is that the four pyrrole groups in 2HTNP are replaced by four isoindole groups in 2HTBNP. Both molecules are displayed in their saddle-shape conformation and the naphthyl group orientation to the surface was set to 26°, which corresponds to the DFT-calculated phenyl angle of the molecule with phenyl instead of naphthyl groups, that is, 2H-tetraphenylporphyrin (2HTPP) on Cu(111) [39]. The two upright standing pyrrole groups of 2HTNP and isoindole groups of 2HBNTP are highlighted in yellow in the structural models.

In order to better understand the adsorption behavior of the different porphyrins on metal surfaces, we start by comparing STM images of 2HTNP and 2HTNBP on Cu(111) at low coverages, where in the absence of island formation the behavior of individual molecules can be studied without the influence of lateral interactions. For 2HTNP, we observed the adsorption of individual molecules on the surface, with no long range order [35]: The molecules adopt the so-called inverted adsorption conformation, that is, two pyrrole groups are standing nearly perpendicular to the surface. For the related 2HTPP molecule, Lepper et al. could demonstrate that on Cu(111) the inverted structure is 0.3 eV more stable than the corresponding saddle shape [39, 40]. In contrast to 2HTNP and also 2HTPP, benzoporphyrins are in general not known for inverted structures, and typically adsorb as saddle shape conformers, which form islands both on Cu(111) and Ag(111) since their attractive intermolecular interactions are stronger than their site-specific molecule/substrate interaction [41–43].

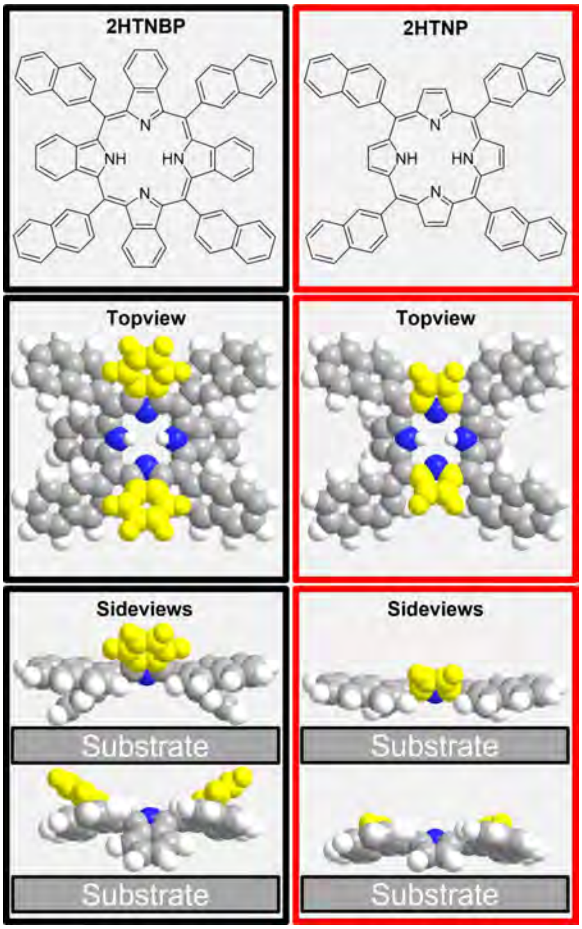

Fig. 1. Chemical structure and top/side views of a space-filling model of the saddle shape of 2H-tetranaphthylbenzoporphyrin (left side) and 2H-tetranaphthylporphyrin (right side). The yellow highlighted isoindole/pyrrole groups are pointing away from the surface.

Fig. 2a and 2b depict a low coverage of 2HTNBP adsorbed on Cu (111) at RT. The molecules appear as singular circular protrusions on the terraces and at step edges of the surface. In addition, we observe streaky features on the terraces, which are attributed to fast diffusing molecules which can be regarded as a 2D gas phase. The molecular appearance unfortunately gives no further information about the conformation and orientation of the naphthyl groups. The behavior of individual adsorbed 2HTNBP molecules is untypical for benzoporphyrins and other comparably large tetrapyrrols like phthalocyanins, which form islands on the surfaces studied so far, that is, Ag(111) and Cu(111) [24, 44, 45]. This indicates a stronger molecule/substrate interaction of 2HTNBP on Cu (111), which indicates a better coordination of the iminic nitrogen atoms of the isoindole groups to Cu substrate atoms, like for 2HTPP and 2HTNP in the inverted structure. An additional driving force for the strong interaction with the substrate could be the larger footprint of the naphthyl groups. For 2HTNP on Cu(111), we found that the orientation of the naphthyl groups had an influence on the mobility of the

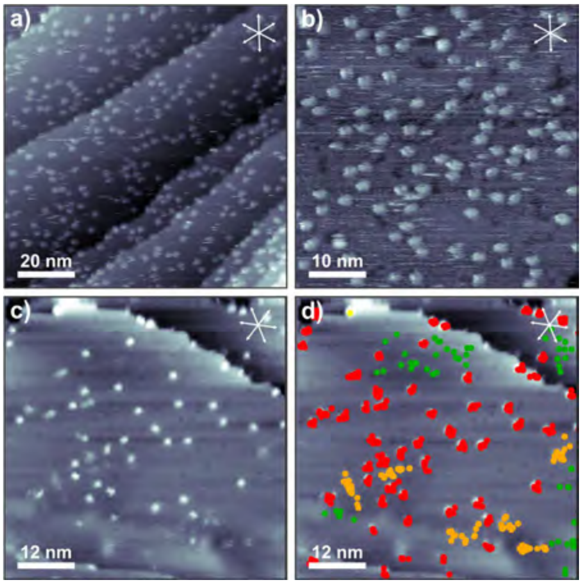

Fig. 2. a) and b) STM images of 2HTNBP on Cu(111) measured at RT. c) Average frame over 14 consecutive taken STM images of 2HTNBP on Cu(111). d) Overview of the position of each molecule in each individual frame and superimposed over the average frame. Molecules are color-coded according to their mobility (red: immobile, orange: medium translation and rotation, green: fast translation and rotation, mostly not even resolvable as molecules). Tunneling parameters: a) U = -1000 mV, I = 290 pA; b) U = -800 mV, I = 300 pA; c, d) U = -1000 mV, I = 300 pA.

molecules: Surface conformers with a larger footprint are less mobile, possibly due to a larger corrugation of the interaction potential and/or due to a larger adsorption energy. 2HTNBP has an even larger footprint compared to 2HTNP (isoindole instead of pyrrole groups) and benzoporphyrins (naphthyl instead of phenyl groups). Both effects could contribute to an increased adsorption energy. Our STM images collected at RT, however, do not provide insights into the actual conformation. Notably, also measurements at lower temperatures (−52 °C) did not improve the image quality (Figure S1).

For further comparison of 2HTNP and 2HTNB, we studied the dynamic behavior of 2HTNBP by acquiring STM movies and motion-pathway-plots (superposition of the position of individual molecules over time); see Fig. 2d. Using similar plots for 2HTNP, we found a strong dependence of its mobility on the molecular conformation, that is, the orientation of the naphthyl groups [35]. For 2HTNBP, we again observe three different behaviors: Most of the molecules are immobile (red) and diffuse only occasionally in close vicinity of the starting spot in the first frame (individual frames are shown in the SI in Figure S2). This diffusion occurs in no preferred direction. Species with medium mobility are marked in yellow. Their diffusion behavior is faster and directed along one of the high symmetry axes (closed packed rows) of the Cu(111) substrate and occasionally hop to a neighboring closed-packed row. Furthermore, these molecules switch the direction of diffusion (alignment with the high symmetry axis) by 120° in consecutive STM images. Finally, very mobile species (green) are observed, which move too fast on the surface at RT to clearly capture their appearance as individual molecules in an STM frame of the movie; they rather appear as streaky protrusions, which diffuse with no preferred direction on the surface. At this point, we want to note that we rule out that the different species are due to decomposition, since we are not aware of any study reporting porphyrin decomposition on Cu(111) at room temperature; also metalation is unlikely, since in this case the number of metalated (mobile) species should increase with time, which is not observed. Further, metalloporphyrins are typically too mobile to be imaged as individual molecules at room temperature [23, 33, 46].

In order to gain deeper understanding of the adsorption behavior of naphthyl-functionalized porphyrins and their intermolecular interaction, we studied 2HTNP and 2HTNBP on Ag(111) at RT. Since on Ag (111) both molecules show island formation already staring at low coverages, we investigate larger coverages than on Cu(111). Fig. 3 shows the adsorption behavior of 2HTNP at coverages below a closed layer of densely packed molecules. We observe the coexistence of perfectly long-range ordered regions and disordered regions of molecules. The molecular appearance is dominated by a central depression, which resembles the cavity of the macrocycle. The four smaller protrusions at the periphery of the macrocycle are assigned to the four naphthyl groups. The molecules are elongated in one direction, which would resemble a $\tau\tau\tau\tau$-orientation of the naphthyl groups according to the annotation established for 2HTNP on Cu(111); this means that all four naphthyl groups point towards the main molecular axis through the iminic isoindole groups [35]. The long-range ordered islands consist of parallel rows of neighboring molecules, with a nearly rectangular unit cell. The unit cell parameters of the islands are $b_1 = 2.01 \pm 0.04$ nm, $b_2 = 1.28 \pm 0.04$ nm and $\alpha = 84^\circ \pm 5^\circ$. The intermolecular distance along b_1 is larger than the length of one molecule (~1.8 nm as estimated from its van-der-Waals dimension). The length of the b_1 vector matches 7 Ag-Ag distances (2.02 nm) within the margin of error and is perfectly aligned along one of the high symmetry axes of the substrate. Since the b_2 vector is also a combination of substrate lattice vectors (see below), we conclude that the molecules have a favorable adsorption site on the surface. Fig. 3c illustrates the island structure by overlaying scaled molecular models over a Ag(111) surface. It clearly shows that molecules of neighboring rows have a higher separation from each other (along the b_1 vector) compared to the molecules within a row (b_2 vector). This indicates that for well-defined adsorption sites the intermolecular interactions at a row distance below the observed 7 Ag-Ag distances are repulsive and cannot be overcome by the molecule/-substrate interaction of additionally adsorbed molecules. Thus, at the given azimuthal orientation stronger repulsive interactions due to a denser packing of neighboring rows (e.g. 6 Ag-Ag distances along the surface vector a) cannot be overcompensated by the energy gained by more molecules at specific adsorption sites. The angle $\alpha = 84^\circ$ reflects, within our experimental margin of error, the closest packable surface site in b_2 direction, which would lead to the proposed stacking behavior along the direction of the lattice vector b_1 for the next row. The proposed $\begin{pmatrix} 7 & 0 \\ -2 & 5 \end{pmatrix}$ structure is commensurable with the surface (Figure S3). The unit cell parameters determined from experiment agree with the parameters calculated for the commensurate superstructure, that is, $b_1 = 2.02$ nm ($7a$), $b_2 = 1.26$ nm ($\sqrt{19}a$) and $\alpha = 83.4^\circ$, within the experimental margin of error.

Site-specific adsorption behavior is normally observed on Cu(111) for inverted porphyrin structures [23, 39, 47]. Notably, on the less reactive Ag(111) surfaces studied in the literature, island formation occurs mostly caused by intermolecular interactions without adsorption site specifity [15, 41, 48]. In Fig. 3e, the outer phenyl ring of the naphthyl groups sits on the same adsorption site as the center of the macrocycle. The top view perspective suggests an apparent overlap of the naphthyl groups, which is not present in the actual structure, since the naphthyl group is tilted against the surface, due to steric hindrance within the molecule. Notably, our STM images give no evidence whether these adsorption sites are on top, bridge or hollow sites.

Upon annealing 2HTNP on Ag(111) to 600 K, the appearance of the molecules remains unchanged and only a change in the island structure is observed (Fig. 3d). The length of unit cell vector c_1 stays comparable to seven close-packed Ag-Ag distances, but the angle between the unit cell vectors decreases to 71°. Furthermore, the orientation of the molecules themselves and their unit cell to the substrate change. The molecules and unit cell are no longer orientated along one of the high symmetry axes, but their main molecular axis (line through iminic

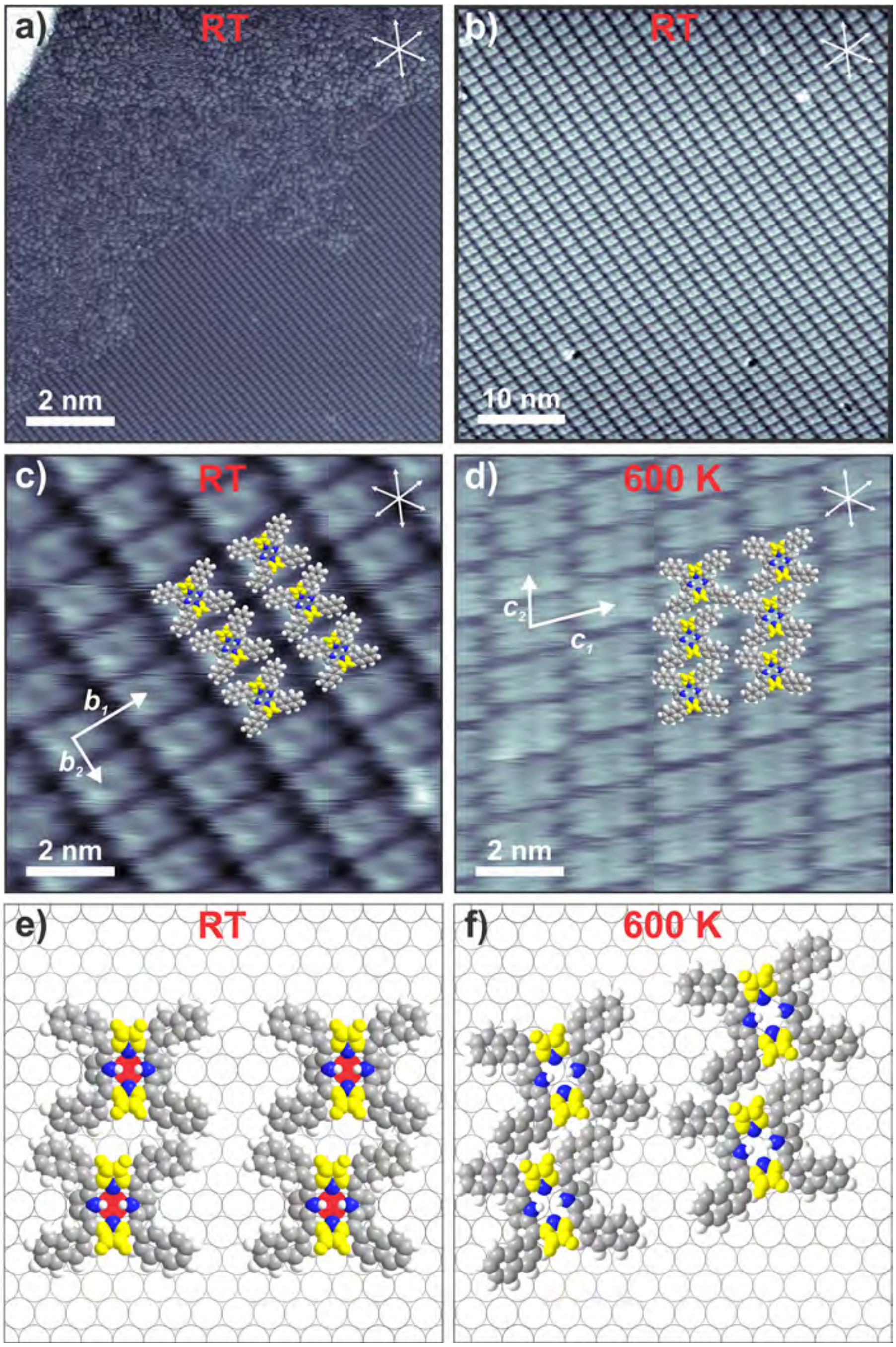

Fig. 3. a) and b) STM images of islands formed by 2HTNP on Ag(111) at RT. c) High resolution STM images overlaid with space-filling molecular models of 2HTNP and its unit cell vectors (white). d) High resolution STM images overlaid with space-filling molecular models of 2HTNP and its unit cell vectors (white). e) Molecular models overlaid on an atomic Ag(111) surface to emphasize the adsorption sites at RT. The on top adsorption site was used for illustration. f) Molecular models overlaid on an atomic Ag(111) surface to emphasize the adsorption sites after annealing to 600 K. The on top adsorption site was used for illustration. Tunneling parameters: a, b , c) U = -100 mV, I = 300 pA; d) U = -1050 mV, I = 290 pA.

pyrrole groups) is rotated by 16° ± 2°. The unit cell parameters are $c_1 = 2.02 \pm 0.04$ nm, $c_2 = 1.22 \pm 0.04$ nm and $\alpha = 71^\circ \pm 5^\circ$. Even though the unit cell vector c_1 is not aligned anymore with one of the high symmetry axes of the surface, it keeps the same length as observed for the structure at RT. Fig. 3f evidences that the overlaid molecules in this structure do not have the same adsorption sites and that the structure is not commensurable with the substrate anymore. Considering the orientation of the molecular unit cell on the surface only every third molecule could sit on the same adsorption site as the first (Figure S4). We propose that the driving force for this change is the increased density of molecules, from 0.39 molecules/nm^2 at RT to 0.43 molecules/nm^2 after annealing. The energy gained by additional adsorbed molecules exceeds the energy the molecules gain by adsorbing on specific adsorption sites.

We next move on to the adsorption of the larger 2HTNBP molecule on Ag(111). Upon deposition of medium coverages in the monolayer range, Fig. 4a and 4b show close-packed, long-range ordered supramolecular structures, which are surrounded by a 2D gas phase of fast diffusing molecules (stripy features). Fig. 4c depicts an enlarged area of the formed islands. The molecular appearances of individual 2HTNBP molecules are different from that of 2HTNP, with the macrocycle and the naphthyl groups not visible. The appearance is rather dominated by two parallel elongated protrusions (yellow circles Fig. 4d), which are assigned to the two upright standing isoindole groups of the macrocycle in the saddle-shape conformation. Fig. 4d shows the superposition of molecules onto the STM images, and the square arrangement of the unit cell with $d_1 = 1.58 \pm 0.04$ nm, $d_2 = 1.54 \pm 0.04$ nm and $\alpha = 90^\circ \pm 5^\circ$. The d_1 and d_2 vectors of the unit cell coincide with one of the [110] and [211] axes of the Ag(111) surface. The molecules are aligned along the d_2 vector of the unit cell; thereby, the main molecular axis is defined as the line separating the two upright standing isoindole units (yellow

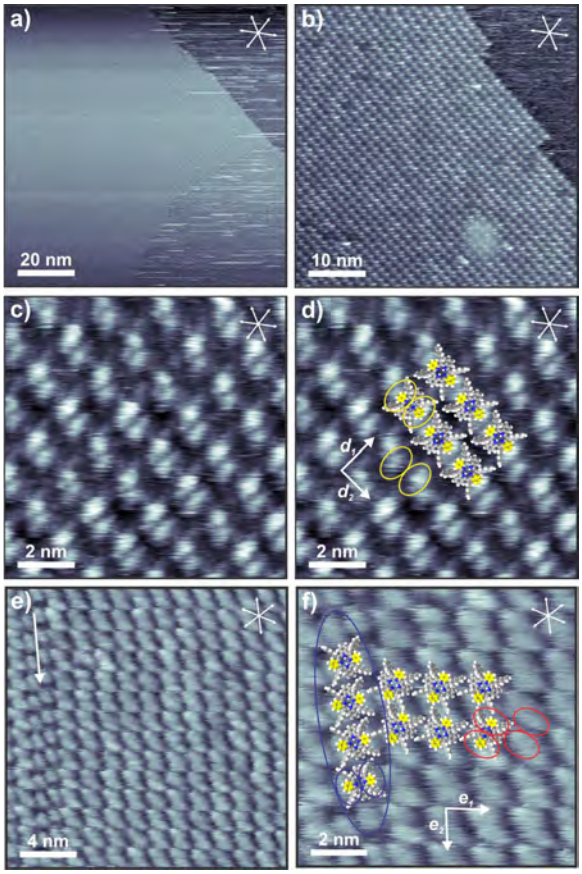

Fig. 4. a, b and c) STM images of islands formed by 2HTNBP on Ag(111) at RT. d) High resolution STM image overlaid with space-filling molecular models of 2HTNBP and its unit cell vectors (white) e) High resolution STM image after annealing to 500 K. The island has a line defect (white arrow), in which the molecules are rotated against the molecules of the main island. f) Overlay of space filling molecules to show the different orientations in the line defect (small blue ovals indicate the upward bent isoindole groups) and the island (red ovals). For further details see text. Tunneling parameters: a) U = -1000 mV, I = 200 pA; b) U = 1000 mV, I = 200 pA; c, d) U = -1910 mV, I = 290 pA; e, f) U = -2500 mV, I = 310 pA.

ellipses). Within the experimental margin of error, every second molecule along d_1 and every molecule along d_2 occupy the same adsorption site. The adsorption behavior is very different from that on Cu(111). We attribute this difference to weaker and less site-specific molecule/substrate interactions due to a weaker porphyrin-Ag-coordination, which leads to a dominance of intermolecular interactions. In the structural arrangement shown in Fig. 4d, each naphthyl group points directly to a neighboring naphthyl group and forms T-type interactions, which are well known in literature for aromatic systems [15, 49, 50].

Fig. 4e depicts an STM image of 2HTNBP molecules on Ag(111) acquired at RT after annealing to 500 K for 10 min, and in Fig. 4f the same image is shown at an enlarged scale with space-filling models overlaid. The big blue oval highlights a domain boundary. At the domain boundary, a domain wall is formed which consists of one row of molecules with a different azimuthal orientation compared to the orientation in the domains right and left of the boundary. The molecular appearance within the domain wall corresponds to a parallel pair of elongated protrusions (small blue ovals) like seen at RT in Fig. 4d. This assignment also helps us to unequivocally assign two parallel protrusions in the larger domains to individual molecules, now marked with small red ovals. The molecules in the domain wall still interact with T-type interactions between neighboring naphthyl groups. Furthermore, the interaction at the domain boundary is T-type as well. The naphthyl groups of neighboring molecules inside the extended domains stand parallel to each other and interact via π-π stacking. The slight apparent overlap of the molecular models in Fig. 4f is only due to the perspective of the top view. The unit cell of the annealed structure is again nearly quadratic $e_1 = 1.50 \pm 0.04$ nm, $e_2 = 1.49 \pm 0.04$ nm and $\alpha = 88^\circ \pm 5^\circ$, with the same alignment with respect to the substrate as the non-annealed structure (see above). Within the experimental margin of error, every third molecule along e_1 and every molecule along e_2 occupy the same adsorption site. The driving force for the structural change is again the energy gain by adsorbing more molecules per surface area. The molecular density increases from 0.41 molecules/nm^2 at RT to 0.45 molecules/nm^2 at 500 K.

Conclusions

The goal of this study was to expand our understanding of the influence of the asymmetric naphthyl group on the adsorption behavior of 2HTNP on Ag(111), and of 2HTNBP on Cu(111) and Ag(111). The difference between the two molecules is that for 2HTNBP in addition to the introduction of the naphthyl group the pyrrole groups are replaced by isoindole groups. Interestingly, we observe no island formation but individual 2HTNBP molecules on the Cu(111) surface, which indicates a strong interaction of this porphyrin with the substrate, as was previously also observed for 2HTPP and 2HTNP on Cu(111). Possible driving forces could be a coordination of the iminic nitrogen atoms of the isoindole groups to Cu substrate atoms, like for 2HTPP and 2HTNP, and the larger footprint of the molecules. For 2HTNP on Ag(111), we observed a commensurable $\begin{pmatrix} 7 & 0 \\ -2 & 5 \end{pmatrix}$ structure, which indicates identical adsorption sites for each molecule. Upon annealing to 600 K, the structure loses its commensurability with the substrate and a transition to a denser packed arrangement occurs. Notably, the molecules keep the same distance along one unit cell vector, which is, however, no longer aligned along one of the surface high symmetry substrate axes. Within the margin of error only every third molecule has the same adsorption site on the surface. For the porphyrin with the pyrrole groups substituted by isoindole groups, that is, 2HTNBP, we observed also on Ag(111) island formation at RT. The non-commensurable structure is stabilized by T-type interactions, between the naphthyl groups of neighboring molecules. Upon annealing to 500 K, the structure converts to a structure with a slightly higher density, which is now stabilized by π-π stacking of neighboring naphthyl groups. Our studies reveal a pronounced difference of the adsorption of the porphyrins on Cu(111) and Ag(111) surfaces, which is maintained when the pyrrole groups are replaced by an isoindole group and the phenyl groups by naphthyl groups. The flexibility of the naphthyl group allows for the formation of different structural motifs based on repulsive interactions occurring at too close specific adsorption sites or attractive interactions via T-type bonding or π-π stacking arrangements.

Declaration of Competing Interest

The authors declare that they have no known competing financial interests or personal relationships that could have appeared to influence the work reported in this paper.

Acknowledgment

The authors gratefully acknowledge funding by the Deutsche Forschungsgemeinschaft (DFG) through Research Unit FOR 1878 (funCOS) and the Collaborative Research Center SFB 953 (project number 182849149) at the Friedrich-Alexander-Universität Erlangen-Nürnberg.

Supplementary materials

Supplementary material associated with this article can be found, in the online version, at doi:10.1016/j.susc.2022.122047.

References

[1] J.V. Barth, G. Costantini, K. Kern, Engineering atomic and molecular nanostructures at surfaces, Nature 437 (2005) 671–679.
[2] L. Sosa-Vargas, E. Kim, A.-J. Attias, Beyond "decorative" 2D supramolecular self-assembly: strategies towards functional surfaces for nanotechnology, Mater. Horiz. 4 (2017) 570–583.
[3] W. Auwärter, D. Écija, F. Klappenberger, J.V. Barth, Porphyrins at interfaces, Nat. Chem. 7 (2015) 105–120.
[4] T. Jung, R. Schlittler, J. Gimzewski, Conformational identification of individual adsorbed molecules with the STM, Nature 386 (1997) 696.
[5] S. De Feyter, F.C. De Schryver, Two-dimensional supramolecular self-assembly probed by scanning tunneling microscopy, Chem. Soc. Rev. 32 (2003) 139–150.
[6] K. Kadish, R. Guilard, K.M. Smith, The Porphyrin Handbook: Applications of Phthalocyanines, Academic Press, 2012.
[7] D.C. Hodgkin, J. Kamper, M. Mackay, J. Pickworth, K.N. Trueblood, J.G. White, Structure of vitamin B12, Nature 178 (1956) 64–66.
[8] H. Marbach, H.-P. Steinrück, Studying the dynamic behaviour of porphyrins as prototype functional molecules by scanning tunnelling microscopy close to room temperature, Chem. Commun. 50 (2014) 9034–9048.
[9] J.M. Gottfried, Surface chemistry of porphyrins and phthalocyanines, Surf. Sci. Rep. 70 (2015) 259–379.
[10] A.J. Mozer, M.J. Griffith, G. Tsekouras, P. Wagner, G.G. Wallace, S. Mori, K. Sunahara, M. Miyashita, J.C. Earles, K.C. Gordon, Zn− Zn porphyrin dimer-sensitized solar cells: toward 3-D light harvesting, J. Am. Chem. Soc. 131 (2009) 15621–15623.
[11] C. Peter, K. Schmitt, M. Apitz, J. Woellenstein, Metallo-porphyrin zinc as gas sensitive material for colorimetric gas sensors on planar optical waveguides, Microsyst. Technol. 18 (2012) 925–930.
[12] J.P. Collman, P. Denisevich, Y. Konai, M. Marrocco, C. Koval, F.C. Anson, Electrode catalysis of the four-electron reduction of oxygen to water by dicobalt face-to-face porphyrins, J. Am. Chem. Soc. 102 (2002) 6027–6036.
[13] F. Klappenberger, Two-dimensional functional molecular nanoarchitectures–complementary investigations with scanning tunneling microscopy and X-ray spectroscopy, Prog. Surf. Sci. 89 (2014) 1–55.
[14] A. Weber-Bargioni, J. Reichert, A. Seitsonen, W. Auwärter, A. Schiffrin, J. Barth, Interaction of cerium atoms with surface-anchored porphyrin molecules, J. Phys. Chem. C 112 (2008) 3453–3455.
[15] F. Buchner, I. Kellner, W. Hieringer, A. Görling, H.-.P. Steinrück, H. Marbach, Ordering aspects and intramolecular conformation of tetraphenylporphyrins on Ag (111), Phys. Chem. Chem. Phys. 12 (2010) 13082–13090.
[16] D. Ecija, M. Trelka, C. Urban, P.d. Mendoza, E. Mateo-Martí, C. Rogero, J. A. Martín-Gago, A.M. Echavarren, R. Otero, J.M. Gallego, Molecular conformation, organizational chirality, and iron metalation of meso-tetramesitylporphyrins on copper (100), J. Phys. Chem. C 112 (2008) 8988–8994.
[17] K. Diller, F. Klappenberger, M. Marschall, K. Hermann, A. Nefedov, C. Wöll, J. Barth, Self-metalation of 2H-tetraphenylporphyrin on Cu (111): an x-ray spectroscopy study, J. Chem. Phys. 136 (2012), 014705.
[18] K. Diller, F. Klappenberger, F. Allegretti, A. Papageorgiou, S. Fischer, A. Wiengarten, S. Joshi, K. Seufert, D. Écija, W. Auwärter, Investigating the molecule-substrate interaction of prototypic tetrapyrrole compounds: adsorption and self-metalation of porphine on Cu (111), J. Chem. Phys. 138 (2013), 154710.
[19] J.M. Gottfried, K. Flechtner, A. Kretschmann, T. Lukasczyk, H.-.P. Steinrück, Direct synthesis of a metalloporphyrin complex on a surface, J. Am. Chem. Soc. 128 (2006) 5644–5645.
[20] M. Eichberger, M. Marschall, J. Reichert, A. Weber-Bargioni, W. Auwärter, R.L. C. Wang, H.J. Kreuzer, Y. Pennec, A. Schiffrin, J.V. Barth, Dimerization boosts one-dimensional mobility of conformationally adapted porphyrins on a hexagonal surface atomic lattice, Nano Lett. 8 (2008) 4608–4613.
[21] L. Smykalla, P. Shukrynau, C. Mende, T. Rüffer, H. Lang, M. Hietschold, Interplay of hydrogen bonding and molecule–substrate interaction in self-assembled adlayer structures of a hydroxyphenyl-substituted porphyrin, Surf. Sci. 628 (2014) 132–140.
[22] S.A. Krasnikov, C.M. Doyle, N.N. Sergeeva, A.B. Preobrajenski, N.A. Vinogradov, Y. N. Sergeeva, A.A. Zakharov, M.O. Senge, A.A. Cafolla, Formation of extended covalently bonded Ni porphyrin networks on the Au (111) surface, Nano Res. 4 (2011) 376–384.
[23] M. Lepper, J. Köbl, L. Zhang, M. Meusel, H. Hölzel, D. Lungerich, N. Jux, A. de Siervo, B. Meyer, H.P. Steinrück, Controlling the self-metalation rate of tetraphenylporphyrins on Cu (111) via cyano functionalization, Angew. Chem. Int. Ed. 57 (2018) 10074–10079.
[24] S. Ditze, M. Stark, F. Buchner, A. Aichert, N. Jux, N. Luckas, A. Görling, W. Hieringer, J. Hornegger, H.-.P. Steinrück, On the energetics of conformational switching of molecules at and close to room temperature, J. Am. Chem. Soc. 136 (2014) 1609–1616.
[25] T. Wähler, R. Schuster, J. Libuda, Self-metalation of anchored porphyrins on atomically defined cobalt oxide surfaces: in situ studies by surface vibrational spectroscopy, Chem. Eur. J. 26 (2020) 12445.
[26] F. Kollhoff, J. Schneider, T. Berger, O. Diwald, J. Libuda, Thermally activated self-metalation of carboxy-functionalized porphyrin films on MgO nanocubes, ChemPhysChem 19 (2018) 2272–2280.
[27] F. Kollhoff, J. Schneider, G. Li, S. Barkaoui, W. Shen, T. Berger, O. Diwald, J. Libuda, Anchoring of carboxyl-functionalized porphyrins on MgO, TiO 2, and Co 3 O 4 nanoparticles, Phys. Chem. Chem. Phys. 20 (2018) 24858–24868.
[28] J. Otsuki, STM studies on porphyrins, Coord. Chem. Rev. 254 (2010) 2311–2341.
[29] M.P. de Jong, R. Friedlein, S. Sorensen, G. Öhrwall, W. Osikowicz, C. Tengsted, S. Jönsson, M. Fahlman, W.R. Salaneck, Orbital-specific dynamic charge transfer from Fe (II)-tetraphenylporphyrin molecules to molybdenum disulfide substrates, Phys. Rev. B 72 (2005), 035448.
[30] P. Donovan, A. Robin, M.S. Dyer, M. Persson, R. Raval, Unexpected deformations induced by surface interaction and chiral self-assembly of coII-tetraphenylporphyrin (Co-TPP) adsorbed on Cu (110): a combined STM and periodic DFT study, Chem. –A Eur. J. 16 (2010) 11641–11652.
[31] M. Stark, S. Ditze, M. Drost, F. Buchner, H.-.P. Steinrück, H. Marbach, Coverage dependent disorder–order transition of 2H-tetraphenylporphyrin on Cu (111), Langmuir, 29 (2013) 4104–4110.
[32] M. Stark, S. Ditze, M. Lepper, L. Zhang, H. Schlott, F. Buchner, M. Röckert, M. Chen, O. Lytken, H.-.P. Steinrück, H. Marbach, Massive conformational changes during thermally induced self-metalation of 2H-tetrakis-(3,5-di-tert-butyl)-phenylporphyrin on Cu(111), Chem. Commun. 50 (2014) 10225–10228.
[33] S. Ditze, M. Stark, M. Drost, F. Buchner, H.-.P. Steinrück, H. Marbach, Activation energy for the self-metalation reaction of 2H-tetraphenylporphyrin on Cu(111), Angew. Chem. Int. Ed Engl. 51 (2012) 10898–10901.
[34] G. Rojas, X. Chen, C. Bravo, J.-.H. Kim, J.-.S. Kim, J. Xiao, P.A. Dowben, Y. Gao, X. C. Zeng, W. Choe, Self-assembly and properties of nonmetalated tetraphenyl-porphyrin on metal substrates, J. Phys. Chem. C 114 (2010) 9408–9415.
[35] J. Kuliga, S. Massicot, R. Adhikari, M. Ruppel, N. Jux, H.-.P. Steinrück, H. Marbach, Conformation controls mobility: 2H-tetranaphthylporphyrins on Cu (111), ChemPhysChem 21 (2020) 423.
[36] P. Mishra, J.P. Hill, S. Vijayaraghavan, W.V. Rossom, S. Yoshizawa, M. Grisolia, J. Echeverria, T. Ono, K. Ariga, T. Nakayama, Current-driven supramolecular motor with in situ surface chiral directionality switching, Nano Lett. 15 (2015) 4793–4798.
[37] C.M. Carvalho, T.J. Brocksom, K.T. de Oliveira, Tetrabenzoporphyrins: synthetic developments and applications, Chem. Soc. Rev. 42 (2013) 3302–3317.
[38] I. Horcas, R. Fernández, J. Gomez-Rodriguez, J. Colchero, J. Gómez-Herrero, A. Baro, WSXM: a software for scanning probe microscopy and a tool for nanotechnology, Rev. Sci. Instrum. 78 (2007), 013705.
[39] M. Lepper, J. Köbl, T. Schmitt, M. Gurrath, A. de Siervo, M.A. Schneider, H.-. P. Steinrück, B. Meyer, H. Marbach, W. Hieringer, "Inverted" porphyrins: a distorted adsorption geometry of free-base porphyrins on Cu(111), Chem. Commun. 53 (2017) 8207–8210.
[40] P. Ryan, P. Lalaguna, F. Haag, M. Braim, P. Ding, D. Payne, J. Barth, T.-.L. Lee, D. Woodruff, F. Allegretti, Validation of the inverted adsorption structure for free-base tetraphenyl porphyrin on Cu (111), Chem. Commun. 56 (2020) 3681–3684.
[41] L. Zhang, M. Lepper, M. Stark, T. Menzel, D. Lungerich, N. Jux, W. Hieringer, H.-. P. Steinrück, H. Marbach, On the critical role of the substrate: the adsorption behaviour of tetrabenzoporphyrins on different metal surfaces, Phys. Chem. Chem. Phys. 19 (2017) 20281–20289.
[42] R. Adhikari, J. Kuliga, M. Ruppel, N. Jux, H. Marbach, H.-.P. Steinrück, Self-assembled 2D-coordination kagome, quadratic, and close-packed hexagonal lattices formed from a cyano-functionalized benzoporphyrin on Cu (111), J. Phys. Chem. C 125 (2021) 7204–7212.
[43] D. Van Vörden, M. Lange, M. Schmuck, J. Schaffert, M.C. Cottin, C.A. Bobisch, R. Möller, Communication: substrate induced dehydrogenation: transformation of octa-ethyl-porphyrin into tetra-benzo-porphyrin, J. Chem. Phys. 138 (2013), 211102.
[44] I. Kröger, B. Stadtmüller, C. Stadler, J. Ziroff, M. Kochler, A. Stahl, F. Pollinger, T.-. L. Lee, J. Zegenhagen, F. Reinert, Submonolayer growth of copper-phthalocyanine on Ag (111), N. J. Phys. 12 (2010), 083038.
[45] B. Stadtmüller, I. Kröger, F. Reinert, C. Kumpf, Submonolayer growth of CuPc on noble metal surfaces, Phys. Rev. B 83 (2011), 085416.
[46] J. Xiao, S. Ditze, M. Chen, F. Buchner, M. Stark, M. Drost, H.-.P. Steinrück, J. M. Gottfried, H. Marbach, Temperature-dependent chemical and structural transformations from 2H-tetraphenylporphyrin to copper (II)-tetraphenylporphyrin on Cu (111), J. Phys. Chem. C 116 (2012) 12275–12282.
[47] M. Lepper, T. Schmitt, M. Gurrath, M. Raschmann, L. Zhang, M. Stark, H. Hölzel, N. Jux, B. Meyer, M.A. Schneider, H.-.P. Steinrück, H. Marbach, Adsorption behavior of a cyano-functionalized porphyrin on Cu(111) and Ag(111): from molecular wires to ordered supramolecular two-dimensional aggregates, J. Phys. Chem. C 121 (2017) 26361–26371.
[48] W. Auwärter, A. Weber-Bargioni, A. Riemann, A. Schiffrin, O. Gröning, R. Fasel, J. Barth, Self-assembly and conformation of tetrapyridyl-porphyrin molecules on Ag (111), J. Chem. Phys. 124 (2006), 194708.
[49] M. Lepper, L. Zhang, M. Stark, S. Ditze, D. Lungerich, N. Jux, W. Hieringer, H.-. P. Steinrück, H. Marbach, Role of specific intermolecular interactions for the arrangement of Ni(II)-5, 10, 15, 20-tetraphenyltetrabenzoporphyrin on Cu(111), J. Phys. Chem. C 119 (2015) 19897–19905.
[50] J. Brede, M. Linares, R. Lensen, A.E. Rowan, M. Funk, M. Bröring, G. Hoffmann, R. Wiesendanger, Adsorption and conformation of porphyrins on metallic surfaces, J. Vac. Sci. Technol. B 27 (2009) 799–804.

Supporting information

On the adsorption of different tetranaphthylporphyrins on Cu(111) and Ag(111)

Jan Brox [a], Rajan Adhikari [a], Majid Shaker [a], Michael Ruppel [b], Norbert Jux [b],
Hubertus Marbach [a] Simon Jaekel [a], and Hans-Peter Steinrück [a*]

a Lehrstuhl für Physikalische Chemie II, Friedrich-Alexander-Universität Erlangen-Nürnberg,
Egerlandstr. 3, 91058 Erlangen, Germany

b Lehrstuhl für Organische Chemie II, Friedrich-Alexander-Universität Erlangen-Nürnberg,
Nikolaus-Fiebiger-Str. 10, 91058 Erlangen, Germany

The supporting material provides additional information demonstrating:

- Low temperature -52°C STM images of 2HTNBP on Cu(111) (**Figure S1**). No improvement of molecular contrast, compared to RT.
- Individual STM frames of the motion-pathway-plot in **Figure 2c, d** (**Figure S2**).
- Schematic ball model of Ag(111) surface with highlighted adsorption sites (red) for the commensurable island structure of 2HTNP at RT (**Figure S3**).
- Orientation of lattice vectors c_1 (blue arrow) and c_2 (orange arrow) for 2HTNP islands after the 600 K annealing treatment overlaid a schematic Ag(111) surface. Red circles illustrate multiples of the of 7 Ag-Ag distances. The structure is not commensurable with the surface. Highlighted with the dotted circle is every third molecule, which could sit on the same adsorption site, as the first, within the margin of error. (**Figure S4**).

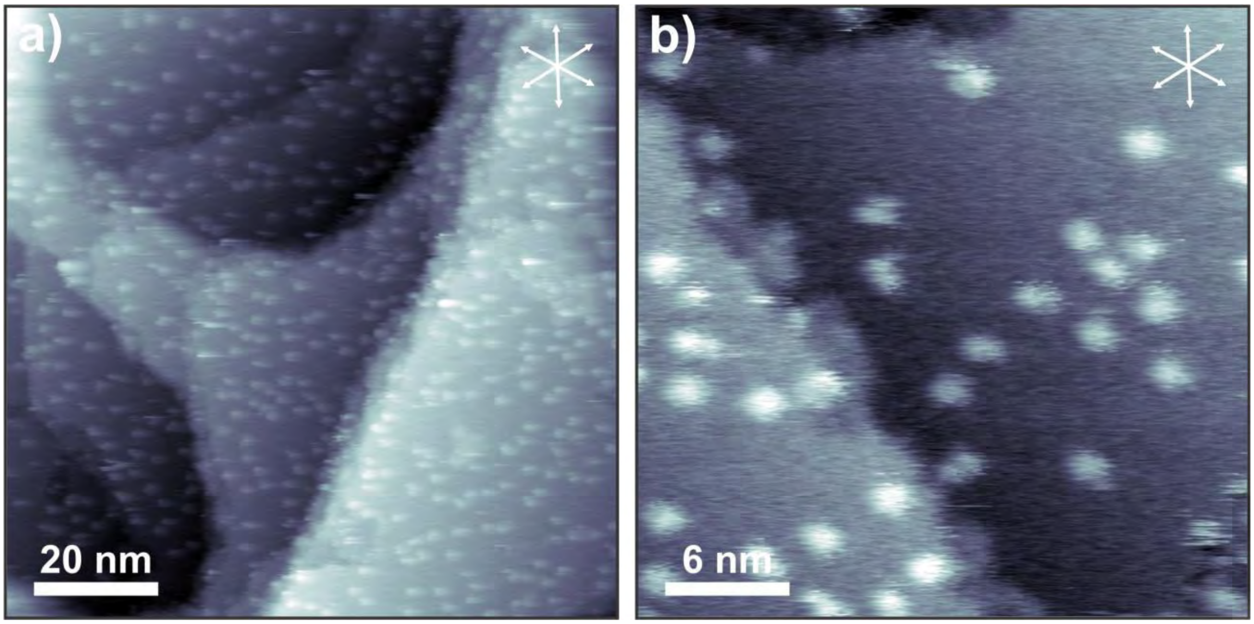

Figure S1: a+b) STM images of 2HTNBP on Cu(111) measured at -52°C.

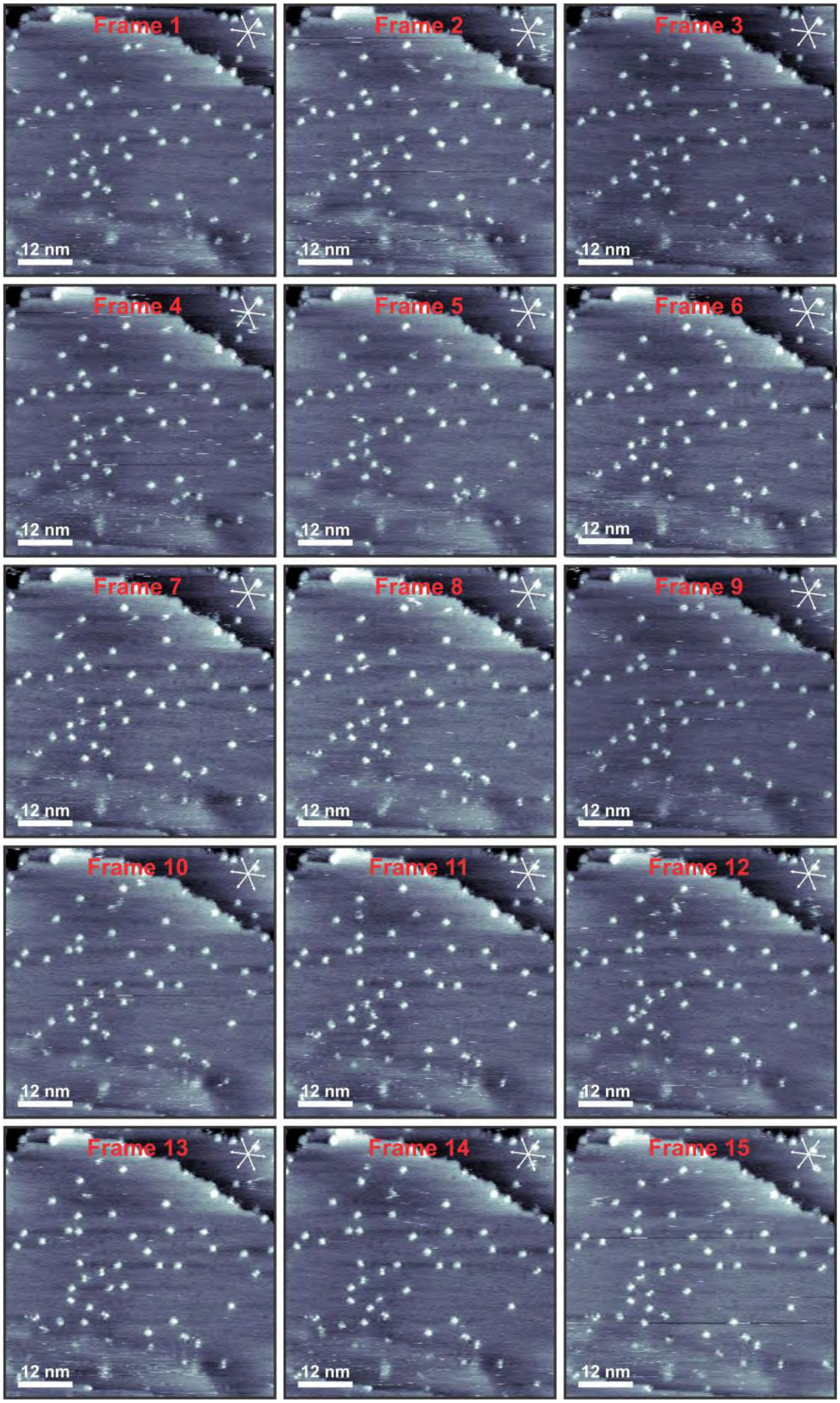

Figure S2: Subsequent STM images taken to acquire a STM movie and to create motion-pathway-plot of 2HTNBP on Cu(111) at RT.

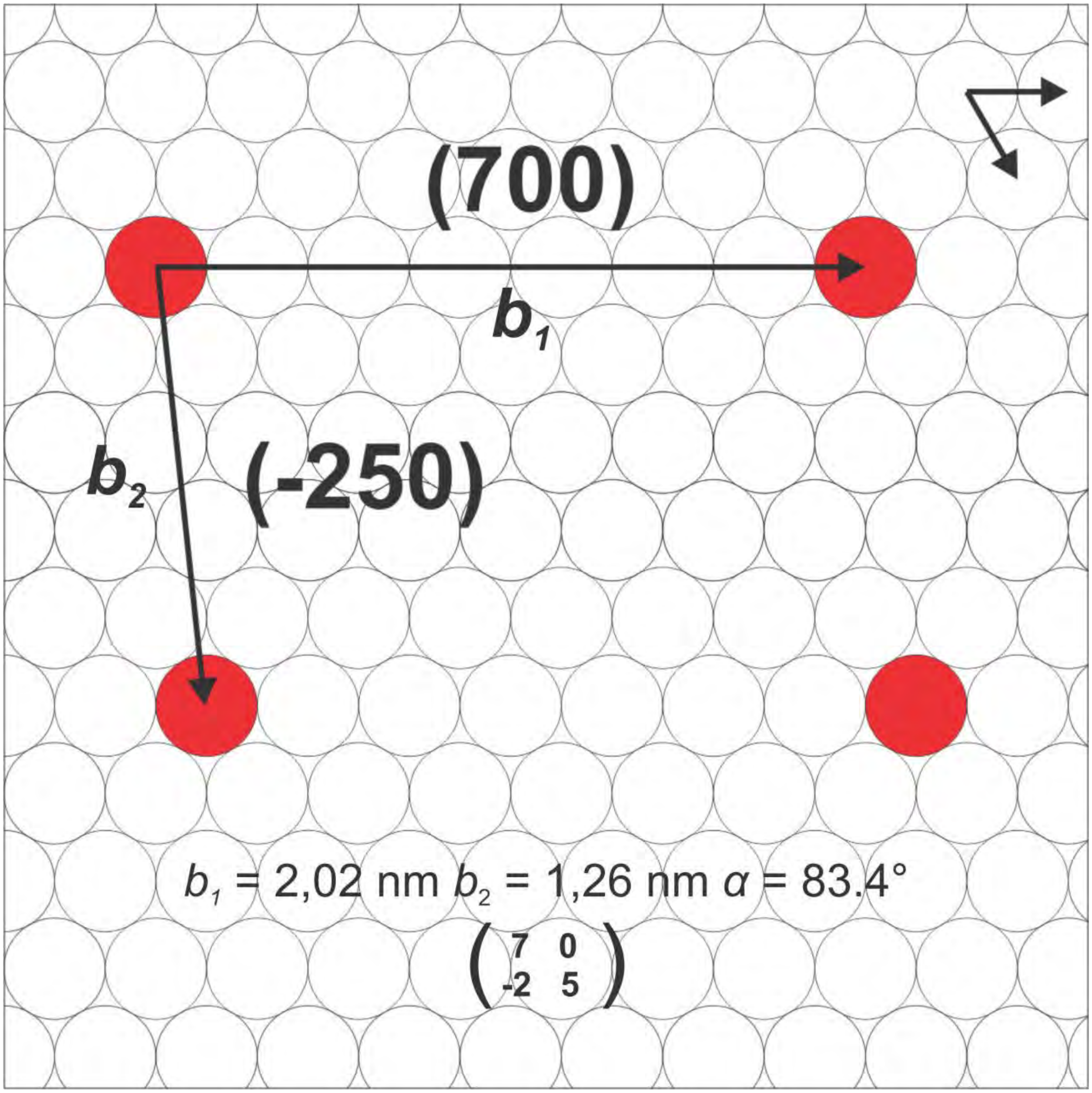

Figure S3: Schematic Ag(111) surface as ball model with highlighted adsorption sites (red) for 2HTNP at RT. The theoretic unit cell vectors and matrix notation for the commensurable structure is given.

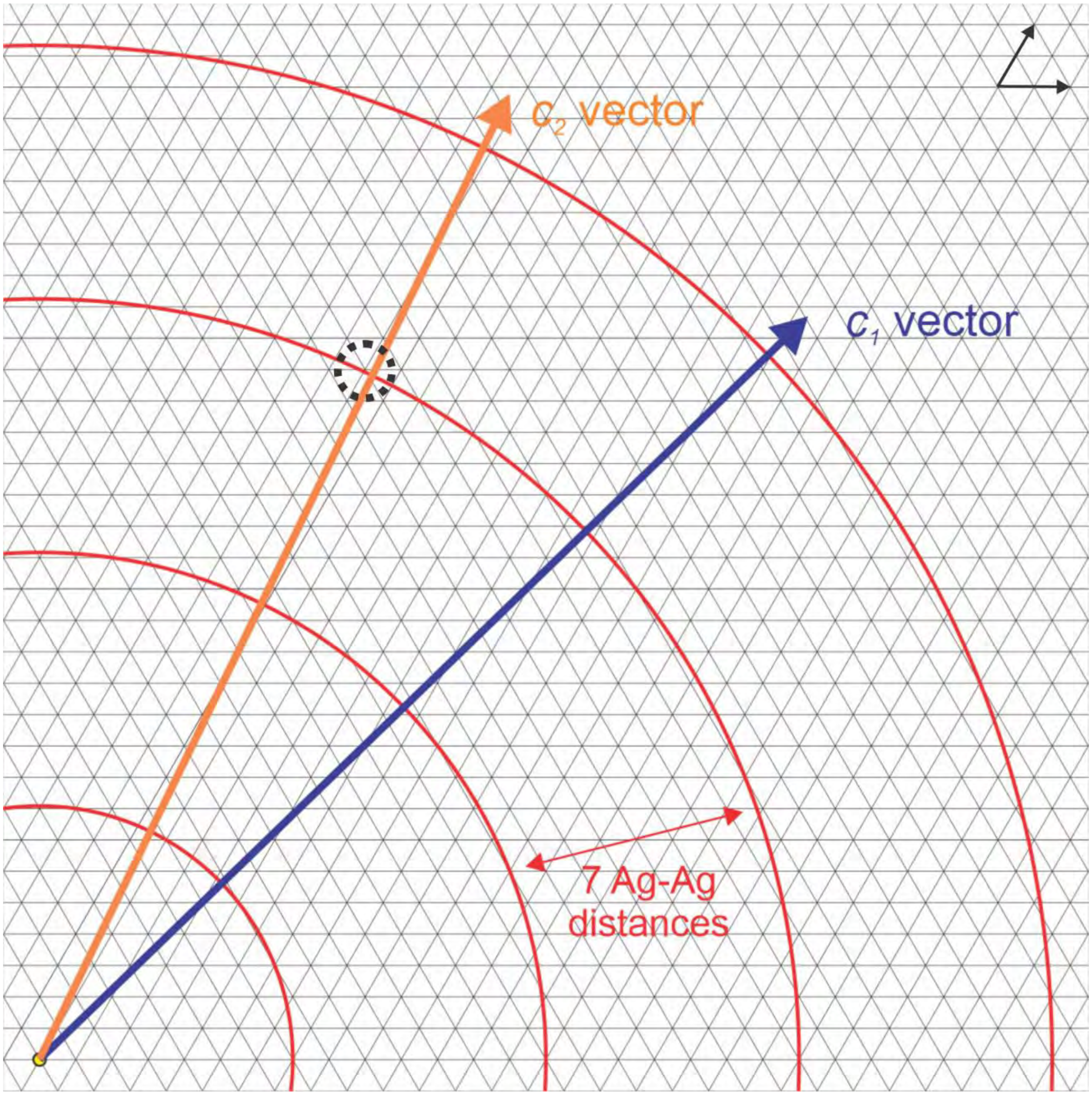

Figure S4: Schematic Ag(111) surface overlaid with the unit cell vectors c_1 and c_2 of 2HTNP after 600 K annealing. The red circles illustrate multiples of the 7 Ag-Ag distances. The dotted circle highlights the nearest matching point of molecules having the same adsorption site.